

2

**MATERIALS FOR ADAPTIVE STRUCTURAL
ACOUSTIC CONTROL**

(M)

Period February 1, 1992 to January 31, 1993

Annual Report

VOLUME II

DTIC
ELECTE
MAY 20, 1993
S B D

**OFFICE OF NAVAL RESEARCH
Contract No. N00014-92-J-1510**

APPROVED FOR PUBLIC RELEASE - DISTRIBUTION UNLIMITED

Reproduction in whole or in part is permitted for any purpose
of the United States Government

L. Eric Cross

PENNSTATE



**THE MATERIALS RESEARCH LABORATORY
UNIVERSITY PARK, PA**

93 5 19 069

93-11221



AD-A264 620



REPORT DOCUMENTATION PAGE

Form Approved

OMB No. 0704-0188

Public reporting burden for this collection of information is estimated to average 1 hour per response, including the time for reviewing instructions, searching existing data sources, gathering and maintaining the data needed, and completing and reviewing the collection of information. Send comments regarding this burden estimate or any other aspect of this collection of information, including suggestions for reducing this burden, to Washington Headquarters Services, Directorate for Information Operations and Reports, 1215 Jefferson Davis Highway, Suite 1204, Arlington, VA 22202-4302, and to the Office of Management and Budget, Paperwork Reduction Project (0704-0188), Washington, DC 20503.

1. AGENCY USE ONLY (Leave blank)		2. REPORT DATE 04/06/93		3. REPORT TYPE AND DATES COVERED ANNUAL REPORT 02/01/92 TO 01/31/93	
4. TITLE AND SUBTITLE MATERIALS FOR ADAPTIVE STRUCTURAL ACOUSTIC CONTROL				5. FUNDING NUMBERS	
6. AUTHOR(S) L. ERIC CROSS					
7. PERFORMING ORGANIZATION NAME(S) AND ADDRESS(ES) MATERIALS RESEARCH LABORATORY THE PENNSYLVANIA STATE UNIVERSITY UNIVERSITY PARK, PA 16802				8. PERFORMING ORGANIZATION REPORT NUMBER N00014-92-J-1510	
9. SPONSORING / MONITORING AGENCY NAME(S) AND ADDRESS(ES) OFFICE OF NAVAL RESEARCH CODE 1513:NRJ 800 NORTH QUINCY STREET ARLINGTON, VA 22217				10. SPONSORING / MONITORING AGENCY REPORT NUMBER DOUGLAS E. HEATON DEPT. NAVY/ONR, RES. REP. THE OHIO STATE UNIV. RES. CTR. 1960 KENNY ROAD COLUMBUS, OH 43210-1063	
11. SUPPLEMENTARY NOTES					
12a. DISTRIBUTION / AVAILABILITY STATEMENT				12b. DISTRIBUTION CODE	
13. ABSTRACT (Maximum 200 words) SEE FOLLOWING PAGE					
14. SUBJECT TERMS				15. NUMBER OF PAGES	
				16. PRICE CODE	
17. SECURITY CLASSIFICATION OF REPORT	18. SECURITY CLASSIFICATION OF THIS PAGE	19. SECURITY CLASSIFICATION OF ABSTRACT	20. LIMITATION OF ABSTRACT		

ABSTRACT

This report documents work carried out in the Materials Research Laboratory of the Pennsylvania State University over the first year of a new ONR sponsored University Research Initiative (URI) entitled "Materials for Adaptive Structural Acoustic Control." For this report the activities have been grouped under the following topic headings:

1. General Summary Papers.
2. Materials Studies.
3. Composite Sensors.
4. Actuator Studies.
5. Integration Issues.
6. Processing Studies.
7. Thin Film Ferroelectrics.

In material studies important advances have been made in the understanding of the evaluation of relaxor behavior in the PLZT's and of the order disorder behavior in lead scandium tantalate:lead titanate solid solutions and of the Morphotropic Phase Boundary in this system. For both composite sensors and actuators we have continued to explore and exploit the remarkable versatility of the flextensional moonie type structure. Finite element (FEA) calculations have given a clear picture of the lower order resonant modes and permitted the evaluation of various end cap metals, cap geometries and load conditions. In actuator studies multilayer structures have been combined with flextensional moonie endcaps to yield high displacement (50 μ meter) compact structures. Electrically controlled shape memory has been demonstrated in lead zirconate stannate titanate compositions, and used for controlling a simple latching relay. Detailed study of fatigue in polarization switching compositions has highlighted the important roles of electrodes, grain size, pore structures and microcracking and demonstrated approaches to controlling these problems. For practical multilayer actuators a useful lifetime prediction can be made from acoustic emission analysis.

New modelling of 2:2 and 1:3 type piezoceramic:polymer composites has given more exact solutions for the stress distribution and good agreement with ultradilatometer measurements of local deformations. Composites with 1:3 connectivity using thin wall ceramic tubes appear to offer excellent hydrostatic sensitivity, unusual versatility for property control and the possibility to use field biased electrostrictors in high sensitivity configurations. Processing approaches have continued to use reactive calcining and have supplied the group with the wide range of ceramics used in these studies. For lead magnesium niobate:lead

ABSTRACT (continued)

titanate solid solutions grain size effects in samples of commercial purity have been traced to a thin (~20 n meter) glassy layer at the grain boundary. In parallel with the ONR URI the laboratory has extensive DARPA and Industry sponsored research on ferroelectric thin films, a very short selection of most relevant papers has been included for the convenience of users.

Accession For		<input checked="" type="checkbox"/>	<input type="checkbox"/>	<input type="checkbox"/>
NTIS AD&I				
DTIC				
Un. Secured				
Int. Secured				
By				
Distribution/				
Availability Codes				
Avail and/or				
Special				
Dist				
A-1				

**MATERIALS FOR ADAPTIVE STRUCTURAL
ACOUSTIC CONTROL**

Period February 1, 1992 to January 31, 1993

Annual Report

VOLUME II

**OFFICE OF NAVAL RESEARCH
Contract No. N00014-92-J-1510**

APPROVED FOR PUBLIC RELEASE – DISTRIBUTION UNLIMITED

Reproduction in whole or in part is permitted for any purpose
of the United States Government

L. Eric Cross

PENNSSTATE



**THE MATERIALS RESEARCH LABORATORY
UNIVERSITY PARK, PA**

TABLE OF CONTENTS

ABSTRACT	6
INTRODUCTION	7
1.0 GENERAL SUMMARY PAPERS	10
2.0 MATERIALS STUDIES	10
3.0 SENSOR STUDIES	12
4.0 ACTUATOR STUDIES	13
5.0 INTEGRATION ISSUES	14
6.0 PROCESSING STUDIES	14
7.0 THIN FILM FERROELECTRICS	15
8.0 HONORS AND AWARDS	15
9.0 APPRENTICE PROGRAM	17
10.0 PAPERS PUBLISHED IN REFEREED JOURNALS	18
11.0 INVITED PAPERS PRESENTED AT NATIONAL AND INTERNATIONAL MEETINGS	21
12.0 INVITED PRESENTATIONS AT UNIVERSITY, INDUSTRY AND GOVERNMENT LABORATORIES	23
13.0 CONTRIBUTED PAPERS AT NATIONAL AND INTERNATIONAL MEETINGS	24

APPENDICES

General Summary of Papers

1. R. E. Newnham, "Memories of Arthur Von Hippel," *Ferroelectrics* 137, 17 (1992).
2. C. Rosen, B. V. Hiremath and R. E. Newnham, "Piezoelectricity," American Inst. of Physics, New York (1991).
3. R. E. Newnham, "Ferroelectric Sensors and Actuators Smart Electroceramics," *Ferroelectric Ceramics*, Editor N. Setter, Proc. of Summer School on Ferroelectrics, Ascona (1991).
4. R. E. Newnham, "Smart Electroceramics in the 1990's and Beyond," J. European Ceramic Soc. (1992).
5. V. Sundar and R. E. Newnham, "Electrostriction and Polarization," *Ferroelectrics* 135, 431 (1992).

Materials Studies

6. J. R. Giniewicz, A. S. Bhalla and L. E. Cross, "Identification of the Morphotropic Phase Boundary in Lead Scandium Tantalate-Lead Titanate Solid Solution System."
7. J. R. Giniewicz, A. S. Bhalla and L. E. Cross, "Variable Structure Ordering in Lead Scandium Tantalate-Lead Titanate Materials."
8. J. R. Giniewicz, A. S. Bhalla and L. E. Cross, "Lead Scandium Tantalate:Lead Titanate Materials for Field Stabilized Pyroelectric Device Applications," *Ferroelectrics Letters* **14**, 21 (1992).
9. A. S. Bhalla, R. Guo, L. E. Cross, G. Burns, F. H. Dacol and R. R. Neurgaonkar, "Glassy Polarization in the Ferroelectric Tungsten Bronze (BaSr) Nb₂O₆," *J. Appl. Phys.* **71** (11), 5591 (1992).
10. J. S. Yoon, V. S. Srikanth and A. S. Bhalla, "The Electrical Properties of Antiferroelectric Lead Zirconate-Ferroelectric Lead Zinc Niobate Ceramics with Lanthanum," *Proc. ISAF 1992, Greenville, South Carolina*, pp. 556.
11. E. F. Alberta, D. J. Taylor, A. S. Bhalla and T. Takenaka, "The DC Field Dependence of the Piezoelectric, Elastic and Dielectric Constants for a Lead Zirconate Based Ceramic," *Proc. ISAF 1992, Greenville, South Carolina*, pp. 560.
12. W. Cao and L. Eric Cross, "The Ratio of Rhombohedral and Tetragonal Phases at the Morphotropic Phase Boundary in Lead Zirconate Titanate," *Japan Journal of Applied Physics* **31** (Pt. 1, No. 5A), 1399 (1992).
13. C. A. Randall, M. G. Matsko, W. Cao and A. S. Bhalla, "A Transmission Electron Microscope Investigation of the R3m - R3c Phase Transition in Pb(ZrTi)O₃ Ceramics," *Solid State Comm.* **85** (3), 193 (1993).
14. Shaoping Li, Chi Yeun Huang, A. S. Bhalla and L. E. Cross, "90° Domain Reversal in Pb(Zr_xTi_{1-x})O₃ Ceramics," *Proc. ISAF 1992, Greenville, South Carolina*.
15. Shaoping Li, Jyh Sheen, Q. M. Zhang, Sei-Joo Jang, A. S. Bhalla and L. E. Cross, "Quasi Lumped Parameter Method for Microwave Measurements of Dielectric Dispersion in Ferroelectric Ceramics," *Proc. ISAF 1992, Greenville, South Carolina*.
16. H. Wang, Q. M. Zhang, L. E. Cross and A. O. Sykes, "Piezoelectric Dielectric and Elastic Properties of Poly (Vinylidene Fluoride/Trifluoroethylene)."
17. H. Wang, Q. M. Zhang, L. E. Cross and A. O. Sykes, "Clamping Effect on Piezoelectric Properties of Poly (Vinylidene Fluoride/Trifluoroethylene) Copolymers."

Composite Sensors

18. Ki-Young Oh, Yutaka Saito, Atsushi Furuta and Kenji Uchino, "Piezoelectricity in the Field Induced Ferroelectric Phase of Lead Zirconate Based Antiferroelectrics," *J. Amer. Ceram. Soc.* **75** (4), 795 (1992).

Composite Sensors (continued)

19. R. E. Newnham, Q. C. Xu, K. Onitsuka and S. Yoshikawa, "A New Type of Flexensional Transducer," Proc. 3rd Int. Mtg. on Transducers for Sonics and Ultrasonics (May 1992).
20. C. A. Randall, D. V. Miller, J. H. Adair and A. S. Bhalla, "Processing of Electroceramic-Polymer Composites Using the Electrorheological Effect," J. Mat. Res. 8 (4), 1 (1993).
21. C. A. Randall, S. Miyazaki, K. L. More, A. S. Bhalla and R. E. Newnham, "Structural-Property Relations in Dielectrophoretically Assembled BaTiO₃ Nanocomposites," Materials Letters 15, 26 (1992).
22. C. A. Randall, S. F. Wang, D. Laubscher, J. P. Dougherty and W. Huebner, "Structure Property Relations in Core-Shell BaTiO₃:LiF Ceramics," J. Mat. Res. (in press).
23. C. A. Randall, G. A. Rossetti and W. Cao, "Spatial Variations of Polarization in Ferroelectrics and Related Materials."
24. Jayu Chen, Qi Chang Xu, M. Blaszkiewicz, R. Meyer, Jr. and R. E. Newnham, "Lead Zirconate Titanate Films on Nickel-Titanium Shape Memory Alloys: SMARTIES," J. Amer. Ceram. Soc. 75 (10), 2891 (1992).

Actuator Studies

25. D. Damjanovic and R. E. Newnham, "Electrostrictive and Piezoelectric Materials for Actuator Applications," J. Intell. Mat. Syst. and Struct. 3, 190 (1992).
26. Y. Sugawara, K. Onitsuka, S. Yoshikawa, Q. C. Xu, R. E. Newnham and K. Uchino, "Metal-Ceramic Composite Actuators," J. Amer. Ceram. Soc. 75 (4), 996 (1992).
27. Q. C. Xu, A. Dogan, J. Tressler, S. Yoshikawa and R. E. Newnham, "Ceramic-Metal Composite Actuators," Ferroelectrics Special Issue.
28. K. Uchino, "Piezoelectric Ceramics in Smart Actuators and Systems," Proc. 1st European Conference on Smart Structures and Materials.
29. A. Furuta, Ki-Young Oh and K. Uchino, "Shape Memory Ceramics and Their Application to Latching Relays," Sensors and Materials 3 (4), 205 (1992).
30. K. Uchino and A. Furuta, "Destruction Mechanisms in Multilayer Ceramic Actuators," Proc. ISAF 1992, Greenville, South Carolina, pp. 195.
31. Q. Jiang, Wenwu Cao and L. E. Cross, "Electric Fatigue Initiated by Surface Contamination in High Polarization Ceramics," Proc. ISAF 1992, Greenville, South Carolina, pp. 107.
32. Q. Jiang, Wenwu Cao and L. E. Cross, "Electric Fatigue in PLZT Ceramics."

Integration Issues

33. Wenwu Cao, Q. M. Zhang and L. E. Cross, "Theoretical Study on the Static Performance of Piezoelectric Ceramic-Polymer Composite with 1-3 Connectivity," *J. Appl. Phys.* 72 (12), 5814 (1992).
34. Q. M. Zhang, Wenwu Cao, H. Wang and L. E. Cross, "Characterization of the Performance of 1-3 Type Piezocomposites for Low Frequency Applications," *J. Appl. Phys.* 73 (3), 1403 (1993).
35. Q. M. Zhang, Wenwu Cao, H. Wang and L. E. Cross, "Strain Profile and Piezoelectric Performance of Piezocomposites with 2-2 and 1-3 Connectivities," *Proc. ISAF 1992, Greenville, South Carolina*, pp. 252.
36. Q. M. Zhang, H. Wang and L. E. Cross, "Piezoelectric Tubes and 1-3 Type Tubular Composites as Tunable Actuators and Sensors."
37. Q. M. Zhang, H. Wang and L. E. Cross, "Piezoelectric Tubes and Tubular Composites for Actuator and Sensor Applications."

Processing Studies

38. Thomas R. Shrout and Scott L. Swartz, "Processing of Ferroelectric and Related Materials: A Review."
39. G. A. Rossetti, D. J. Watson, R. E. Newnham and J. H. Adair, "Kinetics of the Hydrothermal Crystallization of the Perovskite Lead Titanate," *J. Crystal Growth* 116, 251 (1992).
40. A. V. Prasadaraao, U. Selvaraj, S. Komarneni and A. S. Bhalla, "Sol-Gel Synthesis of $\text{Ln}_2(\text{Ln} = \text{La}, \text{Nd}) \text{Ti}_2\text{O}_7$," *J. Mat. Res.* 7 (10), 2859 (1992).
41. A. V. Prasadaraao, U. Selvaraj, S. Komarneni and A. S. Bhalla, "Sol Gel Synthesis of Strontium Pyroniobate and Calcium Pyroniobate," *J. Amer. Ceram. Soc.* 75 (10), 2697 (1992).
42. A. V. Prasadaraao, U. Selvaraj, S. Komarneni and A. S. Bhalla, "Fabrication of $\text{La}_2\text{Ti}_2\text{O}_7$ Thin Films by A Sol-Gel Technique," *Ferroelectrics Letters* 14, 65 (1992).
43. S. F. Wang, U. Kumar, W. Huebner, P. Marsh, H. Kankel and C. G. Oakley, "Grain Size Effects on the Induced Piezoelectric Properties of 0.9 PMN-0.1PT Ceramic," *Proc. ISAF 1992, Greenville, South Carolina*, pp. 148.
44. C. A. Randall, A. D. Hilton, D. J. Barber and T. R. Shrout, "Extrinsic Contributions to the Grain Size Dependence of Relaxor Ferroelectric $\text{Pb}(\text{Mg}_{1/3}\text{Nb}_{2/3})\text{O}_3\cdot\text{PbTiO}_3$ Ceramics," *J. Mat. Res.* 8 (4) (1993).
45. B. V. Hiremath, R. E. Newnham and L. E. Cross, "Barrier Layer Capacitor Using Barium Bismuth Plumbate and Barium Plumbate," *J. Amer. Ceram. Soc.* 75 (11), 2953 (1992).
46. U. Kumar, S. F. Wang, S. Varanasi and J. P. Dougherty, "Grain Size Effects on the Dielectric Properties of Strontium Barium Titanate," *Proc. ISAF 1992, Greenville, South Carolina*, pp. 55.

Processing Studies (continued)

47. U. Kumar, S. F. Wang and J. P. Dougherty, "Preparation of Dense Ultra-Fine Grain Barium Titanate-Based Ceramics," Proc. ISAF 1992, Greenville, South Carolina, pp. 70.

Thin Film Ferroelectrics

48. J. Chen, K. R. Udayakumar, K. G. Brooks and L. E. Cross, "Dielectric Behavior of Ferroelectric Thin Films at High Frequencies," Proc. ISAF 1992, Greenville, South Carolina, pp. 182.
49. K. Uchino, N-Y. Lee, T. Toba, N. Usuki, H. Aburatani and Y. Ito, "Changes in the Crystal Structure of RF-Magnetron Sputtered BaTiO₃ Thin Films," J. Chem. Soc. Japan 100 (9), 1091 (1992).
50. R. E. Newnham, K. R. Udayakumar and S. Trolier-McKinstry, "Size Effects in Ferroelectric Thin Films," *Chemical Processing of Advanced Materials*, Edited by Larry L. Hench and Jon K. West, John Wiley and Sons, Inc. (1992).
51. S. Trolier-McKinstry, H. Hu, S. B. Krupanidhi, P. Chindaudom, K. Vedam and R. E. Newnham, "Spectroscopic Ellipsometry Studies on Ion Beam Sputter Deposited Pb(Zr, Ti)O₃ Films on Sapphire and Pt-Coated Silicon Substrates."

MATERIALS-STUDIES
(continued)

APPENDIX. 16

PIEZOELECTRIC, DIELECTRIC, AND ELASTIC PROPERTIES OF
POLY(VINYLDENE FLUORIDE/TRIFLUOROETHYLENE)

H. Wang, Q. M. Zhang, and L. E. Cross

Materials Research Laboratory

The Pennsylvania State University

University Park, PA 16802

A. O. Sykes

Acoustical Research and Applications

Vienna, VA 22180

The complete piezoelectric coefficient, dielectric constant, and elastic compliance matrices have been determined on poly(vinylidene fluoride/trifluoroethylene) (PVDF-TrFE) (75/25) copolymer at room temperature and a frequency of 500 Hz. The temperature dependence of each of the complex piezoelectric coefficients and complex dielectric constants has been measured in the temperature range of $-100 \sim 65$ °C. The frequency dependence of these coefficients has also been measured at room temperature. It is found that the relaxation observed in the tensile piezoelectric coefficients of this material is different from that of the dielectric constants, whereas the relaxation of the piezoelectric shear constants shows behavior similar to that of the dielectric constants.

PACS numbers: 77.60. +v, 77.20. +y.

INTRODUCTION

Polyvinylidene fluoride (PVDF) and its copolymers with trifluoroethylene (TrFE) or tetrafluoroethylene (TFE) have become important piezoelectric materials for transducer applications. Compared with inorganic piezoelectric materials, these materials have high mechanical flexibility, low acoustic impedance, and can be easily molded into desirable forms. The piezoelectric coefficients of the materials are higher compared with other piezoelectric polymeric materials. In the past two decades, a large number of investigations have been conducted to improve the performance and to explore the physical bases of piezoelectricity and ferroelectricity of these materials.¹⁻⁴

Like other piezoelectric materials, the linear coupling of mechanical and electrical effects of PVDF and its copolymers is described by the constitutive equations. These equations contain the piezoelectric, dielectric, and elastic coefficients which are all important material parameters for both device design and fundamental understanding of the materials. For a stretched and poled PVDF-type polymer, its symmetry properties belong to point group $mm2$. The piezoelectric coefficient, dielectric constant, and elastic compliance matrices have the forms of:

$$\begin{pmatrix} 0 & 0 & 0 & 0 & d_{15} & 0 \\ 0 & 0 & 0 & d_{24} & 0 & 0 \\ d_{31} & d_{32} & d_{33} & 0 & 0 & 0 \end{pmatrix},$$

$$\begin{pmatrix} K_{11} & 0 & 0 \\ 0 & K_{22} & 0 \\ 0 & 0 & K_{33} \end{pmatrix},$$

$$\text{and } \begin{pmatrix} s_{11} & s_{12} & s_{13} & 0 & 0 & 0 \\ s_{12} & s_{22} & s_{23} & 0 & 0 & 0 \\ s_{13} & s_{23} & s_{33} & 0 & 0 & 0 \\ 0 & 0 & 0 & s_{44} & 0 & 0 \\ 0 & 0 & 0 & 0 & s_{55} & 0 \\ 0 & 0 & 0 & 0 & 0 & s_{66} \end{pmatrix},$$

where the coordinate axis 1 refers to the polymer chain direction (stretch direction), 3 the poling direction, and 2 the axis orthogonal to 1 and 3 axes. Experimental evidence has

shown that these coefficients vary with polymer processing methods even for samples with the same composition and the same measuring conditions. For the purpose of application and fundamental understanding of these materials, it is desirable to establish a complete data base to characterize all these properties on samples with similar processing conditions. However, as can be seen in table I, which presents the typical experimental results for piezoelectric, dielectric, and compliance coefficients of PVDF materials available in the literature, in spite of extensive investigations in the past, the characterization of the materials, especially copolymers, is far from being complete. For example, although the piezoelectric tensile coefficients, especially d_{31} , have been studied extensively using quasistatic methods, there is little information about the imaginary part of these coefficients. Furthermore, few measurements of the shear coefficients have been made. The experiment results from various groups differ significantly and they cannot be used to consistently describe the physical properties of the materials.

In this paper, the experimental results from recent studies on a P(VDF-TrFE)(75/25) copolymer are presented. The matrix elements of the piezoelectric, dielectric, and elastic compliance coefficients have been measured at room temperature (22 °C) and a frequency of 500 Hz. Both real and imaginary parts of the piezoelectric and dielectric constants were measured over wide frequency and temperature ranges.

EXPERIMENTAL WORK

(1) Sample preparing

Poled P(VDF-TrFE) (75/25) copolymer plates purchased from Atochem North America Inc. (Part No. A002335-00) were in two thicknesses of 0.5mm and 10 mm. From these plates, test samples were cut into suitable shapes and sizes for measuring the dielectric, piezoelectric, and elastic compliance constants. Samples for the measurements of the tensile piezoelectric coefficients d_{3i} ($i=1, 2$, and 3) and dielectric constant K_{33} were cut from 0.5 mm thick plate while samples for the measurements of the shear piezoelectric

coefficients d_{15} and d_{24} and dielectric constants K_{11} and K_{22} were cut from 10 mm thick plate. For elastic compliance measurements, samples were made into square rods from the 10 mm thick plate with their length along the direction in which the measurement was made.

(2) Measurement details

Complex piezoelectric coefficient, dielectric constant and elastic compliance are defined as following:⁵

$$\begin{aligned} d_{ij} &= d'_{ij} - j d''_{ij} \\ K_{ii} &= K'_{ii} - j K''_{ii} \\ s_{jk} &= s'_{jk} - j s''_{jk} \end{aligned} \quad (1)$$

where $i = 1, 2, 3$, and $j, k = 1, 2, \dots, 6$.

The piezoelectric coefficients were measured by utilizing a laser ultra-dilatometer.⁶ Making use of the converse piezoelectric effect, strain x_j induced by an alternating electric field E_i was measured and the piezoelectric coefficients were determined by

$$d_{ij} = \frac{\partial x_i}{\partial E_j} \Big|_{T=0} \quad (2)$$

Depending on the coefficient to be measured, either the single beam or double beam laser dilatometer was used.⁷ As demonstrated previously,⁸ the system is capable of detecting both the amplitude and phase angle of the field induced strain, thus yielding the real and imaginary part of the piezoelectric strain coefficients.

It should be pointed out that in general, for piezoelectric constant measurement, the quantity determined from the direct piezoelectric effect is $\frac{\partial Q_i}{A_i \partial T_j}$, where A_i is the area of the electrodes in the unstrained sample with its normal along i direction, Q_i the charges on the electrodes, and T the stress applied on the sample. It can be shown that

$$\frac{\partial Q_i}{A_i \partial T_j} = \frac{\partial D_i}{\partial T_j} + \frac{D_i \partial A_i}{A_i \partial T_j} \quad (3)$$

where D is the electric displacement. The first term on the right hand side of the equation is the d_{ij} defined in IEEE standard.⁹ For conventional piezoelectric ceramics, the second term on the right hand side is much smaller than the first term and therefore the quantity measured from the direct piezoelectric effect is practically equal to d_{ij} . However, for polymeric piezoelectric materials, the second term is not negligible. It can also be shown that the piezoelectric strain coefficients d_{ij} determined from the converse effect (Eq. (2)) is equal to the right hand side of Eq. (3).³ Hence, the direct effect and converse effect yield the same piezoelectric constants, and in practice, they are the physical parameters of interest.

A capacitance bridge (General Radio) was used to measure the dielectric constants. For K33, an impedance analyzer(HP) was used to carry out the measurement at higher frequencies.

In the piezoelectric and dielectric constant measurements, temperature was regulated by a microminiature refrigerator system (MMR Technologies Inc.). The temperature variation throughout the measurement was less than 0.1 K.

The principal diagonal components of the elastic compliance matrix were measured by a dynamic compliance measuring apparatus (DCA), developed at Acoustical Research and Applications. The off-diagonal components were measured by using the DCA in conjunction with the double beam laser interferometer. The DCA, shown in Fig. 1, consisted of a massive stiff frame, a calibrated piezoelectric displacement generator and a force gage. Both the generator and the force gage were rigidly attached to the frame, between which a sample of the material to be tested can be inserted.

RESULTS AND DISCUSSION

The results of the complex piezoelectric, dielectric, and elastic constants on P(VDF-TrFE) (75/25) samples acquired at room temperature and a frequency of 500Hz are presented in the column I of table I for comparison with those from the literature. To our

knowledge, this set of piezoelectric, dielectric, and compliance coefficient data is the most complete currently available for any PVDF copolymeric materials.

To avoid the possible clamping effect of the two ends of the sample rods inserted in the DCA on the measured elastic compliance, samples with length to width ratio (aspect ratio) of 10 were used. All the measurements were repeated several times and the data can be reproduced within 5 %. To further confirm that the end clamping effect is negligible here, we also performed the measurement with samples of aspect ratio of 5 and the results are basically the same as those acquired from the samples with aspect ratio of 10. For a piezoelectric material, its elastic compliance can also be measured by piezoelectric resonance technique. For the copolymer samples, s_{31}^E was also measured by utilizing the resonance technique and the result was consistent with that from the DCA.

Shown in Fig. 2 and Fig.3 respectively are the temperature dependences of the piezoelectric and dielectric constants at a frequency of 500Hz. The measured Curie temperature of this material is 115 °C. These results reveal several interesting features. In contrast to drawn PVDF, which is very anisotropic piezoelectrically in the plane perpendicular to the poling direction, and for which d_{31} and d_{32} exhibit very different magnitudes and temperature dependences, very small difference in magnitude and temperature dependence were observed between d_{31} and d_{32} for this copolymer. The piezoelectric constants d_{31} and d_{32} increase with temperature much faster than d_{33} , d_{15} , and d_{24} . Additionally, higher losses were measured. On the other hand, the dielectric constants along three axes exhibit nearly identical temperature dependences.

For PVDF and its copolymers, experimental evidence has shown that the mesoscopic morphology is that of crystalline lamellae embeded in an amorphous region of disordered polymer chains. Hence, the piezoelectric response is governed by the mechanically induced change of the mechanical and electrical fields distribution within the amorphous and crystalline regions. It has been proposed that there are two major contributions to the piezoelectric response in these materials: the intrinsic change of polarization (biased

electrostriction effect), and the change of the sample dimensions while electric moments are fixed (dimensional effect). The dimensional effect contribution was calculated by using a model of dipoles dispersed in an amorphous medium.⁴ For example, the dimensional contribution to d_{33} , from this model, is $-P_r s_{33}$, where P_r is the remanent polarization and s_{33} is the elastic compliance. P_r measured for this sample is $5.4 \mu\text{C}/\text{cm}^2$, hence, the dimensional effect contribution to d_{33} is $-16.2 \text{ pC}/\text{N}$, which is about 50 % of the total d_{33} . However, for the shear components, this contribution is extremely large when calculated using this model. For example, the dimensional effect contribution to d_{15} is $-520 \text{ pC}/\text{N}$. If the model is correct the contributions from the intrinsic and dimensional effects are in opposite signs in shear constants and they almost cancel out, resulting in a small total coefficient.

For PVDF homopolymer there usually exist three relaxation processes associated with different types of segment motion in the material. The α relaxation occurs at temperature above 55°C , β near -40°C , and γ near -70°C . Previous studies have shown that α relaxation is associated with molecular motion in crystalline regions of α -phase, the β relaxation with the segment motion in the amorphous regions and hence signifies the glass transition, and the γ relaxation with local motion in the amorphous regions. For this P(VDF-TrFE) (75/25) copolymer, only β relaxation was observed at temperature around -30°C . This together with the x-ray diffraction data¹⁰ indicate that the crystalline phase in this copolymer is β -phase. The interesting feature is that the loss peaks related to the β relaxation in the dielectric curves are about 20 degrees higher than those in the tensile piezoelectric coefficient curves, i. e., the dielectric loss peaks are at about -20°C while the loss peaks in the tensile piezoelectric coefficients are at -40°C . More interestingly, the loss peaks in the shear piezoelectric coefficient curves are almost at the same temperature as those of the dielectrics.

Fig. 4 shows the frequency dependence of the dielectric constant K_{33} . The relaxation observed near 1 MHz in the K_{33} spectrum is associated with β -relaxation, as has been

identified from the earlier studies on the PVDF homopolymer.¹¹ K_{11} and K_{22} were measured in the frequency range from 100 Hz to 100 KHz and their dependences on frequency are similar to that of K_{33} . No frequency dispersion was observed for piezoelectric d constants in the range of 100Hz-5KHz.

In conclusion, the complete piezoelectric coefficient, dielectric constant, and elastic compliance matrices have been determined on P(VDF-TrFE) (75/25) copolymer at room temperature and a frequency of 500 Hz. The frequency and temperature dependences of all five complex piezoelectric coefficients as well as three complex dielectric constants have been characterized.

ACKNOWLEDGMENT

This work was supported by the Naval Undersea Warfare center's Small Business Innovation Research (SBIR) program under contract N66604-90-C1558 (Low Cost Acoustic Sensor Technology), and the Office of Naval Research.

REFERENCES:

- 1 G. M. Sessier, J. Acoust. Soc. Am. **70**, 1596 (1981).
- 2 M. G. Broadhurst, G. T. Davis, and J. E. McKinney, J. Appl. Phys., **49**, 4992 (1978).
- 3 R. G. Kepler and R. A. Anderson, J. Appl. Phys., **49**, 4490 (1978).
- 4 T. Furukawa, J. X. Wen, K. Suzuki, Y. Takashina, and M. Date, J. Appl. Phys., **56**, 829 (1984).
- 5 R. Holland and E. P. EerNisse, "Design of Resonant Piezoelectric Devices", (Cambridge, Mass., M. I. T. press, 1969).
- 6 Q. M. Zhang, S. J. Jang and L. E. Cross, J. Appl. Phys., **65**, 2807 (1989).
- 7 W. Y. Gu, W. Y. Pan, and L. E. Cross, Materials Letters, **8**, 3 (1989).
- 8 W. Y. Pan, H. Wang and L. E. Cross, Jpn. J. Appl. Phys. **29**, 1570 (1990).
- 9 IEEE Standard on Piezoelectricity, ANSI/IEEE Std 176-1987.
- 10 Unpublished data from the authors.
- 11 T. T. Wang, "The Application of Ferroelectric Polymers", (New York, Chapman and hall, 1988).

FIGURE CAPTIONS

Fig. 1 Schematic drawing of the Dynamic Compliance Apparatus.

Fig. 2 Piezoelectric strain coefficients as functions of temperature.

Fig. 3 Dielectric constants as functions of temperature.

Fig. 4 Dielectric constant K_{33} as function of frequency.

TABLE I The Piezoelectric, Dielectric, and Elastic coefficients of PVDF-Type Materials

(Unit: d-pC/N; s-x10⁻¹⁰m²/N)

Properties	P(VDF-TrFE) (75/25)	DRAWN PVDF				P(VDF-TrFE)	P(VDF-TFE)
d' ₃₁	10.7	12.5 ^b	21 ^{e, h, k}	28 ^{c, f}	16.8 ^a	9.8 ^a	11.6 ^d
d'' ₃₁	0.18			0.4 ^b			
d' ₃₂	10.1	2.3 ^{h, k}	1.5 ^c	2 ^c	4.8 ^f	2.2 ^a	
d'' ₃₂	0.19						
d' ₃₃	-33.5	-26 ⁿ	-32.5 ^e	-17.4 ^f	-28 ⁱ	-14.8 ^a	-30 ~ -44 ⁿ
d'' ₃₃	-0.65						
d' ₁₅	-36.3			-27 ^e			
d'' ₁₅	-0.32						
d' ₂₄	-40.6			-23 ^e			
d'' ₂₄	-0.35						
K' ₁₁	7.40			6.9 ^l			
K'' ₁₁	0.07						
K' ₂₂	7.95			8.6 ^l			
K'' ₂₂	0.09						
K' ₃₃	7.90	13 ^m	7.6 ^l	6.2 ^d	16 ⁿ	15.1 ^b	198 10.4~15.4 ⁿ
K'' ₃₃	0.09			0.24 ^b			10j 1.5j
s' ₁₁	3.32	3.65 ^p	3.3 ^o	5.9 ^a	2.5 ^f		
s'' ₁₁	0.10						
s' ₂₂	3.24		4.24 ^p	2.3 ^f			
s'' ₂₂	0.07						
s' ₃₃	3.00			4.72 ^p			
s'' ₃₃	0.07						
s' ₁₂	-1.44			-1.10 ^p			
s' ₁₃	-0.89			-2.09 ^p			
s' ₂₃	-0.86			-1.92 ^p			
s' ₄₄	94.0						
s'' ₄₄	2.50						
s' ₅₅	96.3						
s'' ₅₅	2.33						
s' ₆₆	3.76						

a reference 1

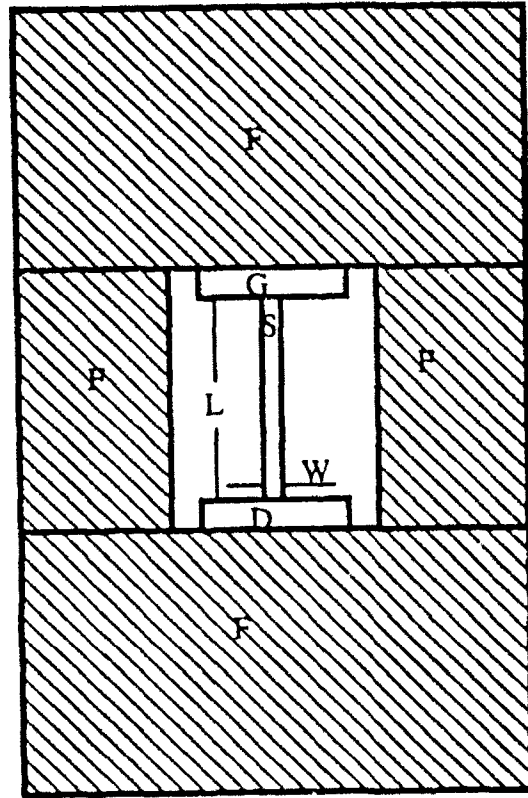
b reference 10

c B. R. Hahn, J. Appl. Phys. 57(4), 1294 (1985).

d K. Koga, H. Ohigashi, J. Appl. Phys. 59(6), 2142 (1986).

e E. L. Nix, I. M. Ward, Ferroelectrics 67, 137 (1986).

- f H. Ohigashi, J. Appl. Phys. **47**, 949 (1976).
- g T. Furukawa, et al., Ferroelectrics, **32**, 61 (1981).
- h ... G. Kepler, Ann. Rev. Phys. Chem. **29**, 497 (1978).
- i Q. C. Xu, et al., IEEE 1987 Ultrasonics Symp., 663(1987).
- j S. Tasaka, S. Miyata, J. Appl. Phys. **57**, 906 (1985).
- k R. Al-Jishi, P. L. Taylor, J. Appl. Phys. **57**, 902 (1985).
- l V. V. Varadan et. al., IEEE 1989 Ultrasonics Symp., 727 (1989)
- m H. Sussner, IEEE 1979 Ultrasonics Symp., 49 (1979).
- n T. Furukawa, N. Seo, Jpn. J. Appl. Phys. **29**, 675 (1990).
- o M. Tamura, K. Ogasawara, N. Ono, S. Hagiwara, J. Appl. Phys. **45**, 3768 (1974).
- p H. Schewe, IEEE 1982 Ultrasonics Symp., Proc. 1 519(1982).



F: Frame

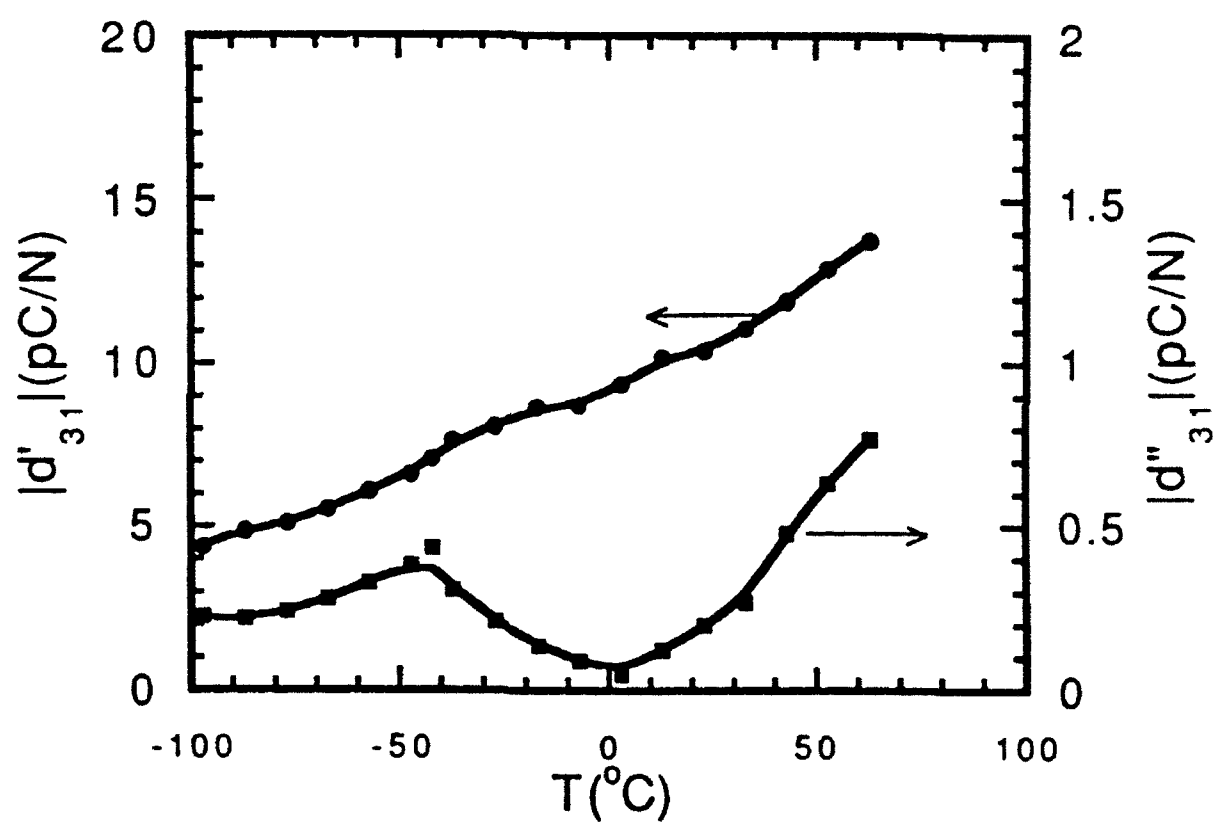
G: Force Gage

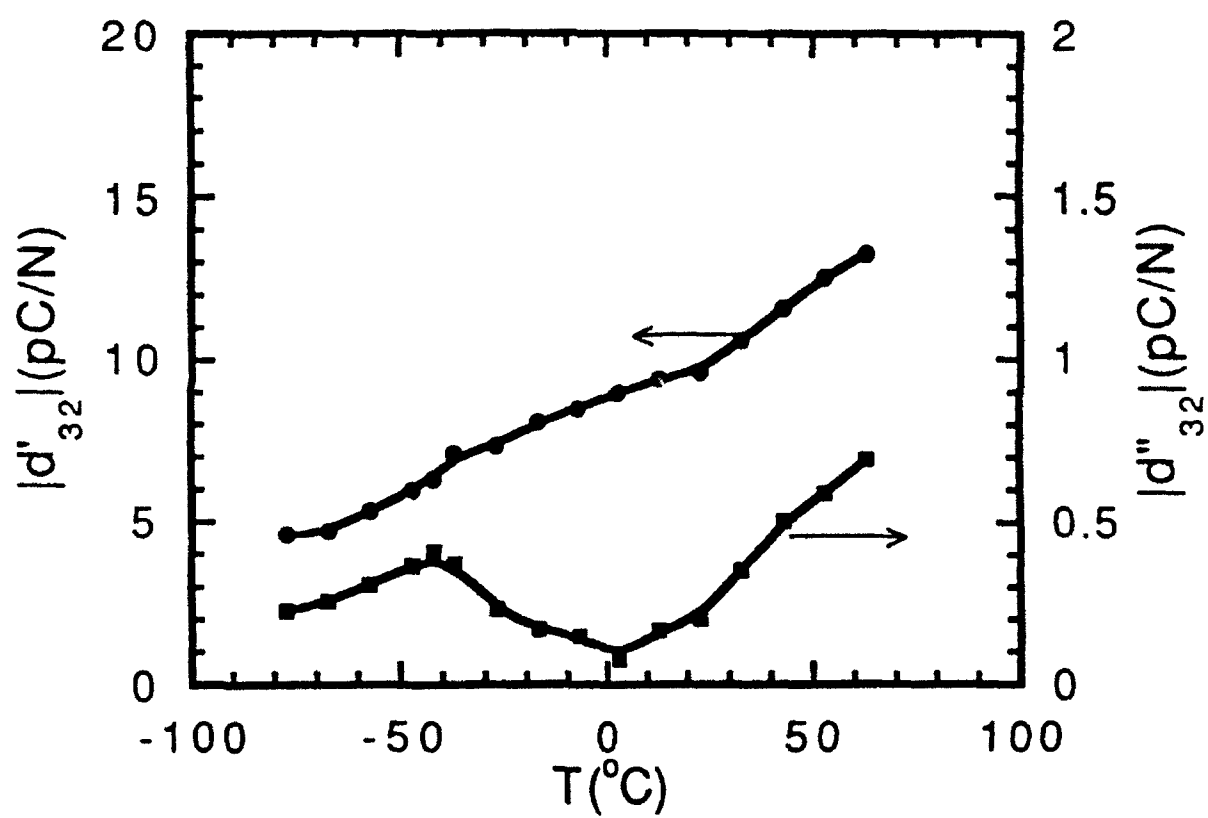
D: Displacement Generator

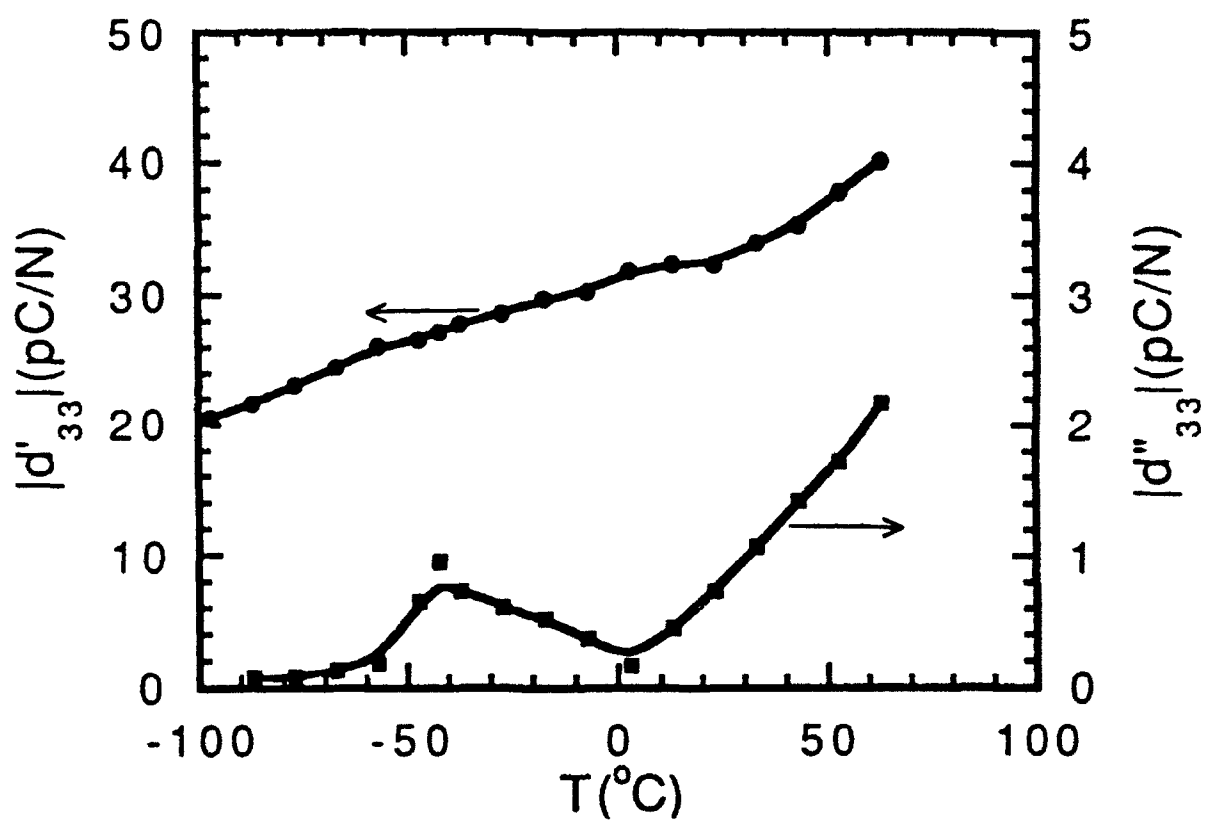
S: Test Sample

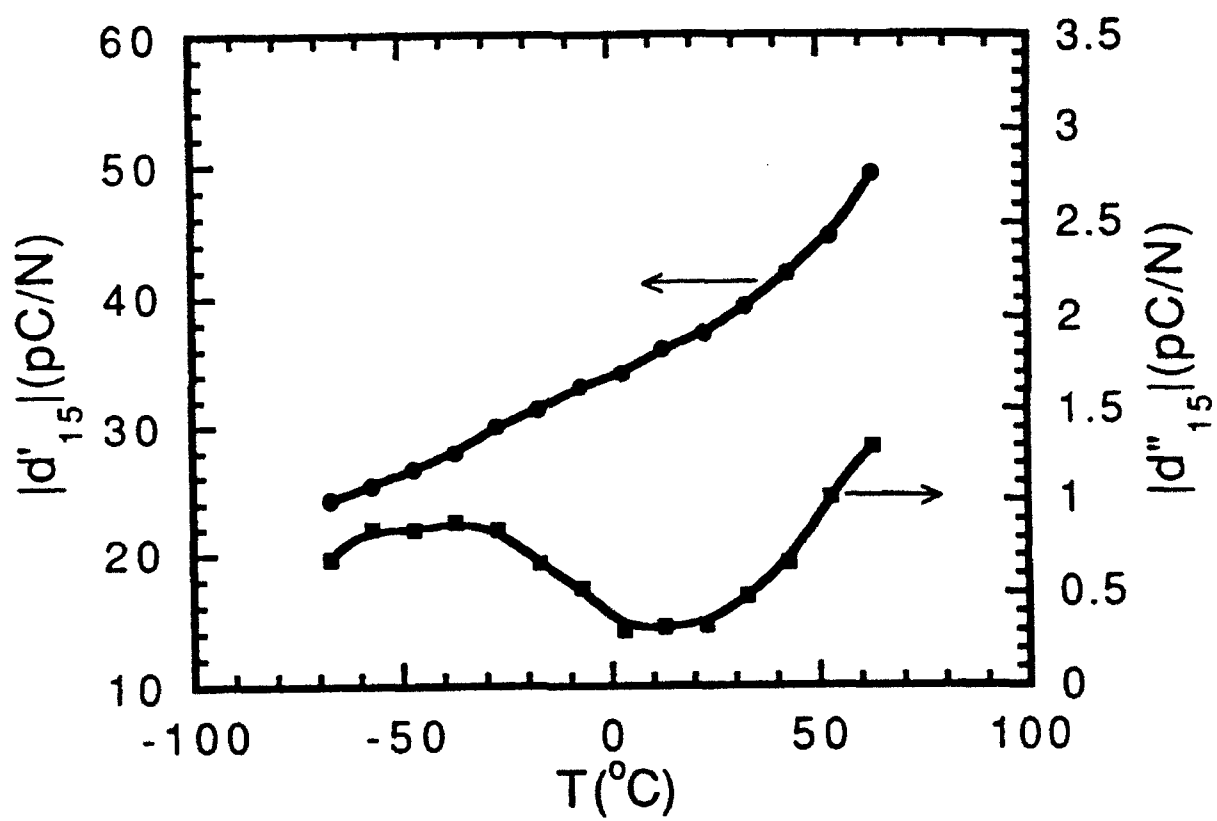
L: Length of the Sample

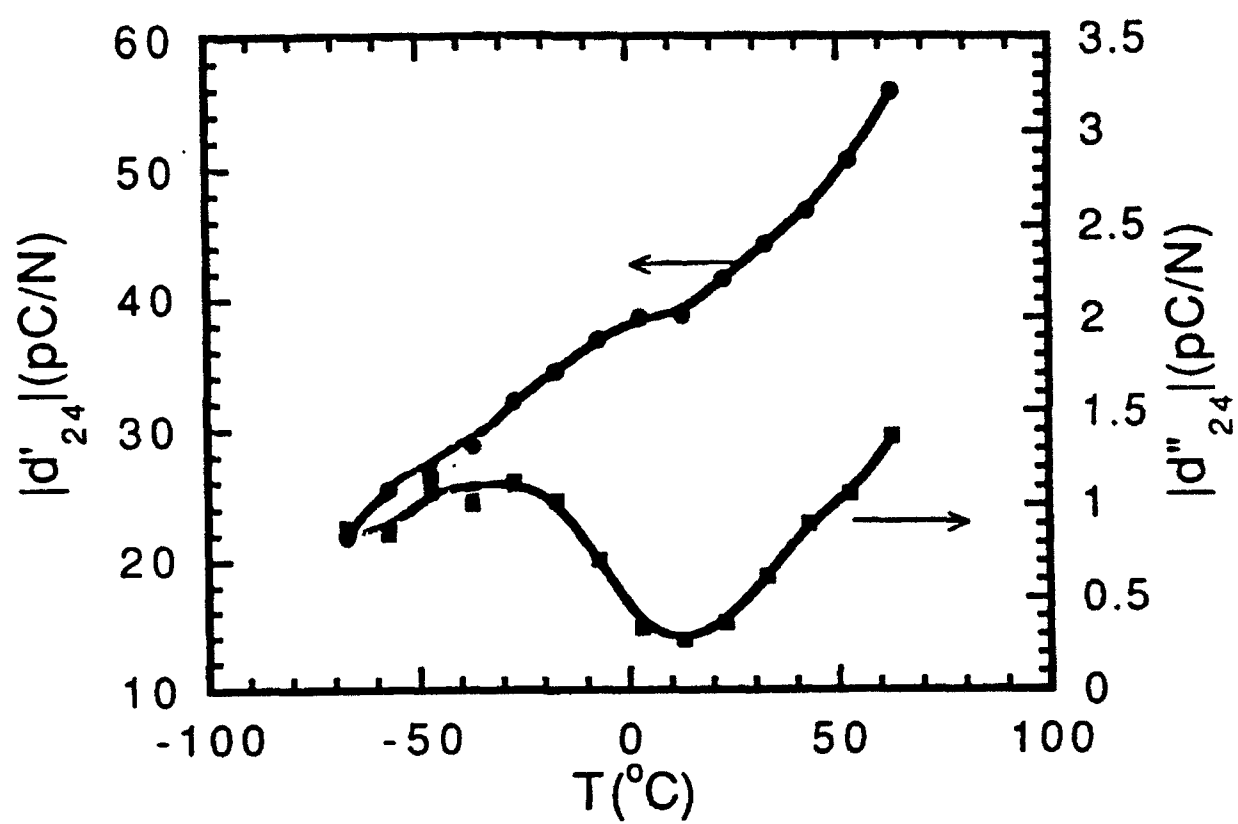
W: Width of the Sample

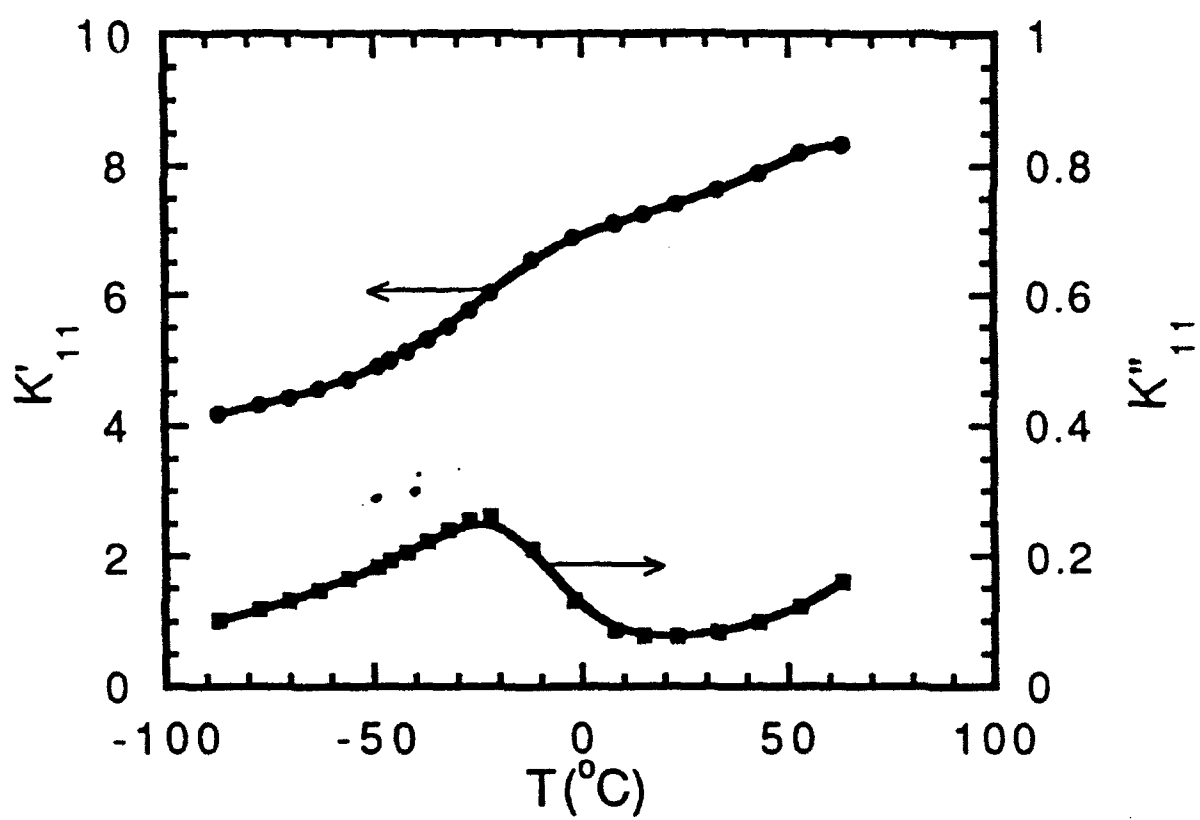


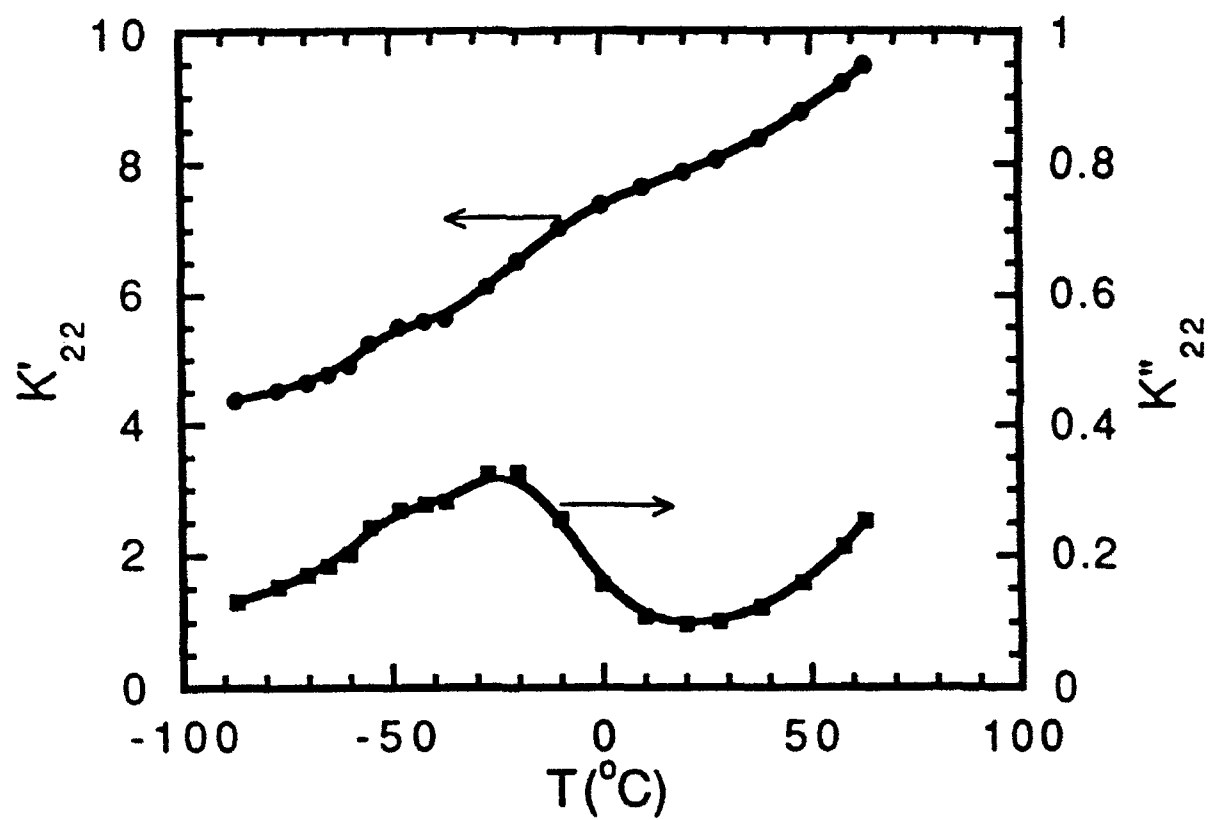


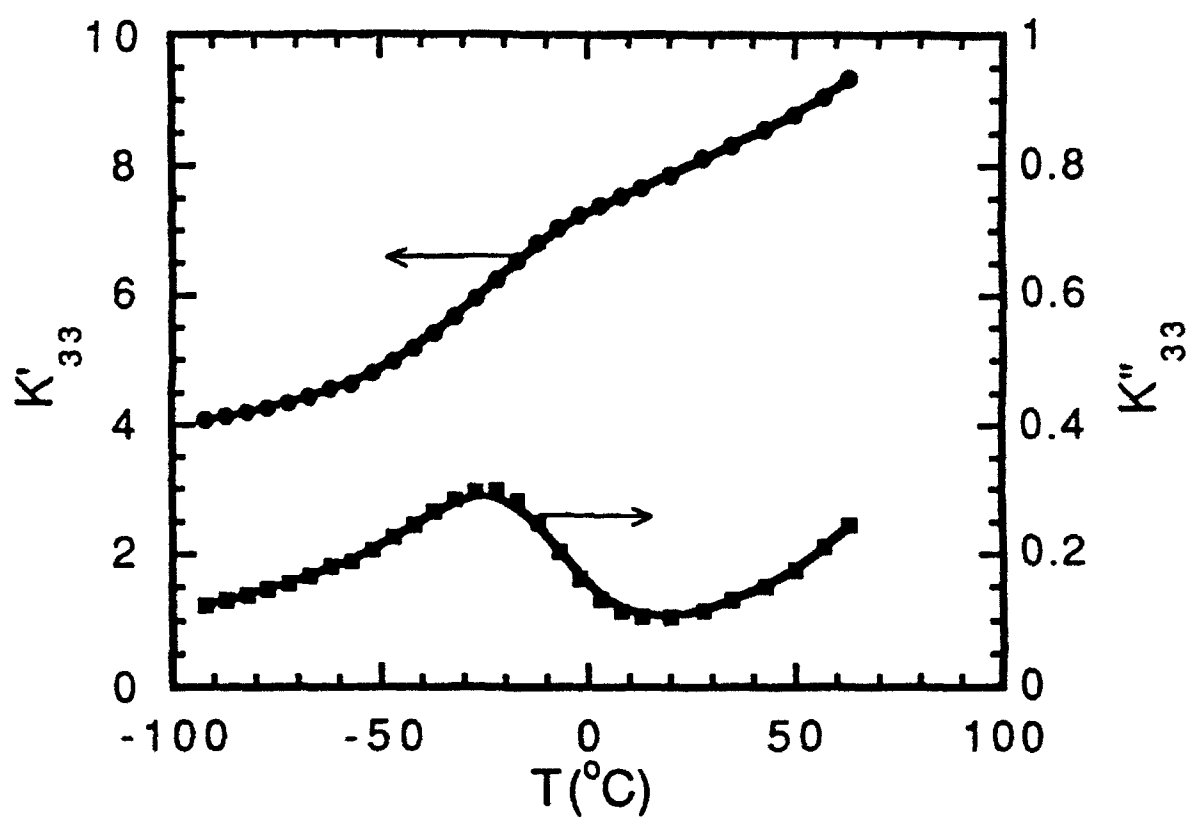


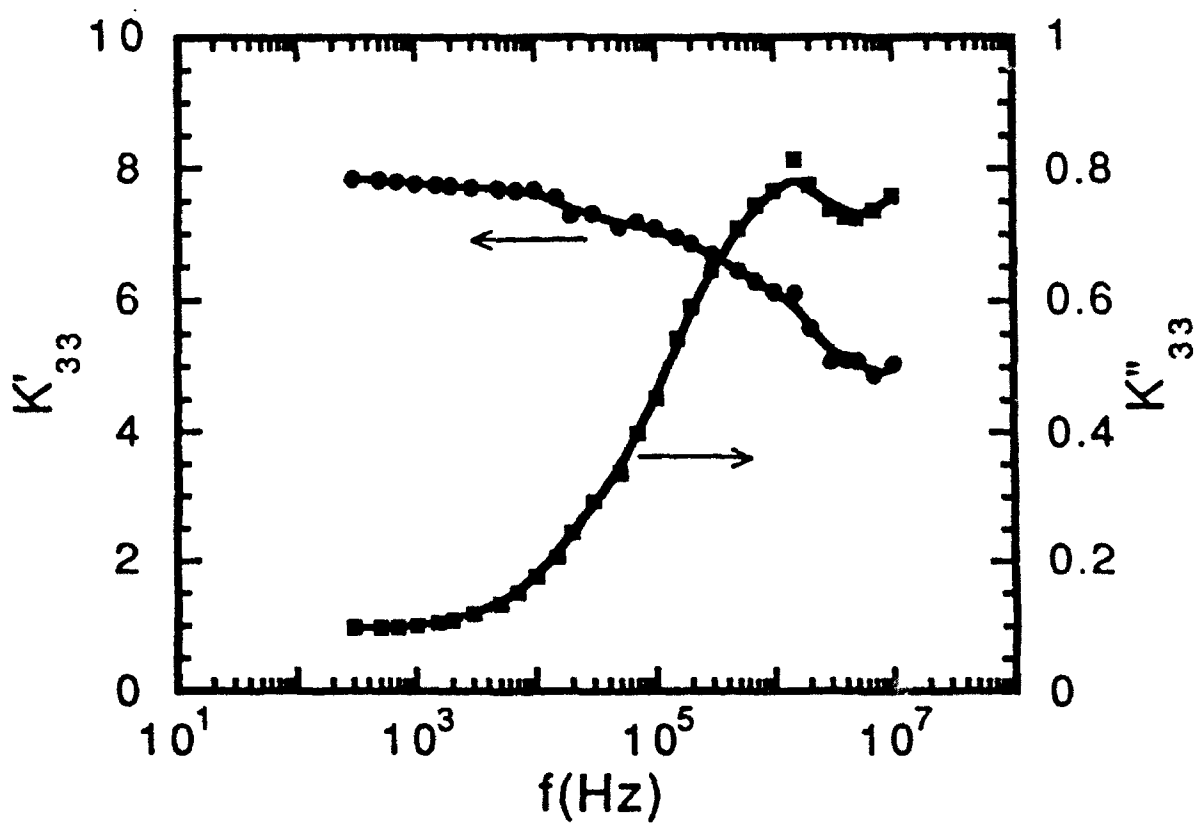












APPENDIX 17

CLAMPING EFFECT ON PIEZOELECTRIC PROPERTIES OF POLY(VINYLIDENE FLUORIDE-TRIFLUOROETHYLENE) COPOLYMER

H. Wang, Q. M. Zhang, and L. E. Cross

Materials Research Laboratory

The Pennsylvania State University

University Park, PA 16802

A. O. Sykes

Acoustical Research and Applications

Vienna, VA 22180

In hydrophone application, PVDF and its copolymers provide high sensitivity because of high piezoelectric voltage coefficient g_h and large figure of merit $d_h g_h$. By using metal plates as electrode, samples can be mechanically clamped in the plane perpendicular to the polar direction, and the transverse piezoelectric responses can be almost eliminated. Compared with non-clamped samples, the hydrostatic coefficient d_h as well as g_h of clamped samples can be increased significantly. In this work, the temperature and pressure dependence of d_h , g_h , and dielectric constant of clamped P(VDF-TrFE) (75/25) copolymer are investigated. The effects of the sample dimensions and other parameters on the clamping are studied. Based on the constitutive equations, the expressions for effective piezoelectric strain coefficient d_{3i}^c ($i=1, 2$, and 3) of a clamped sample are derived, and the hydrostatic strain coefficient d_h derived from the direct and the converse piezoelectric effects are compared. The experimental results are in good agreement with the calculations.

INTRODUCTION

In hydrophone applications, piezoelectric materials are used as a sensor of hydrostatic pressure wave. The sensitivity of a hydrophone is measured by the piezoelectric voltage coefficient $g_h (=g_{31}+g_{32}+g_{33})$, the strain coefficient $d_h (=d_{31}+d_{32}+d_{33})$, and most importantly the figure of merit $d_h g_h$ of the material. The coefficient g_h is defined as the ratio of electric field to the change of hydrostatic pressure, while d_h is the ratio of charges induced on a sample to the change of hydrostatic pressure. The relationship of these two coefficients is as follow:

$$g_h = \frac{d_h}{\epsilon_0 \epsilon_{33}} \quad (1)$$

where ϵ_{33} is the dielectric constant along the polar direction and ϵ_0 is the free space permittivity.

Recently, polyvinylidene fluoride (PVDF) and its copolymers with trifluoroethylene (P(VDF-TrFE)) have attracted increasing attention for hydrostatic applications.¹⁻³ Although the magnitude of the piezoelectric strain coefficient d_{33} of PVDF is almost one order lower than those of conventional piezoelectric ceramics, such as lead zirconia titanate, its d_h coefficient is about the same order. Moreover, because of the significantly lower dielectric constant, the piezoelectric voltage coefficient g_h of PVDF polymer is much higher, thus resulting in a higher hydrostatic figure of merit $d_h g_h$. The relatively low acoustic impedance of PVDF type materials closely matches that of water and, therefore, allows good acoustic coupling from the polymers into water and vice versa. PVDF type materials also possess several other advantages over conventional piezoelectric ceramics such as, mechanical flexibility, low cost, and the ability to be formed into different shapes easily.

Since the cancellation between the longitudinal(d_{33}) and the transverse(d_{31} and d_{32}) piezoelectric responses reduces d_h value, it is conceivable to increase d_h by modifying the stress distribution pattern in a sample so that one of these responses is significantly reduced while the other is kept almost intact. For PVDF and its copolymers, because of their low elastic moduli compared with metals, it is possible to clamp a sample in the plane perpendicular to the poling

direction by using metal plates as electrodes to eliminate the hydrostatic responses from that plan. As shown in Fig. 1, the pressure in the plane direction is borne mostly by the metal electrodes which effectively shield the polymer from the pressure in that direction, resulting in a larger d_h value of the sample.

In this paper, the results of the recent investigations on the clamping effect of metal plates on piezoelectric and dielectric responses of P(VDF-TrFE) (75/25) copolymer are presented. The experimental data are compared with the results derived from the constitutive relations. Several parameters affecting the clamping effect are discussed. The temperature and pressure dependences of these properties were also studied.

EXPERIMENTAL WORK

P(VDF-TrFE) (75/25) poled samples were provided by Atochem North America Inc.. Samples of two different thicknesses were used to study the influence of thickness ratio of polymer to metal plate on the clamping effect. As shown in Fig. 1, the thickness of the metal plates (brass) t^b was fixed at 0.17 mm for all the samples. For copolymer, the two thicknesses (t^p) were 0.5 mm and 2.0 mm, respectively. The 0.5 mm thick copolymers were directly from extrusion and the 2.0 mm thick ones were made by bonding four layers of 0.5 mm thick copolymer together using non-conductive epoxy. The total thickness of samples was, therefore, $2t^b + t^p$. For comparison, copolymer samples without metal plates were also studied. For these samples, silver ink was used for electrodes.

A laser interferometer was employed to measure the longitudinal and the transverse strains x_i^p ($i=1, 2$, and 3 ; the superscript p refers to the strain in copolymer) induced by an electric field. The effective piezoelectric coefficient d_{3i}^c ($i=1, 2$, and 3) of a sample was determined through converse piezoelectric effect, that is, $d_{3i}^c = \frac{x_i^p}{E_3}$, where E_3 is the applied electric field. For a

piezoelectric material with free boundary condition, the hydrostatic piezoelectric coefficient d_h can be determined through its tensile coefficients, i.e., $d_h = d_{33} + d_{31} + d_{31}$. However, for clamped samples, the d_h coefficient determined from the converse piezoelectric effect is not equal to that obtained from the direct effect. Hence, d_h was also measured through the direct piezoelectric effect in which electrical charges induced on electrodes were measured when a sample was subjected to a hydrostatic pressure. The dielectric constants were measured by a capacitance bridge (General Radio). A microminiature refrigerator system (MMR Technology Inc.) was used to provide the temperature regulation for the temperature dependence of the piezoelectric and dielectric constants measurements.

CLAMPING EFFECT ON PIEZOELECTRIC COEFFICIENTS

(1) Tensile coefficients

When an electric field along the 3-direction is applied to a clamped sample, as schematically drawn in Fig. 1, a strain field is induced in the polymer. Clearly, the brass electrodes tend to reduce this strain field, and this effect is equivalent to having external stresses T_1^p and T_2^p applied on the polymer in the plane perpendicular to the poling direction. It is assumed in the following discussion that T_1^p and T_2^p are uniform in the polymer. From the constitutive equations, when subjected to an electric field E_3 , a clamped polymer sample has strains

$$x_1^p = d_{31}E_3 + s_{11}^p T_1^p + s_{12}^p T_2^p \quad (2a)$$

$$x_2^p = d_{31}E_3 + s_{12}^p T_1^p + s_{11}^p T_2^p \quad (2b)$$

$$x_3^p = d_{33}E_3 + s_{13}^p T_1^p + s_{13}^p T_2^p \quad (2c)$$

where s^p is the elastic compliance, d is the piezoelectric strain coefficient of the polymer under stress free condition. The superscript p refers to copolymer. In the above equations it is assumed that $d_{31} = d_{32}$, $s_{11} = s_{22}$, and $s_{13} = s_{23}$ because the piezoelectric and elastic anisotropies in the plane

perpendicular to the poling direction of this material are very small.⁴ The effective piezoelectric strain coefficient d_{3i}^c of a laterally clamped sample can be defined by the following equation:

$$x_i^p = d_{3i}^c E_3 \quad (i=1, 2, 3) \quad (3)$$

For a given electric field, the three effective tensile coefficients are not independent. They are related by the following equation:

$$d_{33}^c = d_{33} + \frac{s_{13}^p (d_{31}^c + d_{32}^c - 2d_{31})}{s_{11}^p + s_{12}^p} \quad (4)$$

To derive d_{3i}^c from Eqs. (2) and (4), it is necessary to find the expressions of T_1^p and T_2^p , which depend upon the properties of the polymer and the brass. In this composite configuration of sample, two conditions can be used. The first one is the static equilibrium condition. From Newton's third law, the total force exerted on the polymer by the brass plates is equal in magnitude and opposite in sign, respectively, to that on the brass plates by the polymer. This can be expressed as follows:

$$T_1^p t^p = -2T_1^b t^b \quad (5a)$$

$$T_2^p t^p = -2T_2^b t^b \quad (5b)$$

where the superscript b refers to the brass electrodes, t^p and t^b are the thicknesses of the polymer and the brass plate, respectively. The lateral strains in the brass plates induced by the stress field in the brass plates are

$$x_1^b = s_{11}^b T_1^b + s_{12}^b T_2^b \quad (6a)$$

$$x_2^b = s_{12}^b T_1^b + s_{11}^b T_2^b \quad (6b)$$

The second condition is the equal strain relation which states that the lateral strains in the two materials should be equal, that is

$$x_1^b = x_1^p \quad (7a)$$

$$x_2^b = x_2^p \quad (7b)$$

It will be shown later that Eqs. (7) are valid only when the electrode dimensions along 1 and 2 directions are much greater than the thickness of the polymer. Solving these equations, we can obtain:

$$d_{31}^c = d_{32}^c = \frac{d_{31}}{1 + \frac{2(s_{11}^p + s_{12}^p)}{\gamma(s_{11}^b + s_{12}^b)}} \quad (8)$$

where $\gamma = t^p/t^b$ is the thickness ratio. Using Eq. (4), the expression for d_{33}^c can be found. From Eq. (8), it is clear that the reduction of d_{31}^c and d_{32}^c can be adjusted through two parameters: the thickness ratio γ and the elastic compliances ratio of the polymer to the brass plate. To effectively eliminate d_{31}^c and d_{32}^c , a smaller γ and metal plates with high elastic moduli are preferred. Also from the Eq. (8), clamping is more effective for polymers with smaller Poisson's ratio.

(2) Hydrostatic strain coefficient d_h

Similar to normal piezoelectric materials, the effective hydrostatic piezoelectric strain coefficient d_h^c of a clamped sample is

$$d_h^c = (d_{33}^c + d_{31}^c + d_{32}^c) \quad (9)$$

Using the results from the preceding section, the hydrostatic strain coefficient under clamping condition is obtained as following:

$$d_h^c = d_{33} + d_{31} \frac{2\gamma(s_{11}^b + s_{12}^b) - 4s_{13}^p}{\gamma(s_{11}^b + s_{12}^b) + 2(s_{11}^p + s_{12}^p)} \quad (10)$$

For a sample under clamping condition, the effective tensile coefficients d_{3i}^c ($i=1, 2$, and 3) derived above through the converse effect are not equal to those derived through the direct effect. So the effective hydrostatic strain coefficient determined by Eq. (10) is not the same as that determined by the direct effect. For the direct effect, d_h can be measured directly without measuring individual tensile coefficients. For comparison, the expression for effective hydrostatic piezoelectric coefficient of a clamped sample derived through the direct effect is given below:

$$d_h^c = d_{33} + d_{31} \frac{2(\gamma+2)(s_{11}^b + s_{12}^b) - 4(s_{13}^p - s_{12}^b)}{\gamma(s_{11}^b + s_{12}^b) + 2(s_{11}^p + s_{12}^p)} \quad (11)$$

The derivation of Eq. (11) is similar to that of Eq. (10). Apparently, the measured results from the two effects, in general, are not equal when a sample is clamped. The difference of d_h value between the two effects is

$$d_{31} \frac{4s_{11}^b + 8s_{12}^b}{\gamma(s_{11}^b + s_{12}^b) + 2(s_{11}^p + s_{12}^p)} \quad (12)$$

Obviously, the more effective the clamping, the bigger the difference. For free samples, there is no such difference. For the samples investigated, this difference is about $0.2d_{31}=2.1pC/N$, which is not very significant. The parameters used in this calculation are listed in table I.

RESULTS AND DISCUSSIONS

(1) Piezoelectric strain coefficients

The transverse piezoelectric responses of a clamped sample depend on the lateral dimensions of the sample. Shown in Fig. 2 (a) and (b) are the dimension dependence of d_{31} and d_{32} for two different thickness ratios of $\gamma=3$ and $\gamma=12$, respectively. In these measurements, d_{31}^c (or d_{32}^c) was measured as a function of the sample dimension along 1 (or 2) direction while the other lateral dimension L_2 (or L_1) was kept constant. As the lateral dimensions increase, d_{31} and d_{32} decrease rapidly. This is the result of incomplete clamping of the polymer by the brass electrodes. When the thickness of the polymer sample t^p , compared with the lateral dimension L , is not small enough, the strains induced by an electric field will not be uniform. This is shown in Fig. 3 (a). The clamping on the polymer by the brass plates is complete only when $t^p/L \rightarrow 0$ and the results derived in the previous sections are valid only under this condition. On the other hand,

for large values of t^p/L , the clamping is not very effective, and d_{3i}^c is still very close to d_{3i} ($i=1, 2$, and 3).

Experimentally, the d_{31}^c and d_{32}^c values of the complete clamping can be obtained by extrapolating the experimental curves of d_{31}^c and d_{32}^c versus the reciprocal of the sample length ($1/L$) to the value at $1/L=0$. These results are listed in Table II along with those calculated from Eq. (8). When $\gamma=3$, the experimental and calculated results are in good agreement. While for $\gamma=12$, the agreement is less satisfactory. It is believed that this difference arises from the fact that for $\gamma=12$ the data points are far from complete clamping and the t^p/L is four times bigger than that for $\gamma=3$. So the clamping is less effective. From Table II and Eq. (8), it is clear that clamping is more effective for thinner polymer samples (smaller γ value).

Longitudinal coefficient d_{33} of a clamped sample also depends on the lateral dimensions of the sample. This can be seen from Eq. (4). When a sample is not fully clamped, d_{31}^c and d_{32}^c change with the dimensions and are not equal to each other. The d_{33}^c values for a completely clamped sample from the experiment and the calculation are also listed in the Table II. The agreement between the experimental result and the theoretical calculation is satisfactory.

Temperature dependence of effective tensile piezoelectric strain coefficients d_{3i}^c ($i=1, 2$, and 3) of clamped sample ($\gamma=3.0$, and $L=9.0$ mm) was measured at a frequency of 500 Hz through the converse piezoelectric effect. From these results, the coefficient d_h^c as a function of temperature is obtained and shown in Fig. 4. For comparison, the temperature behavior of d_h coefficient of a non-clamped sample measured at 500 Hz through the converse piezoelectric effect is also presented in Fig. 4. Examination of the figure indicates that the clamping changes not only the magnitudes of the tensile piezoelectric strain coefficients, but also their temperature behaviors. For the non-clamped copolymer, d_h does not change with temperature noticeably even though all three tensile piezoelectric strain coefficients are significantly temperature dependent. In the temperature interval studied, the d_h for the non-clamped copolymer is in the range of 12-14 pC/N.

For a clamped sample, the d_h value at high temperature ($\sim 60^\circ\text{C}$) is about twice of that of a non-clamped sample. As the temperature is reduced, the difference in d_h between the clamped and non-clamped samples becomes smaller. At very low temperature, they become the same. This kind of temperature behavior can be explained by Eqs. (8) and (10). The clamping effect becomes less effective as the elastic compliances of the copolymer decrease while the elastic compliances of the brass plates are practically unchanged in this temperature region. It is well known that for a semicrystalline polymer, the elastic modulus changes greatly around the glass transition temperature T_g (about -30°C for this copolymer).⁵ At the temperature well below T_g , a polymer becomes stiffer and the clamping is less effective. So the d_h value of the sample with the brass plates approaches that of the unclamped sample. Although d_h coefficient is more temperature dependent for clamped samples, the curve is quite flat around the 0°C , which is the working temperature of most underwater sensors. In this temperature region, the clamping is very significant and d_h value of a clamped sample is much higher than that of the non-clamped sample.

Shown in Fig. 5 are the pressure dependence of d_h measured at the frequency of 50 Hz and room temperature for both clamped and non-clamped copolymers through the direct piezoelectric effect. It can be seen that for both clamped and non-clamped samples, d_h decreases slightly with pressure. For both kinds of samples, when the pressure was lowered back to one atmosphere, the samples returned to their initial level of activity with no noticeable irreversible degradation.

It is noticed that for clamped samples, the difference between d_h values measured through the converse and the direct piezoelectric effects at room temperature is about 3.3pC/N which is greater than predicted value (2.1pC/N) by Eq. (12). It is believed that there are two main sources causing this error: (1) the calculated difference is for a sample with complete clamping, while the measured difference is for a sample with incomplete clamping; (2) the systematic error in the measurement between the two set-ups.

(2) Dielectric constants

The temperature dependence of dielectric constant ϵ_{33} for both non-clamped and clamped samples are shown in Fig. 6. As seen from the curves, there is no noticeable difference between them. For a piezoelectric material, the difference between the dielectric constants under stress free and strain free conditions arises from its piezoelectricity. From the constitutive equations, this difference is

$$\epsilon_0 (\epsilon_{33}^T - \epsilon_{33}^S) = d_{31}e_{31} + d_{32}e_{32} + d_{33}e_{33} \quad (12)$$

where the superscripts T and S refer to stress free and strain free conditions, respectively, and e is the piezoelectric coefficient of the material. For PZT ceramics, the difference can be more than 100% due to their high electromechanical coupling coefficients. However, for piezoelectric polymers, this difference is very small because of their relatively low piezoelectricity compared with PZT. Calculated from the above equation, the difference is only about 5% for P(VDF-TrFE) (75/25). The dielectric constant ϵ_{33} of a clamped sample measured here is not exactly strain free dielectric constant ϵ_{33}^S because the sample is only partially clamped in the 3-direction. Therefore, it is not surprised that the dielectric constant of a clamped sample is experimentally almost the same as that of a non-clamped sample.

(3) Hydrostatic Voltage Coefficient and Figure of Merit

The hydrostatic voltage coefficient g_h can be obtained from the hydrostatic strain coefficient d_h and the dielectric constant ϵ_{33} through Eq. (1). In Fig. 7, g_h as a function of temperature for both clamped and non-clamped samples is presented, where d_h 's are taken from Fig. 4. The temperature behavior of g_h for a clamped sample is much different from that of a non-clamped sample due to the different d_h and the almost-same dielectric constants. Even for non-clamped samples, the g_h value is about 180×10^{-3} Vm/N around temperature of 0°C , which is two orders of magnitude higher than those of PZT ceramics.⁶ By mechanical clamping, both the magnitude and

the temperature dependence of g_h coefficient of the PVDF copolymer are further improved in a wide range of temperature. The pressure dependence of g_h is shown in Fig.8.

In Fig. 9, the hydrostatic figure of merit d_{hg} are shown for clamped and non-clamped samples as a function of temperature. Clearly, in operation temperature range of hydrostatic applications ($T > 0^\circ\text{C}$), the clamping effect provides an effective means to significantly improve the hydrostatic figure of merit of the copolymer.

In summary, Table III presents the room temperature hydrostatic figure of merit for both non-clamped and clamped P(VDF-TrFE) copolymers along with their dielectric, piezoelectric coefficients. For the comparison, the properties for commonly used PZT ceramics and 0-3 piezoceramic-polymer composite are also listed. It is obvious that the clamped PVDF copolymer shows superior hydrostatic figure of merit.

CONCLUSIONS

Polarized PVDF and its copolymer are versatile materials which have shown to have excellent piezoelectric properties. It is anticipated the application range of the materials will be further broadened with continued research aimed at further improvement in basic material-performance parameters. By mechanical clamping in the plane perpendicular to the poling direction, nearly all the effective piezoelectric responses in that plane can be eliminated. As a result, the effective hydrostatic response can be improved significantly. It is also shown that the dimension and the elastic properties of both metal plates and copolymer can have great influence on the effectiveness of this clamping effect. To improve the clamping, a smaller thickness ratio of polymer to metal plate, a smaller aspect ratio (t_p/L), and a large difference in the elastic properties between polymer and metal plate are preferred.

ACKNOWLEDGMENT

This work was supported by the Naval Undersea Warfare center's Small Business Innovation Research (SBIR) program under contract N66604-90-C1558 (Low Cost Acoustic Sensor Technology), and the Office of Naval Research.

REFERENCES

1. H. R. Gallantree, IEEE proceedings, **130**, 219 (1983).
2. J. M. Powers, Electronics and Aerospace Systems Conf., Oct. 517 (1979).
3. T. T. Wang, J. M. Herbert, A. M. Glass. Glasgow, Blackie, The Applications of Ferreelectric polymers, Chapman and Hall, 1988.
4. H. Wang, Q. M. Zhang, and L. E. Cross, submitted to JAP.
5. P. Flory, Principles of Polymer Chemistry, Ithaca, Cornell University Press, 1953.
6. R. Y. Ting, Jpn. Appl. Suppl., **24**, 982 (1985).
7. R. C. Weast, CRC Handbook of Chemistry and Physics, CRC Press, Inc. 1980-1981.
8. K. A. Hanner, A. Safari, R. E. Newnham, J. Runt, Ferroelectrics, **100**, 255 (1989).

FIGURE CAPTIONS

Fig. 1. Schematic drawing of a clamped sample by metal plates.

Fig. 2. The effective transverse coefficients as a function of the lateral dimension of a clamped sample.

Fig. 3. Deformation of a clamped sample under an Electric field. (a). Nonuniform deformation; (b). uniform deformation.

Fig. 4. Hydrostatic d_h coefficient as a function of temperature for non-clamped and clamped samples.

Fig. 5. Pressure dependence of d_h coefficient for non-clamped and clamped samples.

Fig. 6. Dielectric constant as a function of temperature for non-clamped and clamped samples.

Fig. 7. Hydrostatic g_h coefficient as a function of temperature for non-clamped and clamped samples.

Fig. Pressure dependence of g_h coefficient for non-clamped and clamped samples.

Fig. 9. The figure of merit $d_h g_h$ as a function of temperature for non-clamped and clamped samples.

Table I Some elastic, piezoelectric, and dielectric properties of P(VDF-TrFE)(75/25) and the elastic compliances of the brass electrode.

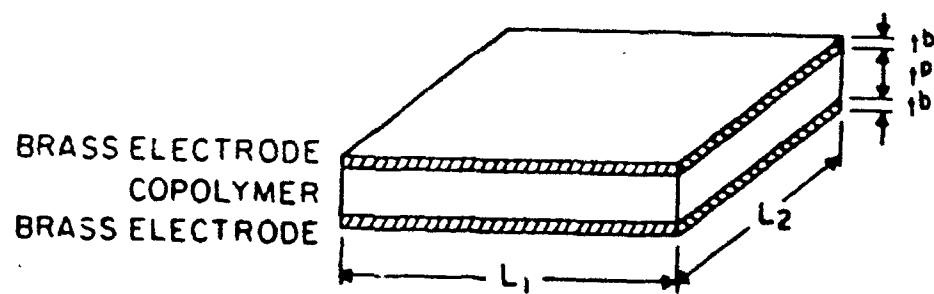
Material	s_{11} ($\times 10^{-10} \text{ m}^2/\text{N}$)	s_{12} ($\times 10^{-10} \text{ m}^2/\text{N}$)	d_{31} (pC/N)	d_{33} (pC/N)	ϵ_{33}	Reference
PVDF-TrFE (75/25)	3.32	-1.44	10.7	33.5	7.90	4
Yellow Brass	0.097	-0.032				7

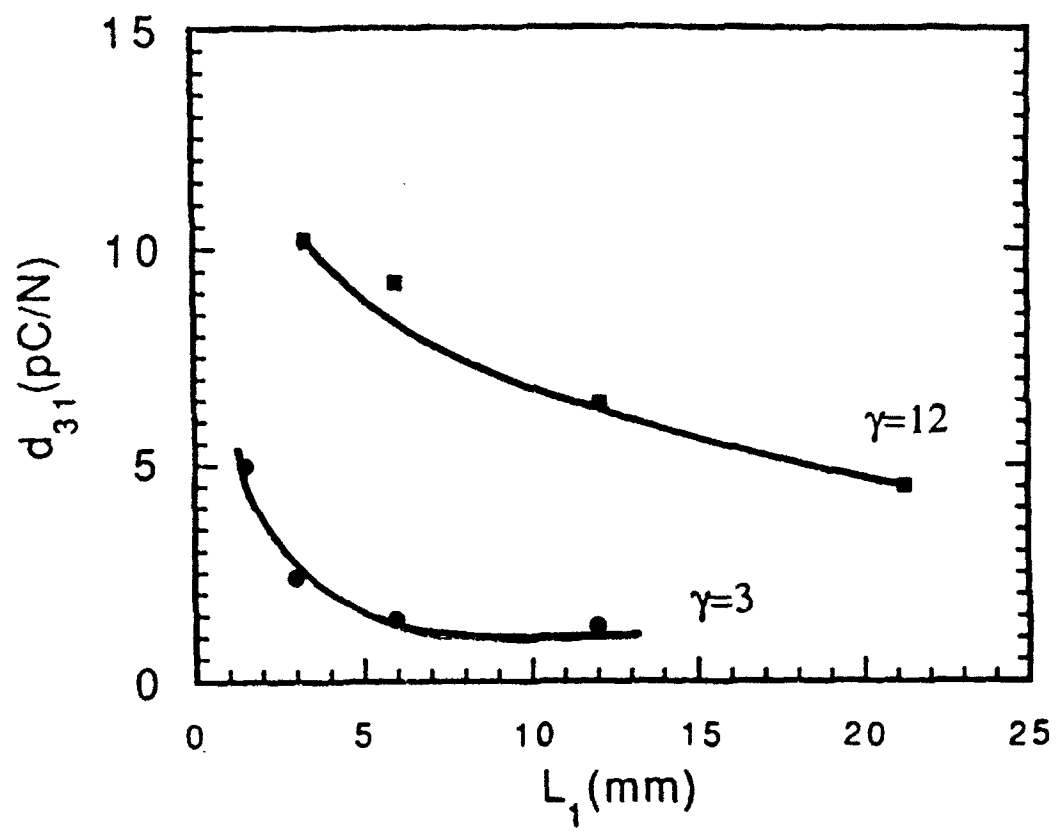
Table II The piezoelectric strain coefficients under complete clamping conditions.

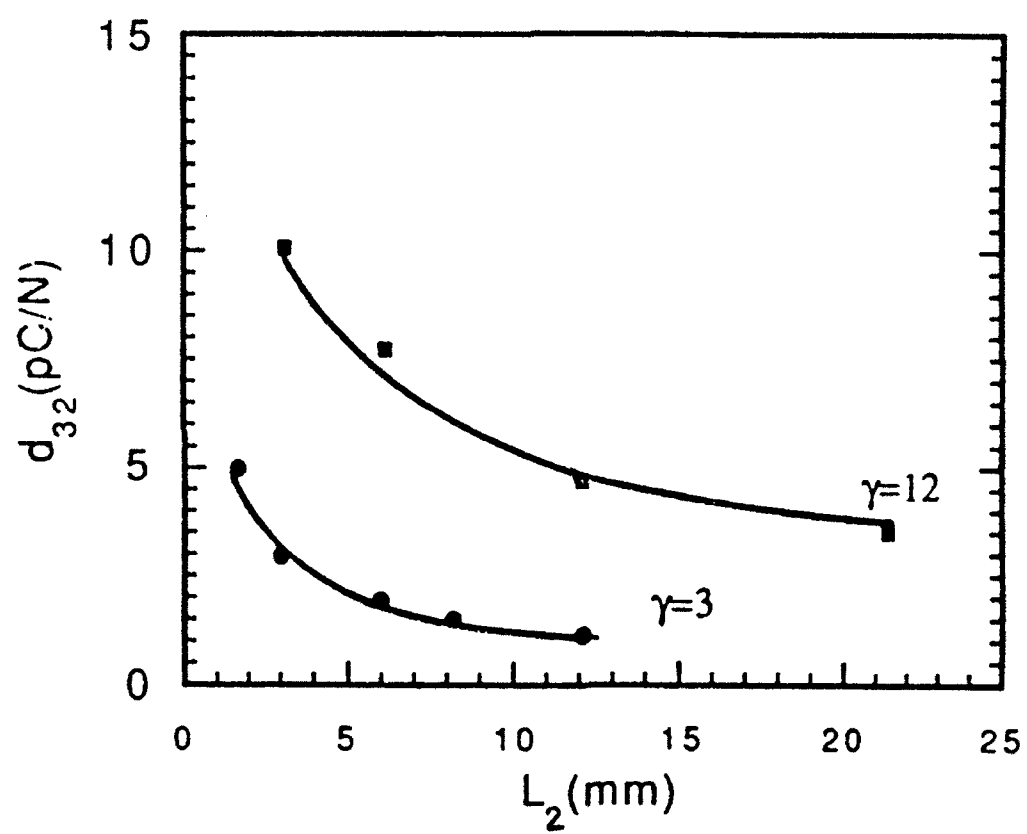
γ	d_{31}^c (pC/N) calculated	d_{31}^c (pC/N) measured	d_{33}^c (pC/N) calculated	d_{33}^c (pC/N) measured
3.0	0.53	0.53	-24.75	-21
12.1	1.85	2.65	-26.00	

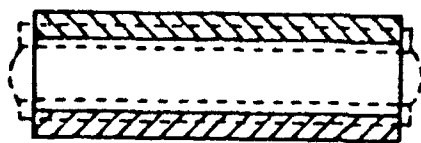
Table III The hydrostatic piezoelectric properties of the P(VDF-TrFE) copolymer and some other materials

Material	ϵ_{33}	d_h (pC/N)	g_h ($\times 10^{-3}$ Vm/N)	$d_h g_h$ (m^2/N)	Reference
P(VDF-TrFE) (75/25) non-clamped	7.9	12.5	170	2125	this work
P(VDF-TrFE) (75/25) clamped	7.4	19.5	275	5363	this work
PZT 4	1300	43	4	172	6
PZT 5	1690	21	2	42	6
0-3 composite of acrylic copolymer/PbTiO ₃	54	32	67	2140	8

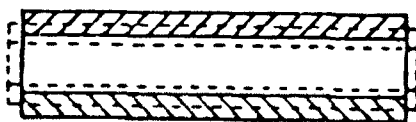
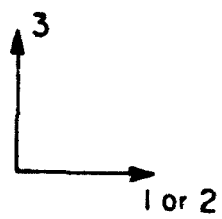




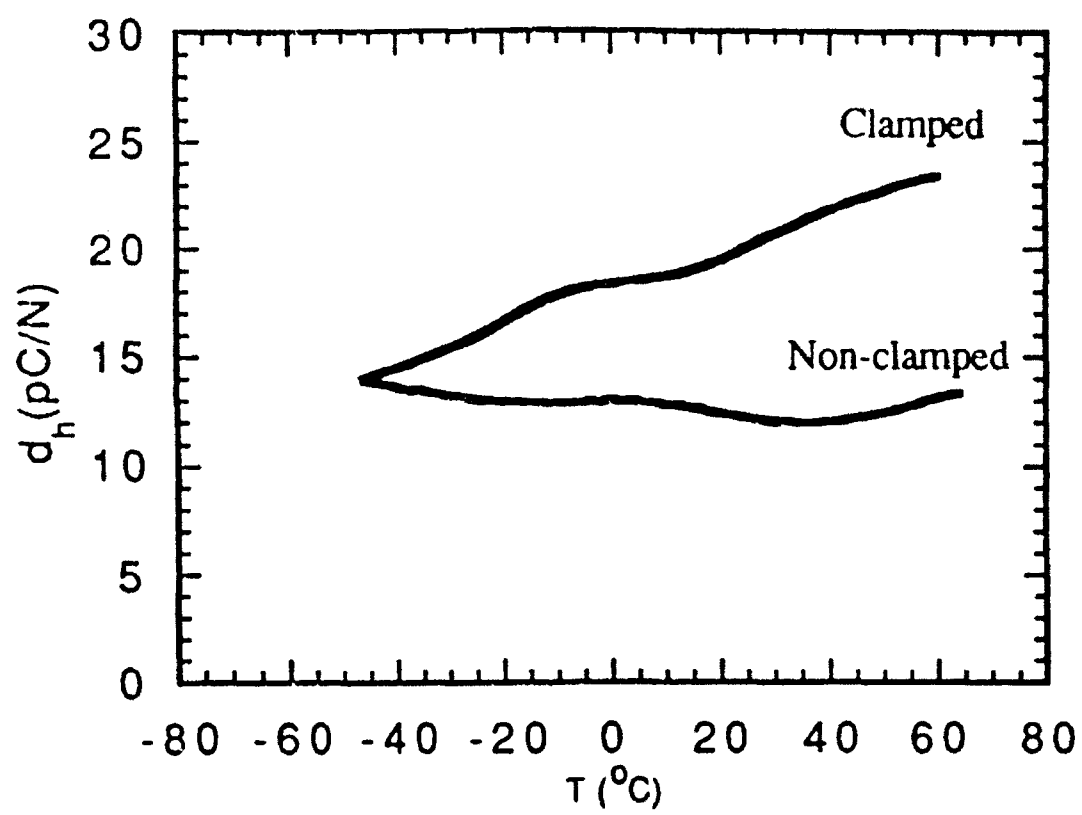


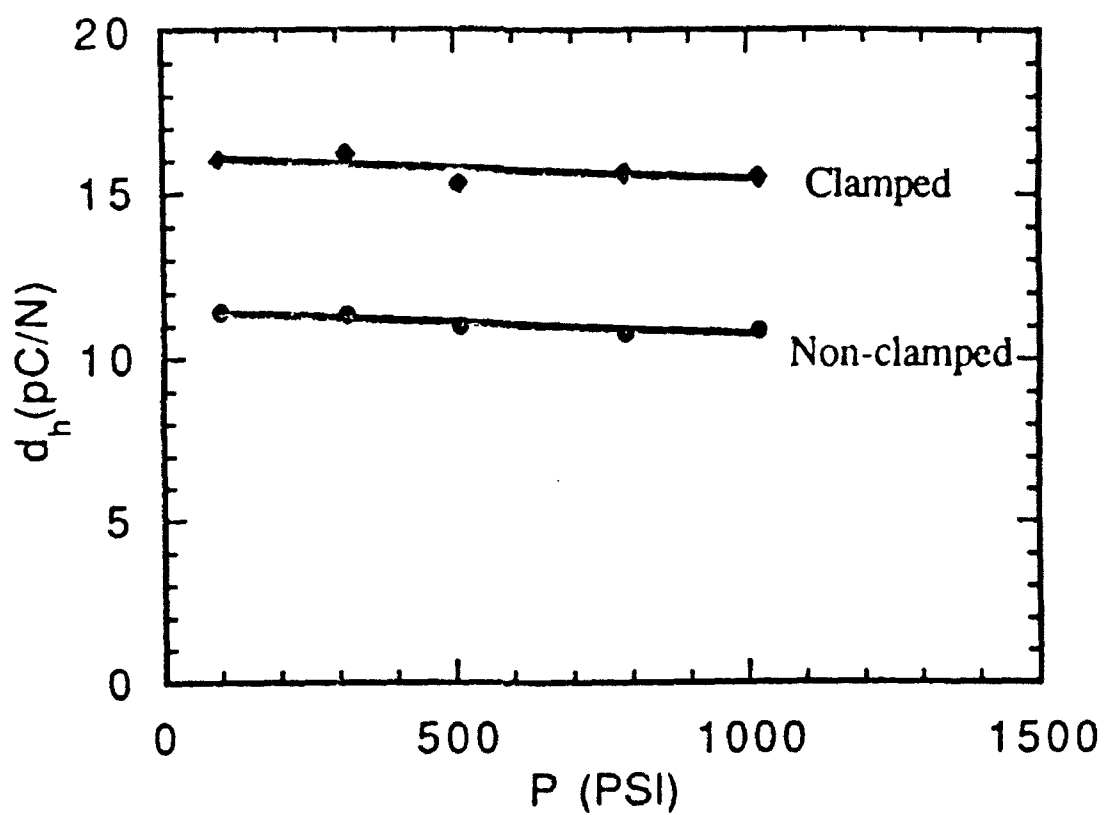


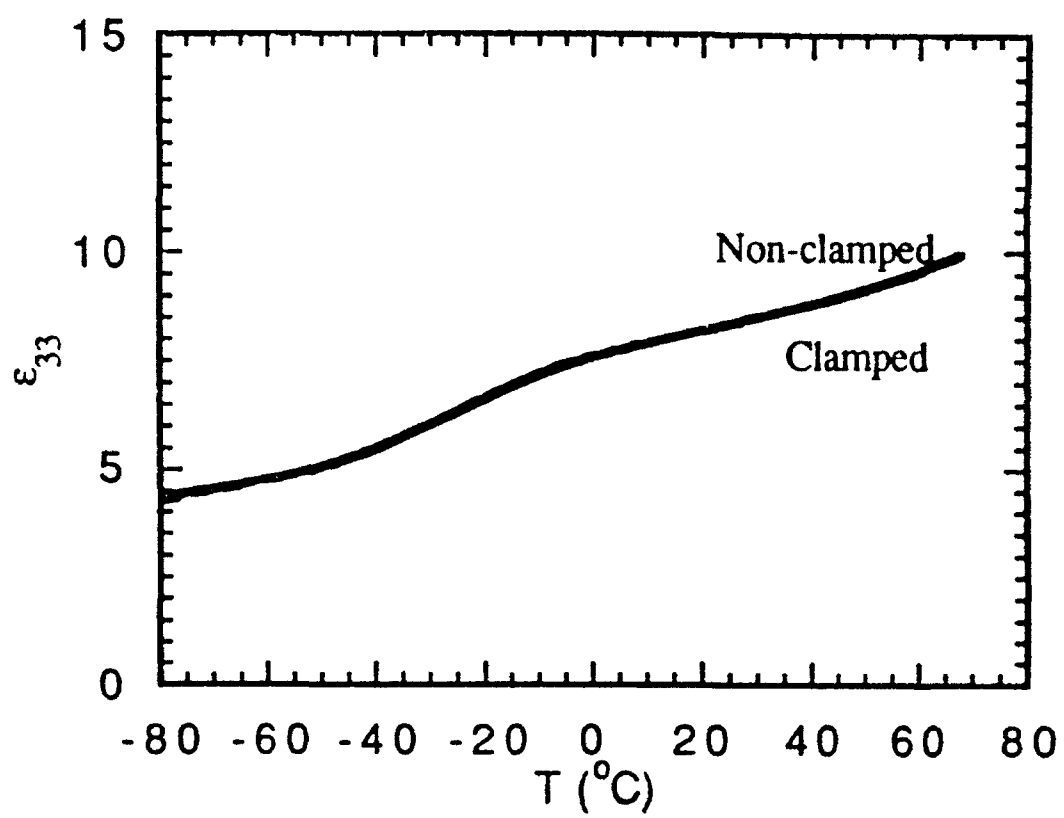
(a)

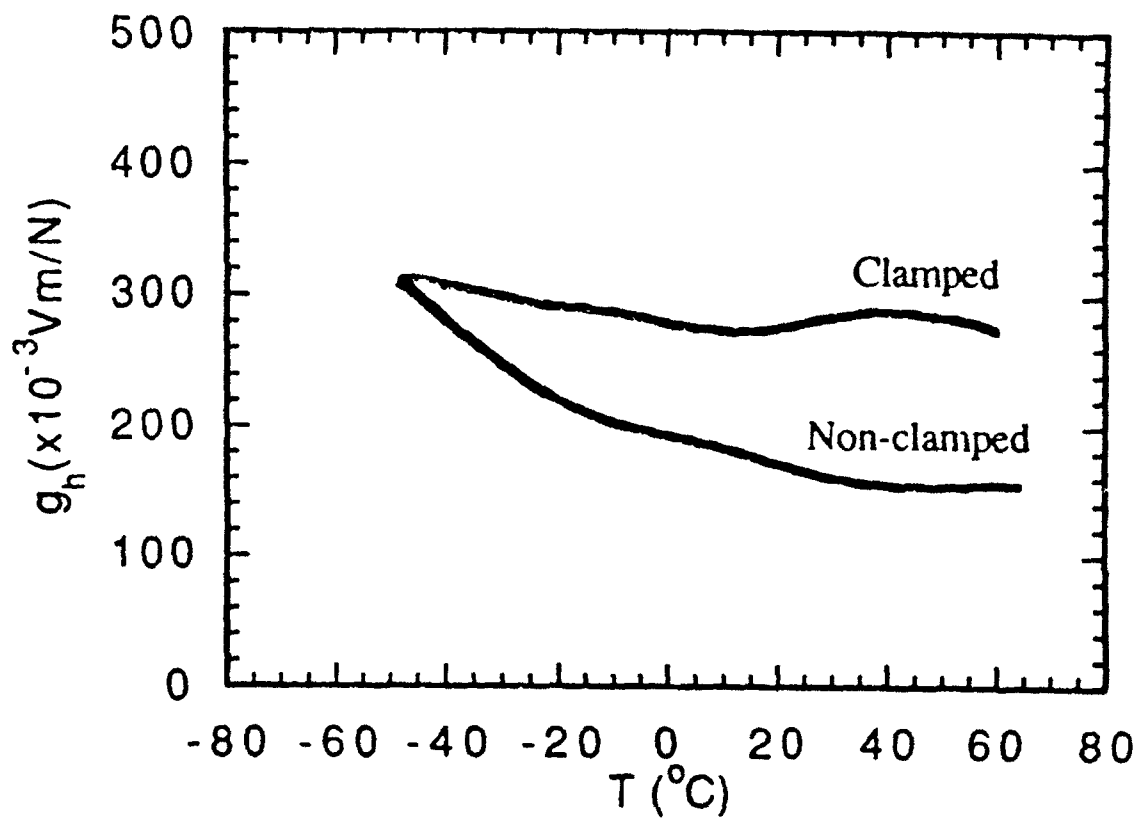


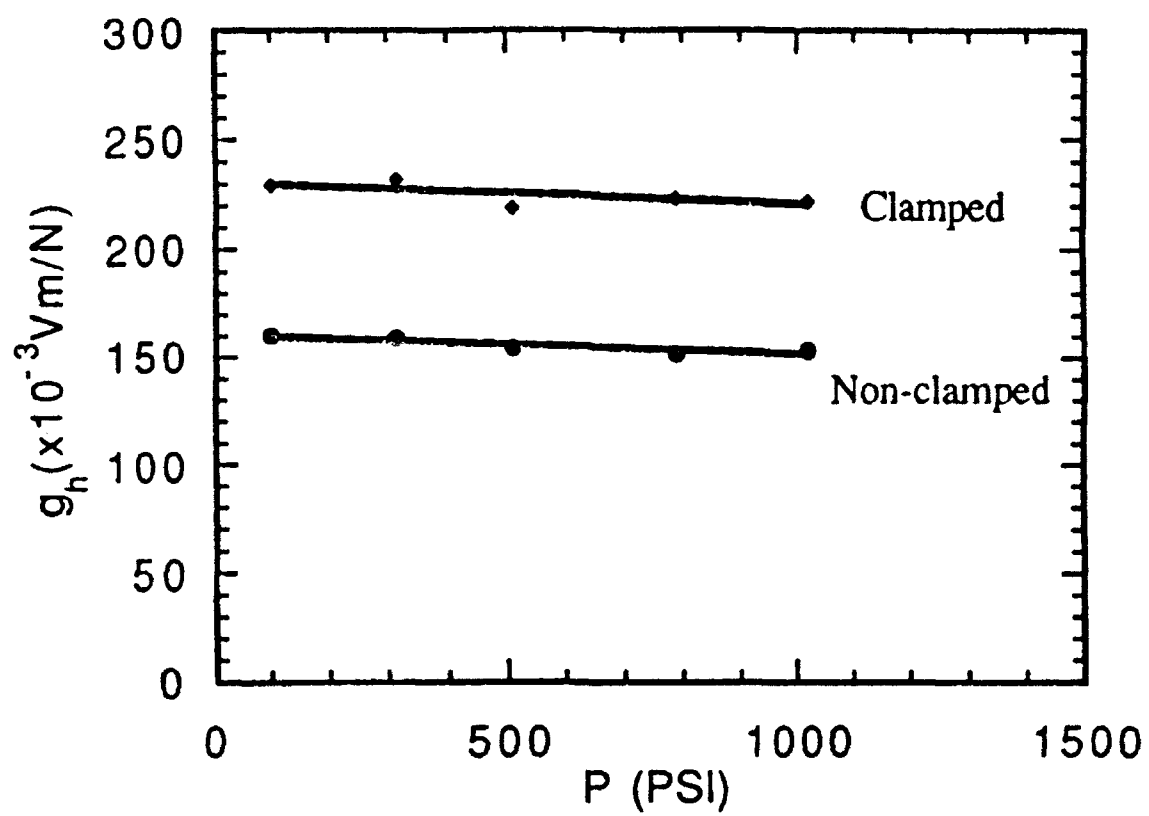
(b)

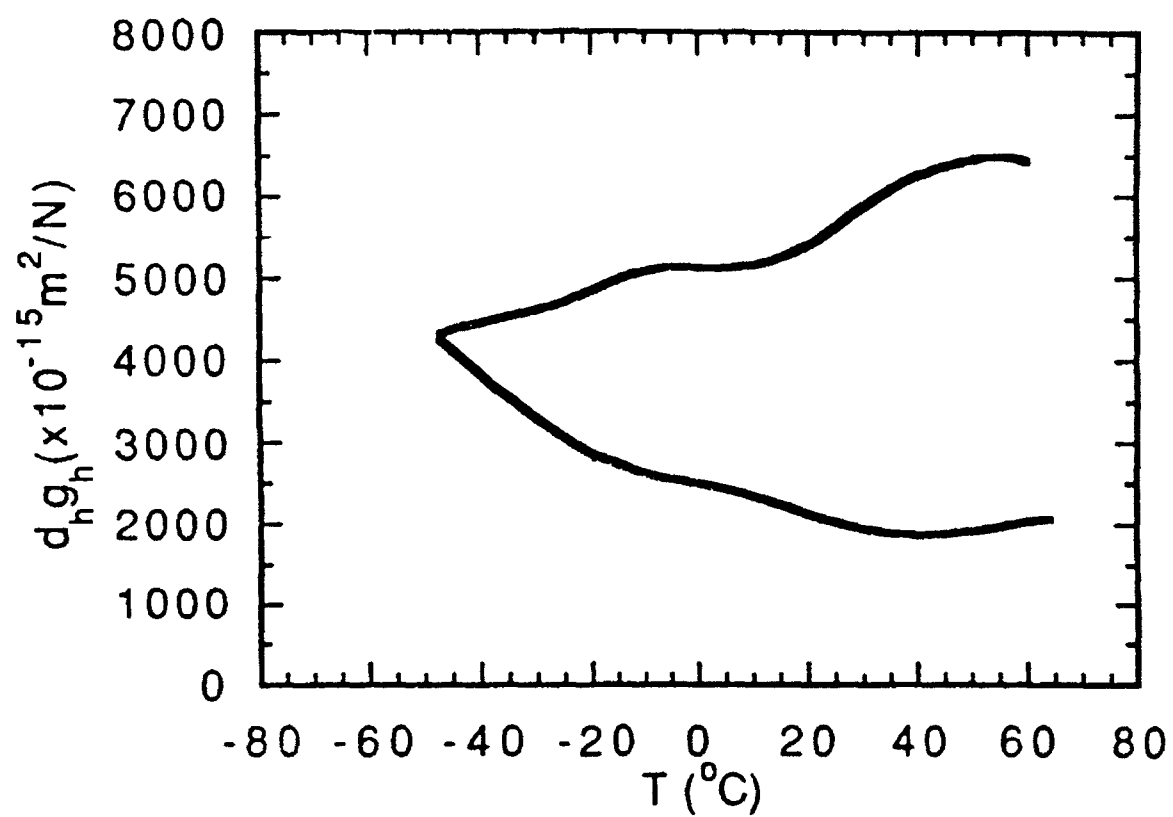












COMPOSITE SENSORS

APPENDIX 18

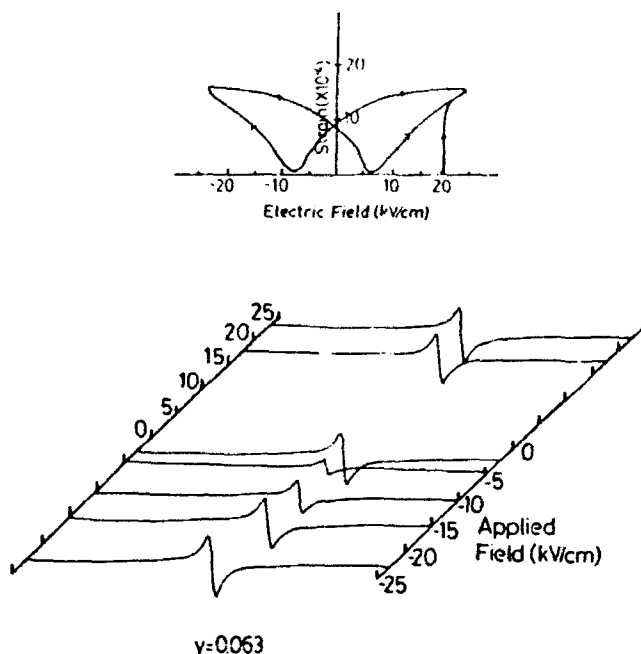


Fig. 2. Field-strain relation and piezoelectric resonance admittance curve of a planar mode with applied pulse field measured in $y = 0.063$.

parison, the PNZST materials ($y = 0.063, 0.064$) with the shape memory effect are confirmed to be very suitable for controlling the piezoelectricity with low energy consumption.

In the case of the specimen with $y = 0.066$ (region III), the resonance and antiresonance peaks will not disappear completely, even after applying the large reverse bias field pulse. This is probably because the specimen sustains the field-induced ferroelectric phase even after the reverse bias is applied, as shown in the upper part of Fig. 3. In the case of $y = 0.090$ (Fig. 4), the field-induced piezoelectricity cannot be removed completely by the reverse bias. It is notable that the electric pulse field required to cause piezoelectricity is

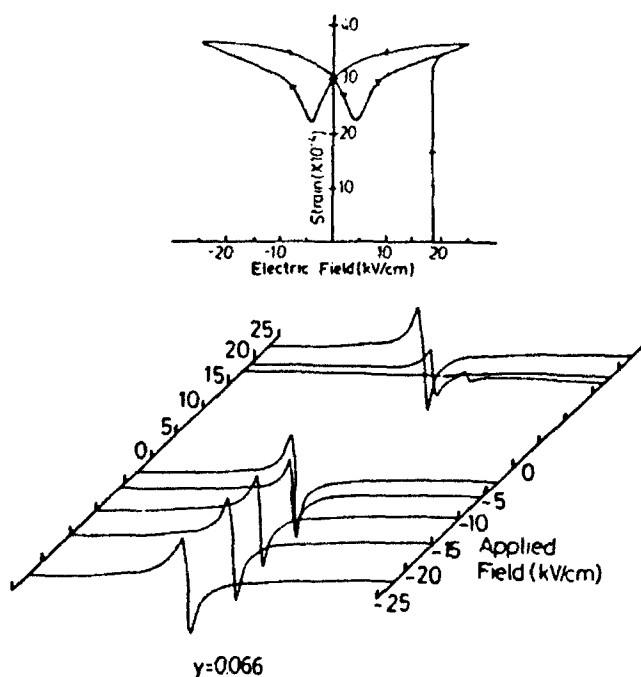


Fig. 3. Field strain relation and piezoelectric resonance admittance curve of a planar mode with applied pulse field measured in $y = 0.066$.

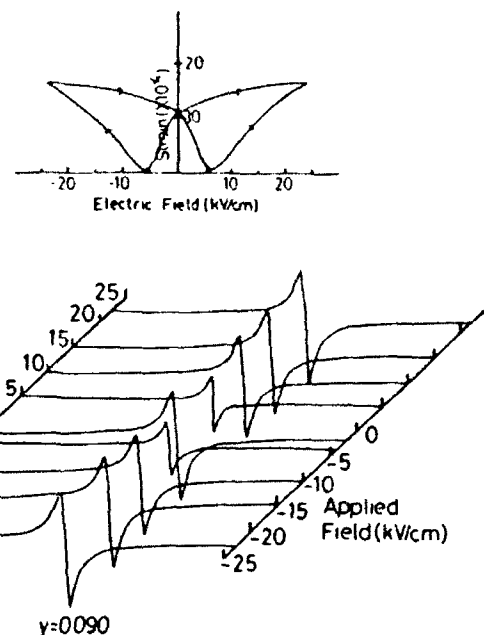


Fig. 4. Field-strain relation and piezoelectric resonance admittance curve of a planar mode with applied pulse field measured in $y = 0.090$.

smaller (5 kV/cm) than that of the other specimens ($y = 0.063$ and 0.066). Since the specimen is originally ferroelectric, it does not need a large electric field to obtain the piezoelectricity and does not lose the piezoelectricity completely by the reverse bias.

Figure 5 shows the variation of admittance characteristics as a function of Ti concentration. The frequencies of the maximum and minimum peaks are shifted to higher frequencies with increasing y , and then decrease as the Ti concentration increases above $y = 0.066$.

Electromechanical coupling factors for the planar and thickness modes are calculated from the measurement by using the following equations:

$$\frac{k_p^2}{1 - k_p^2} = \frac{\pi}{2} \frac{\omega_A}{\omega_R} \tan \left(\frac{\pi}{2} \frac{\omega_A - \omega_R}{\omega_R} \right) \quad (\text{planar mode})$$

$$k_t^2 = \frac{\pi}{2} \frac{\omega_R}{\omega_A} \tan \left(\frac{\pi}{2} \frac{\omega_A - \omega_R}{\omega_A} \right) \quad (\text{thickness mode})$$

where k is an electromechanical coupling factor and ω_R and ω_A are the resonance and antiresonance frequencies, respectively.

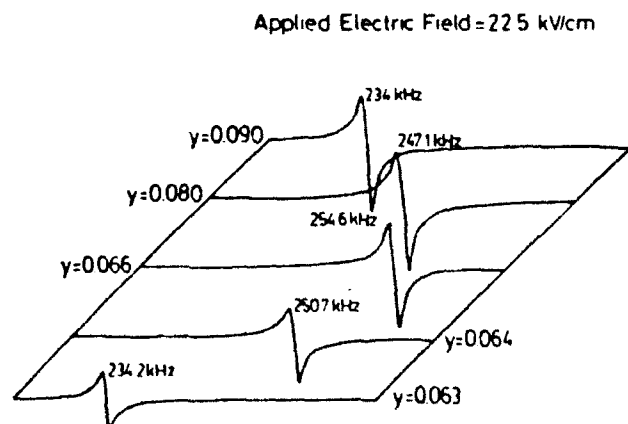


Fig. 5. Variation of resonance and antiresonance frequencies with Ti concentration (planar mode).

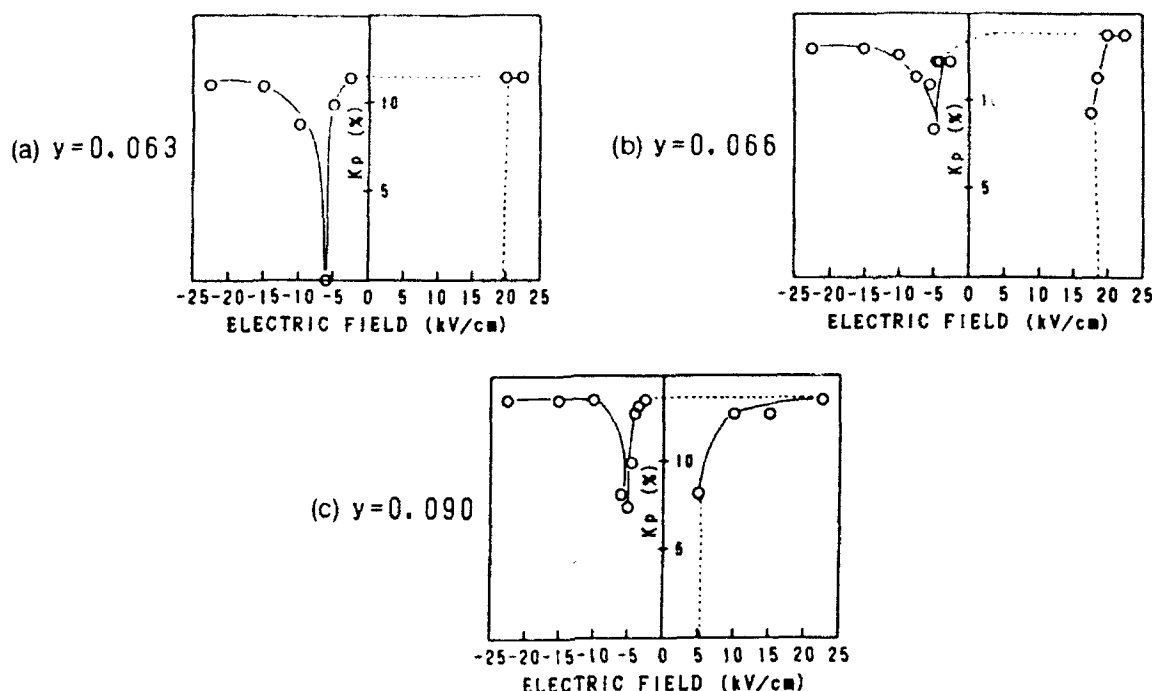


Fig. 6. Dependence of k_p on pulse field, measured in various Ti concentrations

Figures 6, 7, and 8 show the variations of k_p (planar mode), k_t (thickness mode), and K_t/k_p (piezoelectric anisotropy) as a function of applied pulse field in the sample of $y = 0.063$, 0.066, and 0.090. As the applied electric field increases, k_p and k_t appear abruptly at the transition point from the anti-ferroelectric to ferroelectric phase, then decrease gradually with the field. A minimum is observed at the domain reversal coercive field. The variations of k_p and k_t (saturated values) as a function of Ti concentration are plotted in Fig. 9. Both k_p and k_t show maxima at a certain Ti concentration. The maximum values of $k_p = 0.145$ and $k_t = 0.622$ appear in the compositions of $y = 0.08$ and 0.066, respectively.

The k_t/k_p is calculated as shown in Fig. 10 for the various compositions. The (k_t/k_p) value is more than 4.0, and the maximum value of 4.5 is observed in the composition of $y = 0.066$ around the phase boundary between regions II and III, which is about two times greater than in conventional piezoelectric materials such as PZT shown in Table I. Large anisotropy in piezoelectricity is also observed in 0.9PbZrO₃-0.1PbTiO₃, which is also a near-antiferroelectric material.

Table I also lists the data of PbTiO₃-based material ((Pb_{0.95}Ca_{0.05})[(Co_{0.5}W_{0.5})_{0.01}Ti_{0.99}]O₃ + 2 mol% MnO), which is a well-known anisotropic piezoelectric developed by Toshiba.⁴ Although the k_t/k_p value is larger, the k_t value itself

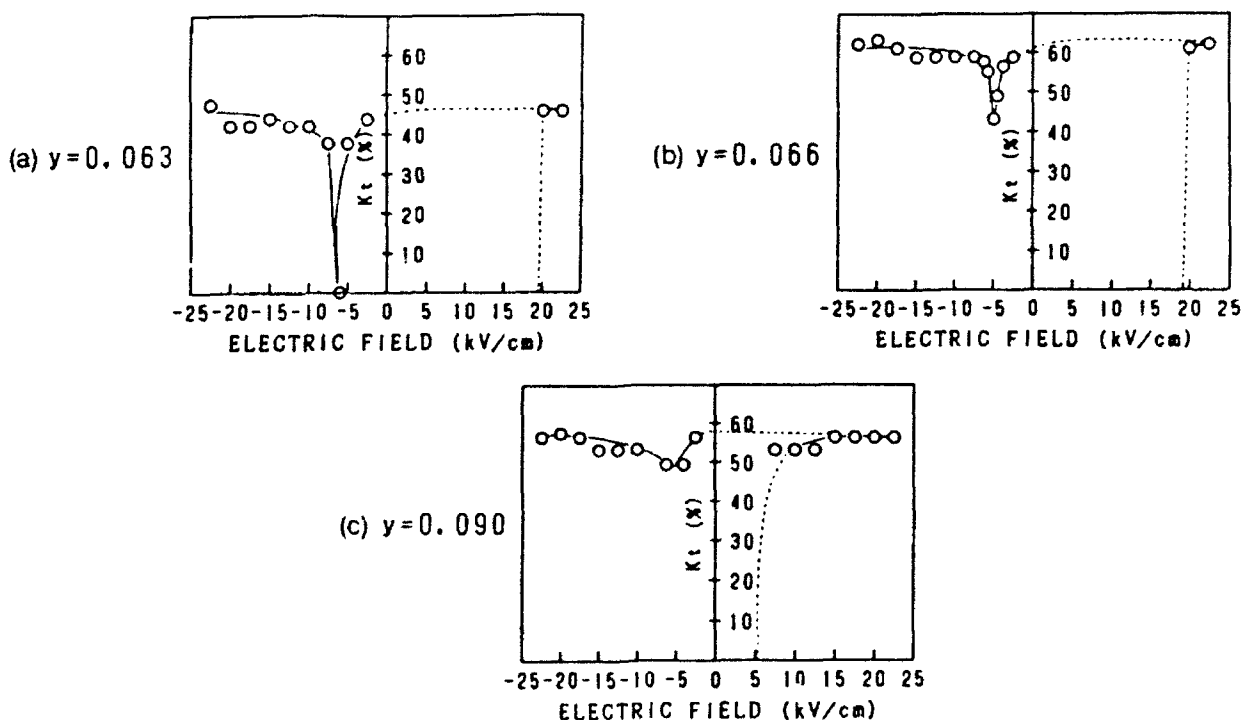


Fig. 7. Dependence of k_t on pulse field, measured in various Ti concentrations.

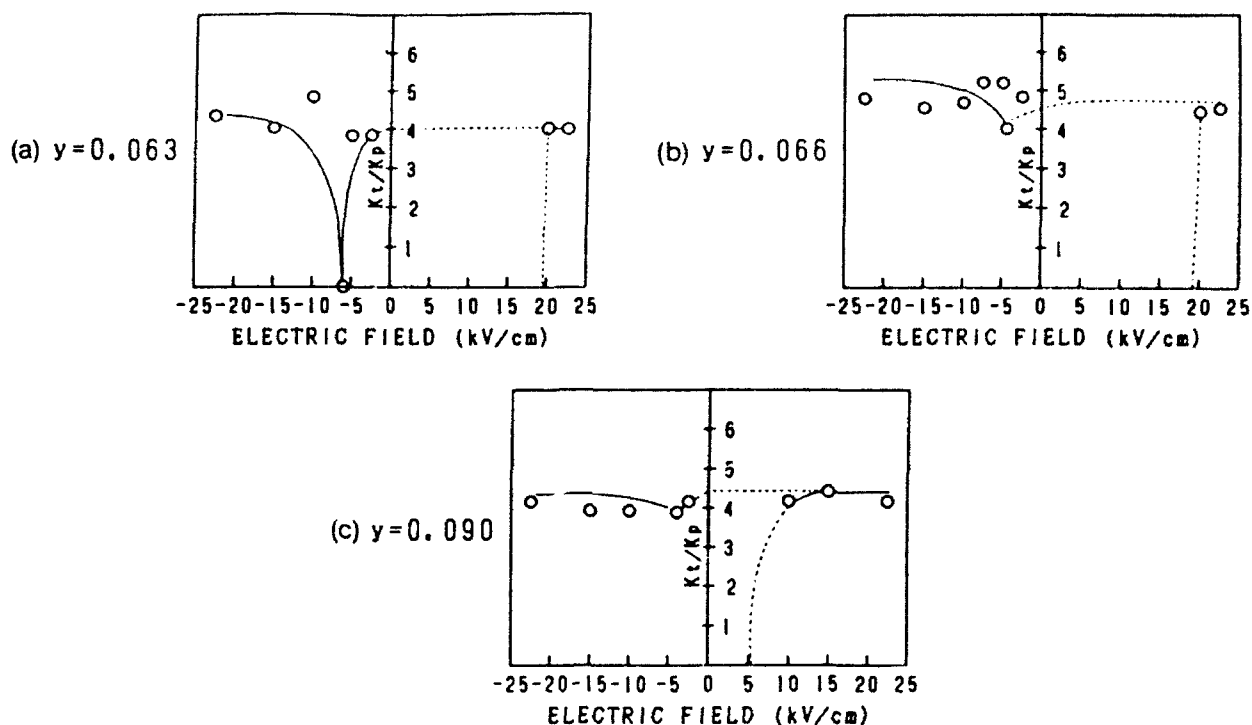


Fig. 8. Dependence of k_t/k_p on pulse field, measured in various Ti concentrations.

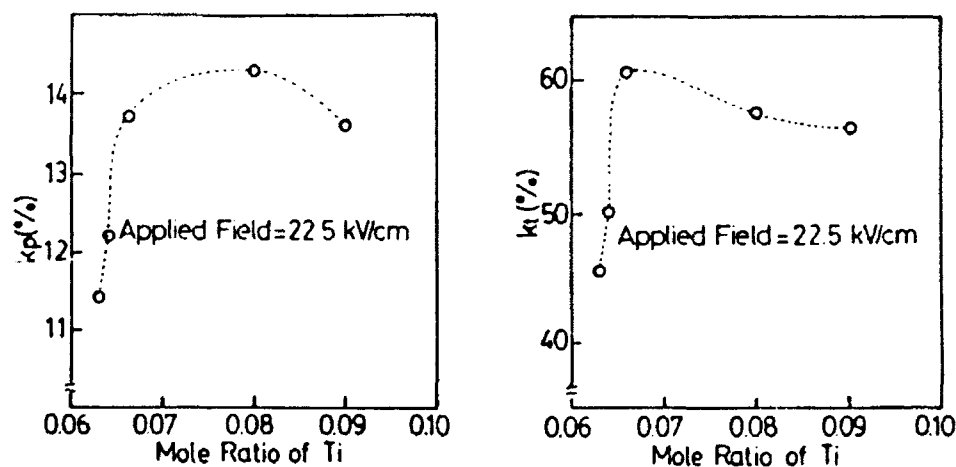


Fig. 9. Variation of k_p and k_t with Ti concentrations.

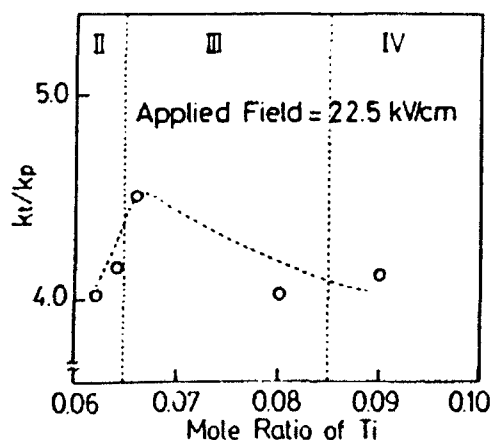


Fig. 10. Variation of k_t/k_p with Ti concentration.

is smaller than that of the PNZST ceramics. The large anisotropy can be explained phenomenologically by using a sublattice system; the two sublattices provide significant contribution to the piezoelectric anisotropy. The detailed explanations for this large anisotropy were discussed in a previous paper.⁵

IV. Conclusions

- (1) Piezoelectricity can be controlled easily by an electric field pulse in the shape memory type PNZST materials ($y = 0.063, 0.064$).
- (2) The field-induced ferroelectric phase shows a piezoelectric anisotropy larger than in conventional PZT-based materials.
- (3) In comparison with the PbTiO_3 -based ceramics, the PNZST exhibits larger electromechanical coupling with smaller anisotropy k_t/k_p .

Table I. Summary of k_p and k_t for Various Ti Concentrations in $\text{Pb}_{0.98}\text{Nb}_{0.02}[(\text{Zr}_{0.6}\text{Sn}_{0.4})_{1-x}\text{Ti}_x]_{0.98}\text{O}_3$ and Other Materials

	PNZST (applied field = 22.5 kV/cm)					0.9PZ + 0.1PT	0.5PZ + 0.5PT	Pb-based*
	$x = 0.3$	$x = 0.064$	$x = 0.066$	$x = 0.080$	$x = 0.090$			
k_p	0.114	0.123	0.137	0.145	0.136	0.072	0.388	0
k_t	0.456	0.501	0.622	0.575	0.564	0.325	0.752	0.53
k_t/k_p	4.0	4.15	4.56	4.02	4.15	4.52	1.938	∞
N_p^* (Hz·m)	2576	2757	2800	2718	2574			
N_t^* (Hz·m)	1691	1970	2018	1831	1736			

* $(\text{Pb}_{0.98}\text{Ca}_{0.02})[(\text{Co}_{0.2}\text{W}_{0.8})_{0.98}\text{Ti}_{0.02}\text{O}_3 + 2 \text{ mol}\% \text{ MnO}]$. N_p^* frequency constant of planar mode. N_t^* frequency constant of thickness mode.

The characteristics mentioned above are expected to be useful for resonators which require control of the piezoelectricity and large piezoelectric anisotropy.

References

- *K. Uchino, "Digital Displacement Transducer Using Antiferroelectrics," *Jpn. J. Appl. Phys.*, **24**, Suppl. 24-2, 46C-62 (1985).
- *K. Uchino, "Shape Memory Effect Associated with the Forced Phase Transition In Antiferroelectrics", pp. 489-503 in Proceedings of the Materi-

als Research Society International Meeting on Advanced Materials, Vol. 9 Materials Research Society, Pittsburgh, PA, 1989.

- *K. Y. Oh, A. Furuta, and K. Uchino, "Shape Memory Unimorph Actuators Using Lead Zirconate-Based Antiferroelectrics," *J. Jpn. Ceram. Soc.*, **98** [8] 905-908 (1990).
- *Y. Yamashita, S. Yoshida, and T. Takahashi, "Effects of MnO Additive on Piezoelectric Properties in Modified (Pb, Ca) TiO₃ Ferroelectric Ceramics," *Jpn. J. Appl. Phys.*, **22**, Suppl. 22-2, 40-42 (1983).
- *K. Uchino and K. Y. Oh, "Piezoelectric Anisotropy and Polarization Sublattice Coupling in Perovskite Crystals," *J. Am. Ceram. Soc.*, **74** [5] 1131-34 (1991). □

APPENDIX 19

A New Type of Flextensional Transducer

Robert E Newnham, Qichang Xu, Katsuhiko Onitsuka, Shoko Yoshikawa
Materials Research Laboratory, Pennsylvania State University
University Park, PA 16802

1. Introduction

Flextensional transducers composed of a piezoelectric ceramic and a shell structure exhibit good electroacoustic performance [1-2] in which the extensional vibration mode of the piezoelectric ceramic is coupled to the flexural vibration mode of the metal or polymer shell. The shell is used as a mechanical transformer for transforming the high acoustic impedance of the ceramic to the low impedance of the medium. The transducer can produce large volume velocity on the shell for a low Q_m , high efficiency projector, high stress in the ceramic for a highly sensitive hydrophone, or large displacement for a compact actuator. [3-5]

This paper describes a new type of flextensional transducer. Its basic structure has little similarity to class V flextensional transducer [6] because there is a different bonding area. It is a high performance transducer. A large effective piezoelectric coefficient d_{33} exceeding 4000pC/N, a high hydrostatic piezoelectric coefficient d_{31} exceeding 600pC/N and a resistance to pressures higher than 1000psi are obtained from this single PZT disk - two metal end caps flextensional transducer [3-5]. The basic configuration and simplified model of the transducer are described in section II. Finite Element Analysis (FEA) for the deformed shape and stress distribution under hydrostatic stress and the vibration dynamic mode is presented in section III. The experimental results for hydrophone, transceiver and actuator applications are discussed in section IV. The bonding materials between PZT and metal are described in section V.

II. Configuration and simplified model

Fig.1 shows the basic configuration of the transducer. The ceramic element can either be a piezoelectric ceramic or an electrostrictive ceramic with single layer or multilayer. An electrostrictive ceramic is expected to reduce the hysteresis of the actuator. A multilayer ceramic element enables lower driving voltages. The "moonie" metal end caps are used as

a displacement magnifier or a mechanical impedance transformer. The relationship between the displacement of the end caps and the size of the caps and the ceramic is explained below. For simplicity consider a beam with small curvature bonded to a ceramic bar (Fig.2). According to elastic theory [7], the bending moment M under an electroactive force from the ceramic is as equation (1)

$$M = \frac{-T_d (b^2 - a^2)^2 - 4a^2 b^2 (\ln \frac{b}{a})}{a} \quad (1)$$

$$4 \left[-\frac{a^2 b^2}{r^2} \ln \frac{b}{a} + b^2 \ln \frac{r}{b} + a^2 \ln \frac{a}{r} + b^2 - a^2 \right]$$

The electroactive force will be transmitted to the moonie metal caps. The stress in the metal is :

$$T_\theta = \frac{dE_3 Y_c A_c}{A_m} \quad (2)$$

where d = piezoelectric strain coefficient of the ceramic,
 E_3 = electric field in the ceramic
 Y_c = Young's modulus of the ceramic,
 A_c, A_m = cross sectional area of the ceramic and metal, respectively,

and $r \sim a \sim b$.

The normal displacement of the metal produced by the piezoelectric effect of the ceramic is:

$$U_p = \frac{-M \left(\frac{h_m}{2}\right)^2}{2 Y_m I_m} - \frac{3}{4} \frac{d Y_c d_c}{b_m Y_m \theta} V \quad (3)$$

h_m = thickness of the metal
 Y_m = Young's modulus of the metal
 V = applied voltage
 I_m = moment of inertia of the metal

$$d_{33} \Big|_{\text{eff}} = \frac{U_p}{V} = \frac{3}{4} \frac{d Y_c d_c}{b_m Y_m \theta} \quad (4)$$

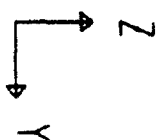
1. Hydrophone application

The dimensions of the sample are $d=d_p=11\text{mm}$, $d_c=9\text{mm}$, $h_m=h_p=1\text{mm}$ and $h=0.2\text{mm}$. The ceramic is PZT-5, the metal is brass and the bonding material is epoxy. The deformed shape of the PZT, when a unit pressure (-1.0 unit) is applied to the exterior surface as a hydrostatic pressure, is given in Fig.4. Fig.5 shows that the stresses in the r and θ direction are extensional stresses and those in the z direction are mainly compressive stresses in the PZT ceramic. (See Fig.5) These stresses in the PZT explain why this type of transducer has very high dh and can withstand high hydrostatic pressure. The first resonant frequency of the flextensional mode as a function of the metal thickness h_m of the hydrophone is presented in Fig.6. The FEA results are given by the calculated curve. Experimental results are in good agreement with FEA results. The first three vibration modes are shown in Fig.7.1, Fig.7.2 and Fig. 7.3 respectively.

2. Transceiver for fishfinder

Flextensional transducers are usually used at frequencies lower than 10kHz. This new type of transducer can reach high performance by adjusting the cavity diameter or the thickness of metal end caps to operate up to 100kHz. The 50kHz flextensional transducer can not only reduce the size and weight but can also keep higher figure of merit and wider directivity patterns measured by Airmar technology corp. than the Langevine type transducer with same diameter. The sizes of the typical samples for 30kHz fishfinder are $d_p=35\text{mm}$, $d_c=28\text{mm}$, $h_m=6$, $h_p=3\text{mm}$ and $h=0.2\text{mm}$. The ceramic is PZT-4, the metal is aluminum and the bonding material is epoxy. To get a good electrical contact between PZT ceramic and aluminum end caps, fine mesh made of brass or stainless steel is inserted into the bonding layer. The typical thickness of this type of bonding layer measured by SEM is 80 μm .

The configuration of the flextensional transducer for fishfinding is shown in Fig.8. The first three flextensional resonance frequency modes vs metal thickness are shown in Fig.9. The first resonance frequency is approximately proportional to $(h_m)^{1/2}$. The cavity diameter has a large effect to the first and third resonance frequencies, the first resonance frequency vs cavity diameter is shown in Fig.10. Fig.11.1 shows the thickness of PZT has little effect on the first three modes. The results of FEA shows that the first resonance frequency is approximately proportional to $1/(d_p)^2$, if keeping the d_c/d_p ratio constant



HP110911

UNDEFORMED
SHAPE

Bond

OPTIONS

ELEMENT IDS
WIRE FRAME

SAP90

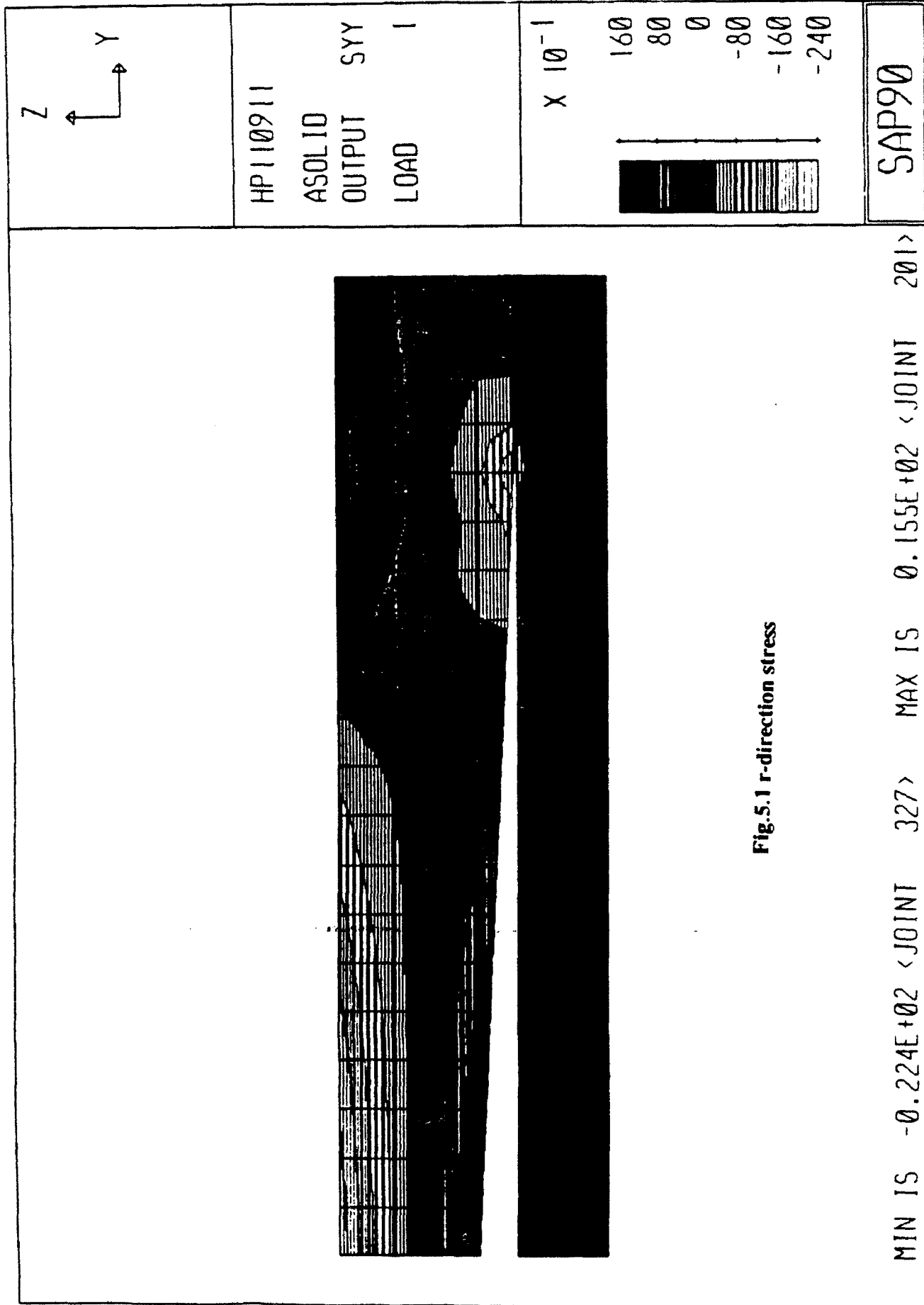
METAL

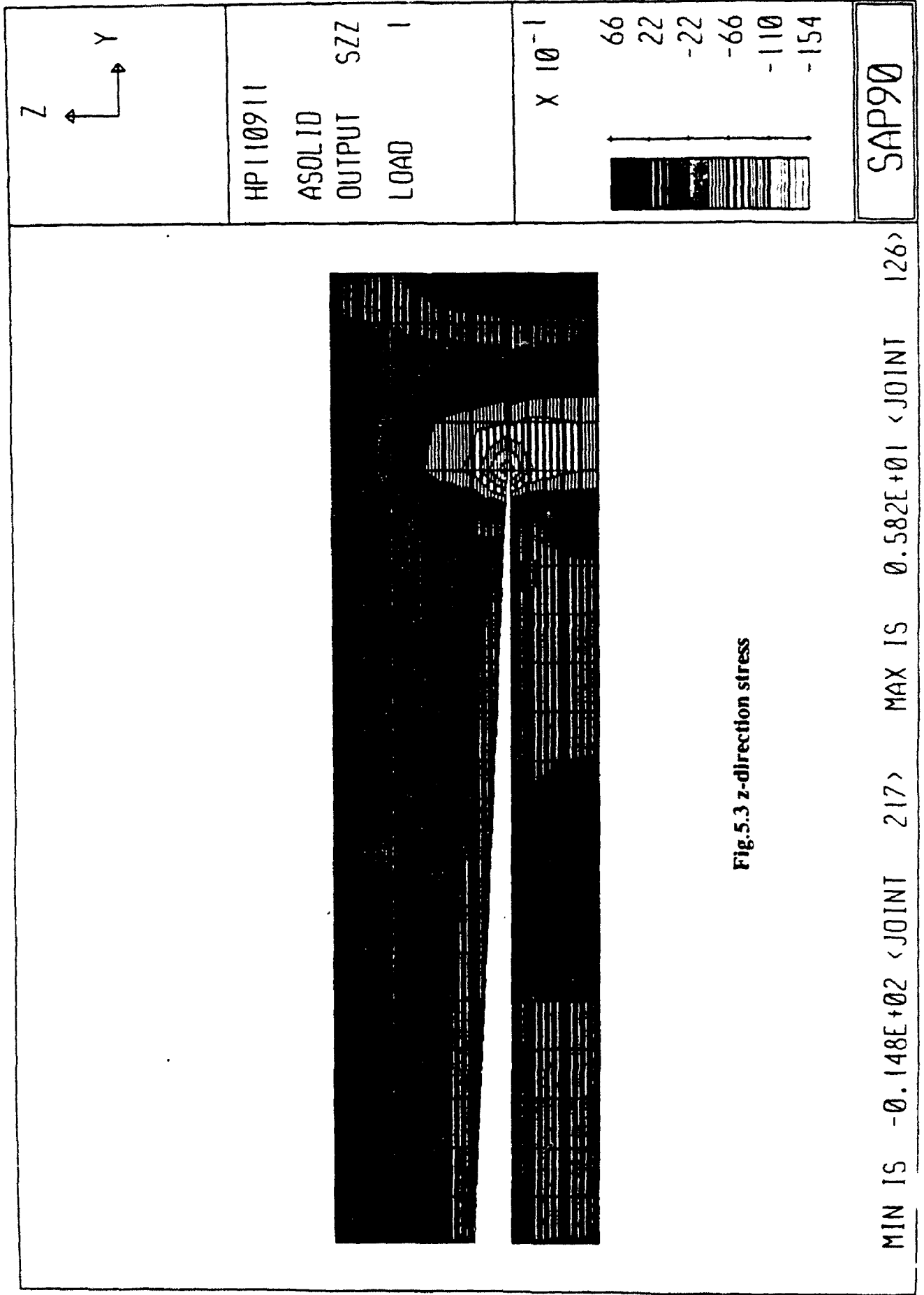
301	302	303	304	305	306	307	308	309	310	311	312	313	314	315	316	317	318	319	320
281	282	283	284	285	286	287	288	289	290	291	292	293	294	295	296	297	298	299	300
261	262	263	264	265	266	267	268	269	270	271	272	273	274	275	276	277	278	279	280
241	242	243	244	245	246	247	248	249	250	251	252	253	254	255	256	257	258	259	260
221	222	223	224	225	226	227	228	229	230	231	232	233	234	235	236	237	238	239	240
201	202	203	204	205	206	207	208	209	210	211	212	213	214	215	216	217	218	219	220

CERAMIC

81	82	83	84	85	86	87	88	89	90	91	92	93	94	95	96	97	98	99	100
61	62	63	64	65	66	67	68	69	70	71	72	73	74	75	76	77	78	79	80
41	42	43	44	45	46	47	48	49	50	51	52	53	54	55	56	57	58	59	60
21	22	23	24	25	26	27	28	29	30	31	32	33	34	35	36	37	38	39	40
1	2	3	4	5	6	7	8	9	10	11	12	13	14	15	16	17	18	19	20

Fig.3





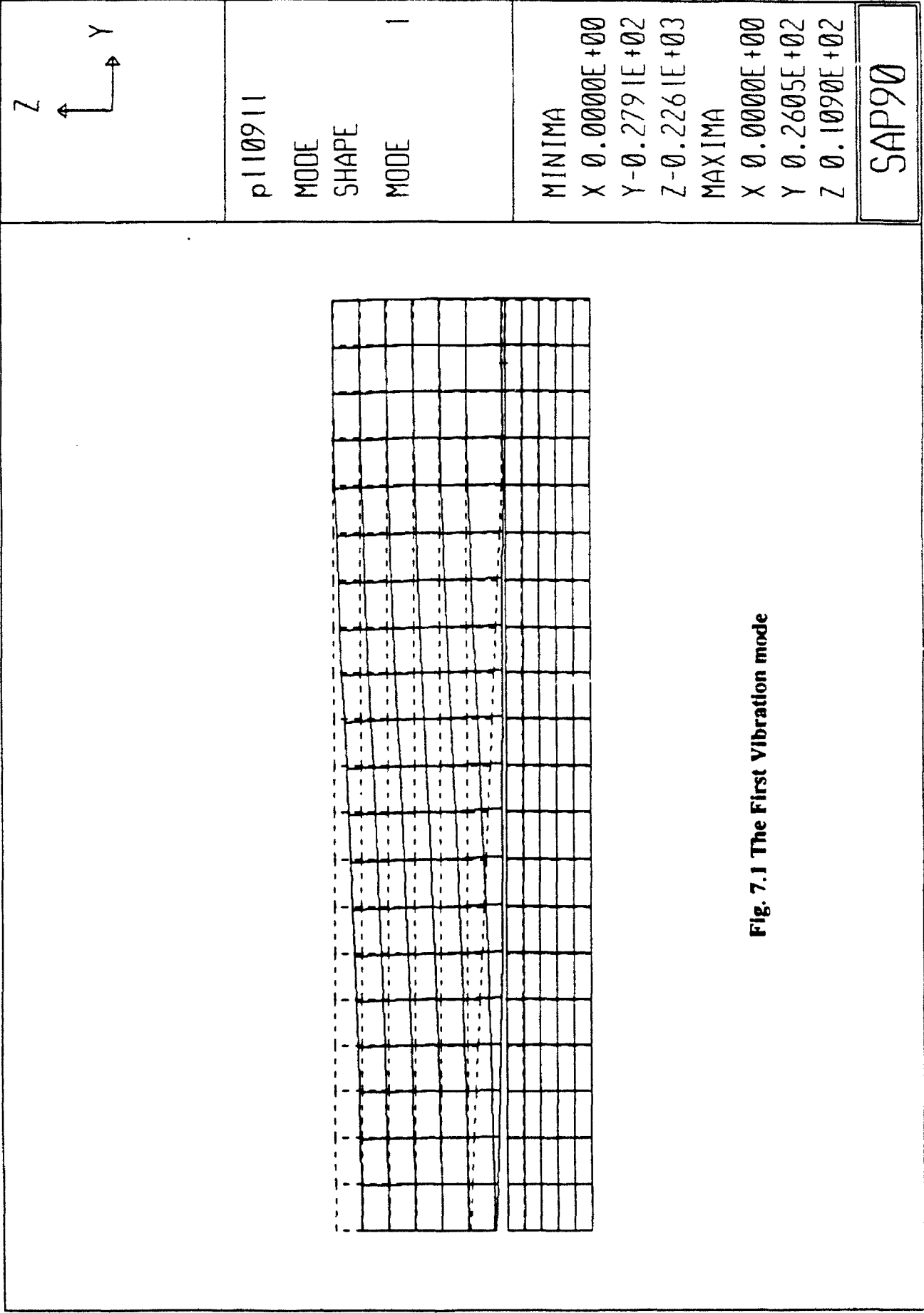


Fig. 7.1 The First Vibration mode

p110911

MODE

SHAPE

MODE

1

MINIMA

X 0.0000E+00

Y -0.2791E+02

Z -0.2261E+03

MAXIMA

X 0.0000E+00

Y 0.2605E+02

Z 0.1090E+02

SAP90

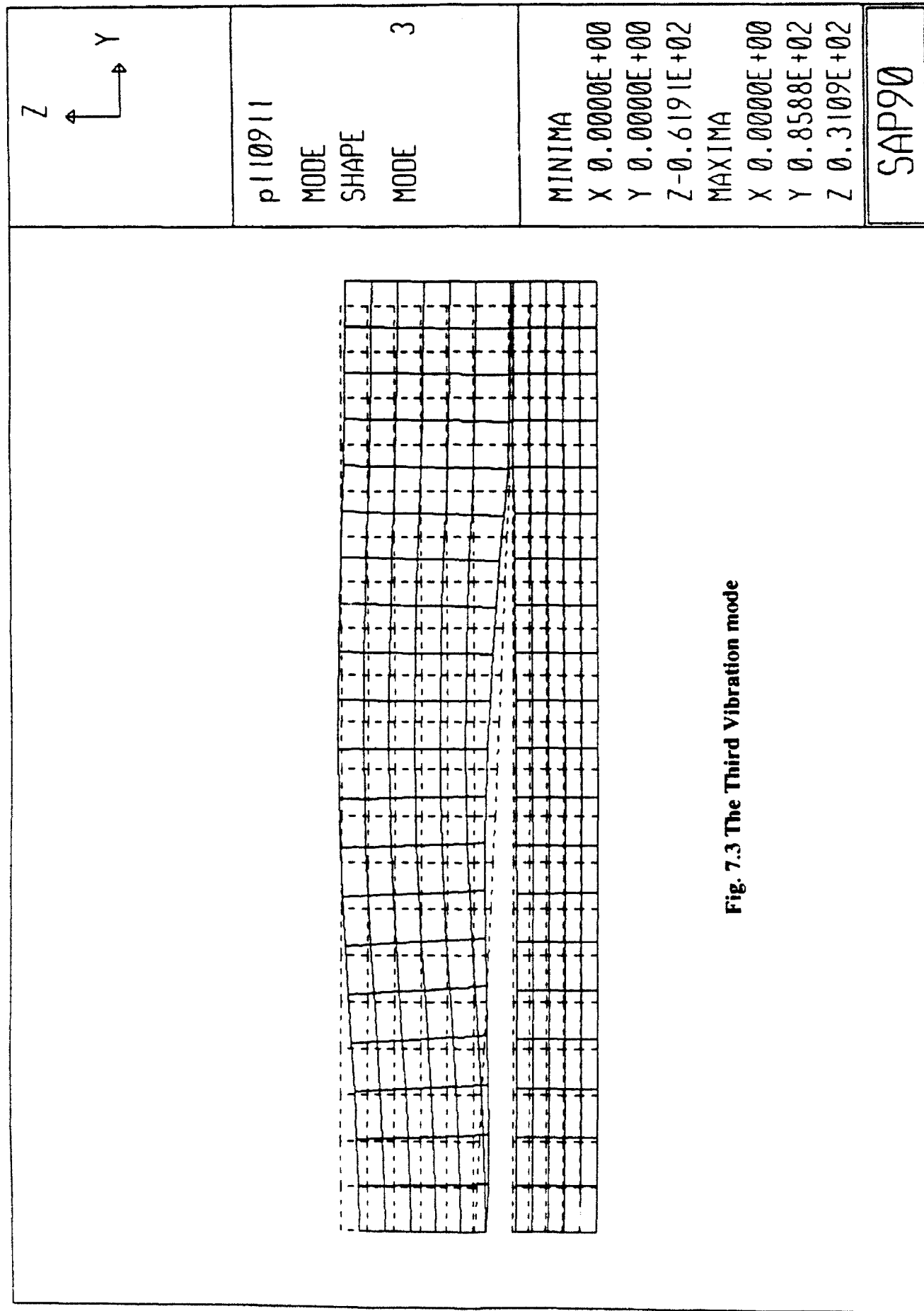


Fig. 7.3 The Third Vibration mode

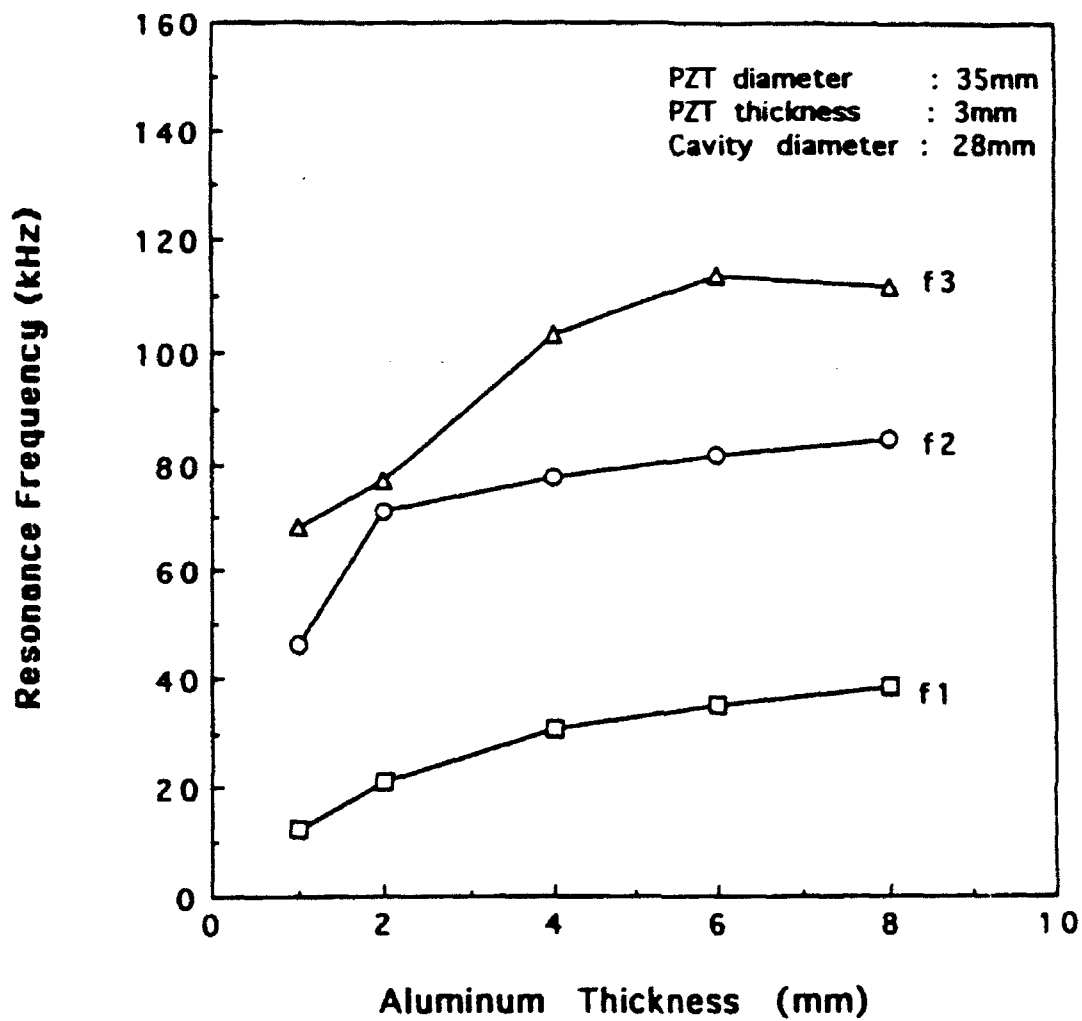


Fig. 9.1 Resonance frequencies calculated by FEM as a function of the Aluminum thickness

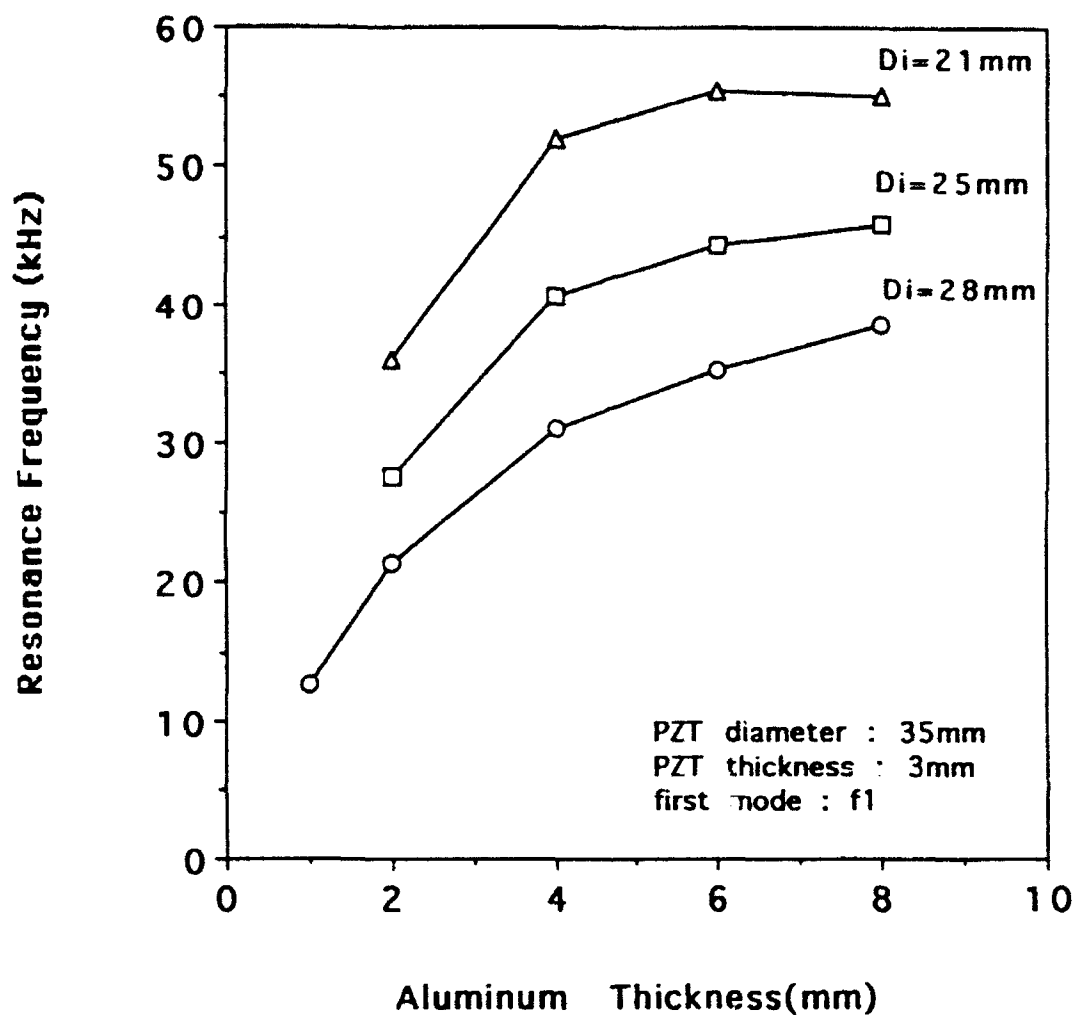


Fig.10 Resonance Frequencies calculated by FEA as a function of aluminum thickness and cavity diameter

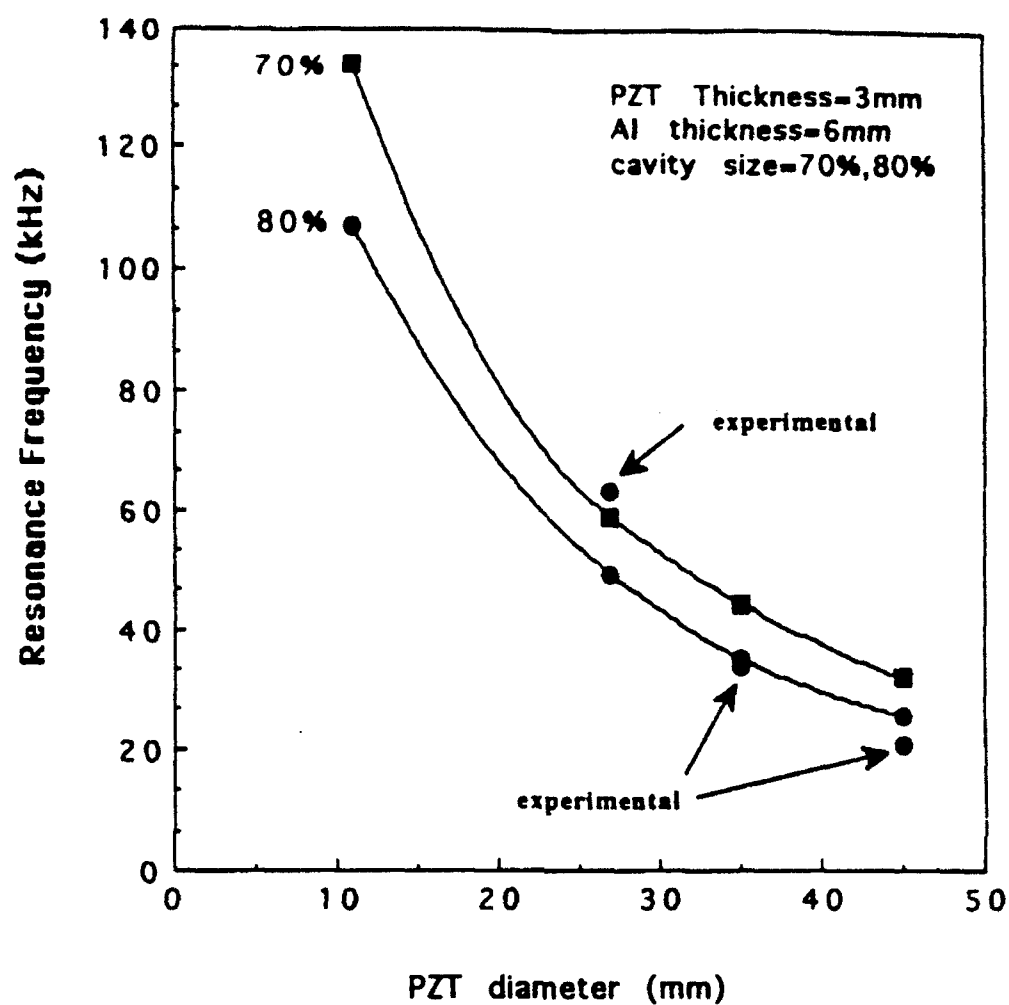


Fig.11.2 The first resonance frequencies as a function of the PZT diameter and relative cavity size.
Cavity size = $d_c/d_p \times 100$ (%)

(Fig.11.2). Fig.12 shows the resonance frequency vs bond thickness from 0 to 100 μm , for two different bonding materials. The thickness of the bonding layer has little effect on the resonance characteristics.

IV. Experimental results

1. Hydrophone

The typical PZT-5 - brass flextensional hydrophone element, with epoxy bonding, has dimensions $d=11\text{mm}$, $h_p=1.0\text{mm}$, $h=0.15\text{mm}$, $d_c=8.5\text{mm}$. The dielectric constant is $K=1450$, $\tan\delta=0.02$ and the lowest flextensional resonant frequency is 54kHz. The dependence of d_h and g_h on hydrostatic pressure P_0 is shown in fig.13.

Experimental results show that (1) the effective d_{33} , d_h and g_h are approximately proportional to $(d_c)^2$ and $1/(h_m)$, and (2) the lowest flextensional resonant frequency is proportional to $(h_m)^{1/2}$. These are confirmed with the simplified model in section II. The aging under hydrostatic pressure at 350psi is very small for experiments up to 10 days. Because of the symmetric configuration of the flextensional element, the vibration noise in the z direction can be very small. A flexible array incorporating four flextensional elements was tested in [3].

2. Fishfinder transceiver

Samples having three different diameters of 27, 35 and 45mm, have been made to obtain different resonance frequency ranges. From the FEA analysis, the first resonant mode is suited for the transmitter. The first resonance frequency, calculated for each sample, is plotted in Fig.11.2. Experimental values are in accordance with calculated values. The slight difference observed in the sample with 45mm diameter is thought to be due to the difference of the cavity diameters because the bonding area is not perfectly circularly shaped.

Wider directivity patterns of the sample with 35mm diameter, 14mm in thickness and 35kHz resonance frequency indicates that this new type of transducer has advantages for fishfinder applications.

3 . Actuator

The actuators were made from electroded PZT-5A or PMN-PT ceramic disk (11mm in diameter and 1mm thickness) and brass end caps (from 11mm to 13mm in diameter

with thickness ranging from 0.2 to 3mm). Shallow cavities from 6mm to 9mm in diameter and about 0.15mm center depth were machined into the inner surface of each brass cap. Most experimental actuator samples are bonded by epoxy or solder. The displacement of the composite actuator in the low frequency range was measured with a linear voltage differential transformer (LVDT) having a resolution of approximately 0.05 μ m. The direct piezoelectric coefficient d_{33} was measured at a frequency of 100Hz using a Berlincourt d_{33} meter.

In Fig.14, the displacements for the PZT-5A and PMN-PT themselves and their flextensional actuators with $h_m=0.5$ mm and $d_c=8.5$ mm are shown. The actuator with dimensions $d_p=11$ mm, $h_p=1$ mm, $h=0.2$ mm, $h_m=0.4$ mm, and $d_c=9.0$ mm exhibits sizable displacement as large as 20 μ m with a pressure capability of 50 g/mm² (see Fig.15).

As expected in Eq.(4), the effective d_{33} is proportional to $1/h_m$. In Fig.16, the d_{33} values were measured at the center of the brass end cap using a Berlincourt d_{33} meter. Values as high as 4000pC/N, approximately ten times of that of PZT-5A, were obtained with the moonie actuator. The displacement is largest near the center of the transducer. The effective d_{33} measured as a function of position are shown in Fig.17. Plots are shown for two brass thicknesses of 0.3mm and 3.0mm. Ample work area of several mm² are obtained with the actuator of 11mm diameter.

The creep experiment revealed that keeping a field of 1kV/mm on the epoxy-bonded actuator for two hours showed no displacement change after 1 hour (Fig.18). Larger displacement can be obtained using stacks (Fig.19). Experimental results show that the total displacement of the stack is the summation of the displacements of all elements.

The 124 layer electrostrictive composite actuator shown in Fig.20 gave the displacement exhibited in Fig.21. More than 15 μ m displacement can be obtained under an applied voltage of 150V. Note that this experimental result is obtained with only one metal end cap on the ceramic stack. If the convex or concave metal end caps are placed on both sides of the ceramic stack, more than 30 μ m displacement will be achieved under the applied voltage of 150V. The smaller displacement for the uncapped multilayer ceramic in the same direction is shown for comparison. Its lowest flextensional resonance frequency is 6.4kHz.

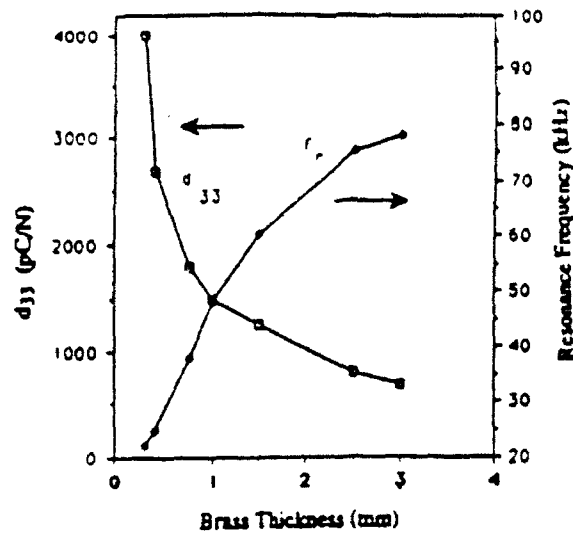


Fig.16 Resonance frequency f_r and d_{33} coefficient plotted as a function of the thickness of the brass endcaps.

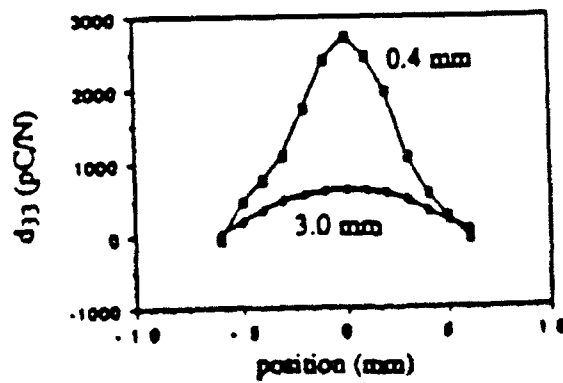


Fig.17 Positional dependance of the d_{33} coefficient for two actuators with brass thicknesses of 0.4mm and 3.0mm.

**THIS
PAGE
IS
MISSING
IN
ORIGINAL
DOCUMENT**

FIG. 18 and 19

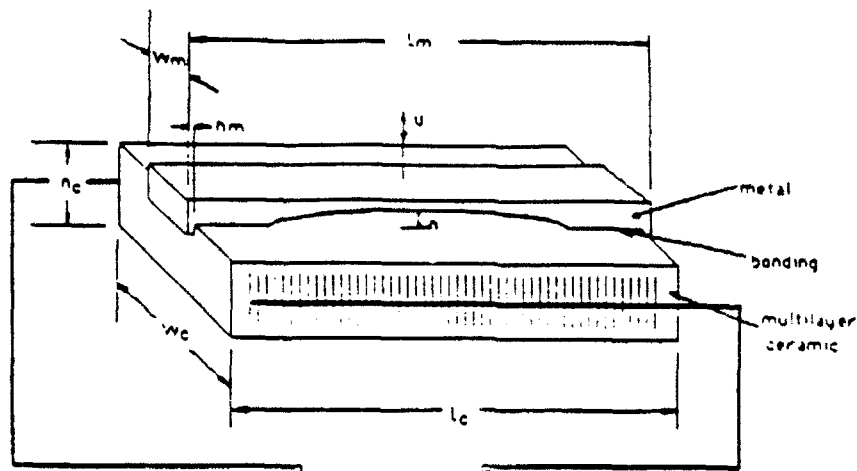


Fig.20. Another type of ceramic-metal composite actuator with multilayered ceramic part.

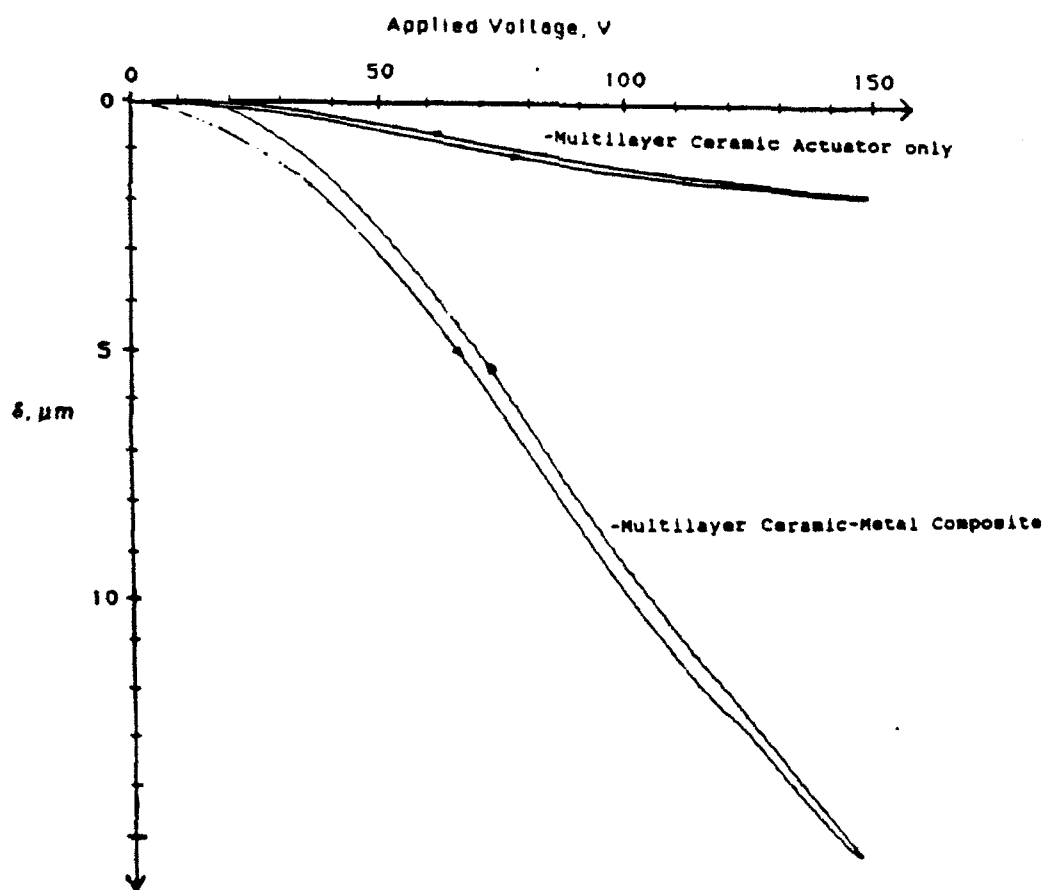


Fig.21 Displacement with increase in applied voltage of the multilayer ceramic-metal composite actuator using a electrostrictive ceramic stack and a brass end cap.

VI. Conclusion

A new type of flextensional transducer has been constructed from piezoelectric PZT or electrostrictive ceramic bonded to metal end caps. Shallow spaces under the end caps produce substantial increase in strain by combining the d_{33} and d_{31} contribution of the ceramic. Very large displacement, effective d_{33} and d_h can be obtained. It is attractive for hydrophone, transceiver and actuator applications, and is especially advantageous for non-resonant, low frequency projector in deep water.

FEA shows that under hydrostatic pressure, the radial and tangential stresses in ceramic are mainly extensional stresses, compressive stresses in z-direction concentration is high near the bonding tip. This is the reason why this flextensional transducer has very high d_h and high hydrostatic pressure tolerance.

The effective piezoelectric coefficient is approximately inversely proportional to the metal thickness and proportional to the square of the cavity diameter.

The lowest flextensional resonance frequency is approximately proportional to the square root of the metal thickness and virtually independent of ceramic and bonding layer thickness.

The lowest flextensional mode can produce large volume velocity with lower side lobe than conventional piston type transducer.

Using this flextensional transducer as an actuator is very attractive. The displacement produced by a single element moonie with total thickness of 1.8 mm can reach 20 μm with load 50g/mm² under the applied electrical field of 1kV/mm. Recent experiments show that a stacked flextensional element with total thickness of 3.8mm can reach 28 μm displacement under an electrical field of 1kV/mm and the pressure up to 50g/mm².

APPENDIX 20.

Processing of electroceramic-polymer composites using the electrorheological effect

C. A. Randall, D. V. Miller, J. H. Adair,¹¹ and A. S. Bhalla

Materials Research Laboratory, The Pennsylvania State University, University Park, Pennsylvania 16802-4801

(Received 4 March 1992; accepted 7 December 1992)

This paper presents a novel approach that demonstrates the usefulness of electrorheological fibril formation to form 1-3 connected ceramic-polymer composites. These fillers include ferroelectric, polar, metal, semiconductor, and superconductor crystallite powders. Patterned distributions of ceramic fillers within the polymer matrix can be induced by electric fields applied between patterned electrodes.

I. INTRODUCTION

A. Electroceramic composites

The study of electroceramic composites has results in several new families of devices with properties superior to those obtained from single phase materials.¹⁻³ Typically, the success of such composites can be traced to a well-designed connectivity of each phase making up the composite. Where connectivity is defined as the number of dimensions a component phase is connected. These connectivity patterns enhance the anisotropy of property coefficients and control transport of heat, charge, and radiation. These connectivity patterns can take on a number of forms. A full nomenclature has been described for diphasic and triphasic component composite systems alike. For readers unfamiliar with this nomenclature and wish to read more, we refer them to Ref. 3. This study involved two diphasic connectivity patterns, namely the subgroups 0-3 and 1-3. These diphasic connectivity patterns are schematically demonstrated in Fig. 1. The 0-3 case that refers to the active filler phase has zero connectivity, while the inactive matrix phase has three-dimensional connectivity, i.e., a dispersed phase in a surrounding matrix. The 1-3 case refers to a filler phase having connectivity in one dimension, while the matrix phase is continuous in all three dimensions.

With many early electroceramic composites, the size of the connected phase has been on a scale ($>100\text{ }\mu\text{m}$) that could be processed with conventional processing techniques.¹⁻³ Hence, desirable composite connectivity patterns could be readily obtained. However, present day and future requirements of component miniaturization bring with it difficulties in assembling more complex connectivities. These difficulties primarily are associated with the mechanical assembly of the component parts

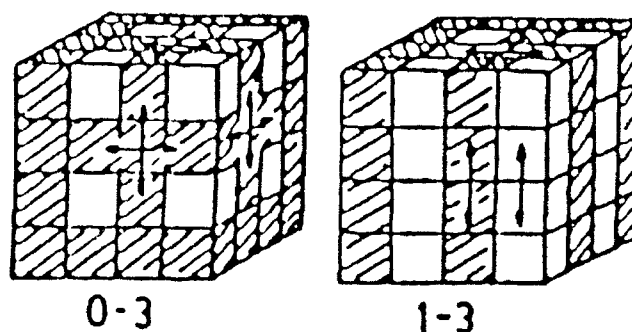


FIG. 1 Schematic representation of the diphasic connectivities 0-3 and 1-3.

and the strong interparticle forces between individual filler components. Engineers and materials scientists are forced to exploit self-assembling composite systems to control intelligently the phase or component segregation. Such examples of self-assembly include unidirectional solidification of eutectic compositions or ceramics of aligned polar-crystallites.⁴⁻⁸ However, these types of self-assembly are exceptional cases and not applicable to all composite systems. Ceramic-polymer and metal-polymer composites require other methods to align or assemble the filler phase. Magnetic fillers have been shown to align under magnetic fields, but of course this has its limitation to paramagnetic or ferromagnetic fillers.^{9,10} Other methods of assembling fillers in ceramic-polymer composites are laminar flow and tape-casting methods. These methods also have their limitations as they are very dependent on particle morphology, rheology, and particle size for successful texturing.

We present here the use of fibril formation in the electrorheological effect to aid 1-3 connectivity and percolation in composite processing.

B. Electrorheological (ER) effect

The electrorheological effect was first discovered by Winslow in 1949.¹¹ Winslow discovered that in certain

¹¹Present address: Department of Materials Science and Engineering, University of Florida, 121 Rhines Hall, Gainesville, Florida

suspensions a change in viscosity can be observed on application of an electric field to these suspensions. The ER effect can be induced by both ac and dc electric fields alike, although the effect is frequency dependent.¹²⁻¹⁵ On application of the electric field there is a redistribution of the dispersed particles into chains of aggregates and/or individual particles running between the oppositely charged electrodes. These chains of particles are known as fibrils. In the connectivity nomenclature we are using here, a change between 0-3 and 1-3 connectivity is induced using the ER effect.

The origins of the ER effect are still unclear.¹⁵⁻¹⁷ It is generally accepted that the electric field induces a net charge separation on the suspended particles to form a dipole. The induced dipoles on one suspended particle then interact with each other in accordance to electrostatic dipolar-dipolar attraction. The many body dipolar interactions drive the particle distribution to form the fibrils.¹⁸ This type of modeling has been successfully demonstrated by a computer simulation study by Bonnecaze and Brady.¹⁹

The basic understanding of induced particle dipolar polarization is more controversial. It has been suggested that the dipole comes from a displacement of the double layer and/or electrostatically induced surface charges at the fluid particle interface; a schematic representation of these two models is shown in Fig. 2. Another confusing aspect in ER fluids is the role of water and hydrated surfaces. Some authors report enhanced viscosity changes with the presence of water, while others have produced "true" ER fluids with large viscosity changes.¹⁶ The details of the ER fluid behavior that obviously need to be resolved. However, the applications using viscosity changes with ER fluids are being seriously

considered for fluid clutches, valves, clamps, and "smart" damping control of vibrations.^{15,17}

The aim of this paper is to demonstrate the potential usefulness of the electrorheological fibril formation in processing ceramic/metal-polymer composites.

C. Experimental

As this paper is mainly concerned with composite microstructural control, much of the experimentation was performed using microscopy. A number of optical cells were developed in order to study *in situ* observations of the electrorheological fibril development.

Solid composites were cured in larger teflon cells (Fig. 3). Fillers were dried for 24 h before testing in order to eliminate water effects. A number of differing polymers were studied; see Table I. Within this group of thermoset polymer, the viscosities were sometimes high, such that during the mixing of the filler, air was incorporated. In these cases the composite mix and teflon cell were put under vacuum for a period of 1 h. After the evacuation, the electric alignment was performed at 65 °C for up to 1 h, depending on the polymer. Further optical microstructural studies to characterize the alignment were made on solid polymer composites after sectioning with a microtome.

II. RESULTS

A. Polymer and filler study

A number of thermoset polymers were tested in their uncured state to determine their fluid states as a possible host for electrorheological fibril formation. Results are shown in Table I. Reasons for the success of one type of polymer over another at a given field

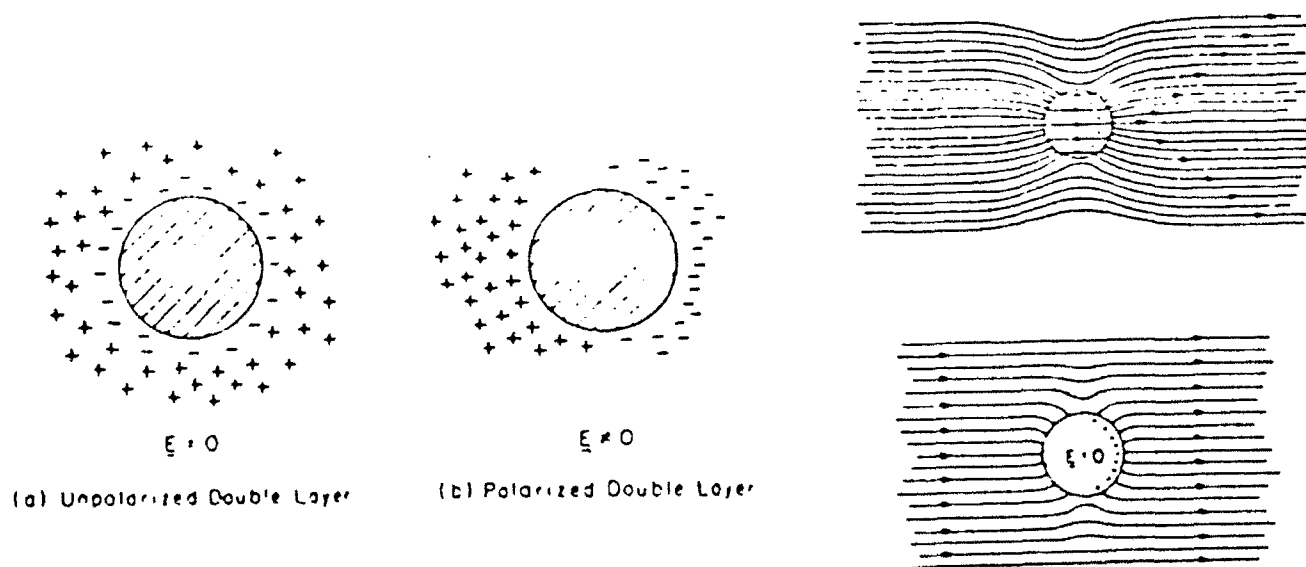


FIG. 2 Schematic representation of the possible mechanisms for the induced polarization in electrorheological fluids: (a) unpolarized double layer and (b) polarized double layer

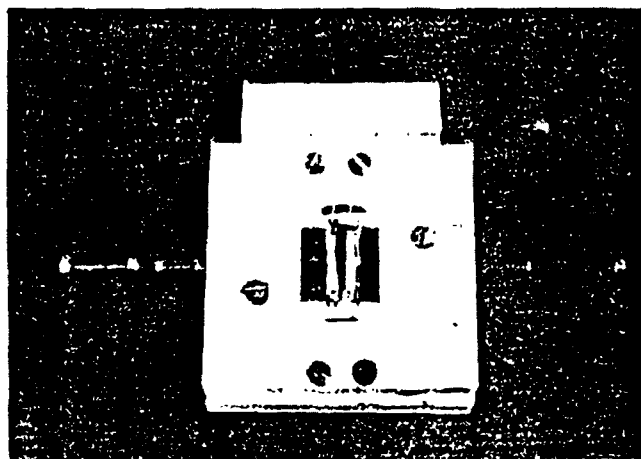


FIG. 3. Photograph of a typical teflon cell used to fabricate solid composites.

strength and alternating frequency are not known at this time. This is the same limitation in our understanding of the electrorheological phenomena itself.

For successful ER uncured polymers, a wide variety of filler materials were tested, including insulators, semiconductors, and metals. Table II shows a list of these various filler materials, which all showed evidence for ER fibril formation in successful polymers. The magnitude of electric field, $\sim 1-2$ kV/mm, was based on previous studies with silicon oil and BaTiO_3 powder.¹⁶ Both direct and alternating electric fields can induce fibril formation of the filler phases. But, with high-voltage direct fields, electrophoretic motion can override the fibril alignment. Hence, alternating fields are preferred in the processing. The frequency conditions were based on direct optical microscopy studies, where the fibril formation was optimized for frequencies ~ 10 Hz for polyurethane and silicone elastomers and for frequencies from 500–700 Hz for epoxy polymers at room temperature.

Alignment was observed for a wide volume fraction range 0.1–25 vol. % in $\text{Pb}(\text{ZrTi})\text{O}_3$ and BaTiO_3 particles in silicone elastomer. Higher volumes of these insulator powders were studied by microstructural studies, but did not resolve alignment owing to the high density of packing. However, electrorheological viscosity

TABLE I. Polymers and suppliers.

	Fibril formation $E \approx 1-2$ kV/mm	Trade name and supplier
Polyurethane	Yes (10 Hz)	Hysol-Dexter, US0048
Silicone elastomers	Yes (10 Hz)	Sylard-184, Dow Corning
Eccogel	Yes (600 Hz)	Eccogel-Emerson Cummings 1365
Epon resin	Yes† (600 Hz)	EPON 815-Shell

TABLE II. Alignment of powders in uncured silicon elastomers.

Insulators	Semiconductors	Metals
BaTiO_3	$\text{YBaCu}_3\text{O}_{6.5}$	Aluminum metal
PbTiO_3	Graphite	Ag cover resin balls ^b
$\text{Pb}(\text{Zr}, \text{Ti})\text{O}_3$	SiC fibers	Ag cover acrylic fibers ^b
$\text{Ba}_2\text{TiSi}_2\text{O}_8$		
ZrO_2		
TiO_2		
Silica glass spheres ^a		

Manufacturers:

^aSpherglass—Potters Industries, Inc.

^bMitsubishi Metal Corporation.

changes are found to exist up to 35 vol. %. Figure 4 shows examples of fibril formation in silicone elastomer with (a) ferroelectric $\text{Pb}(\text{ZrTi})\text{O}_3$ 5 vol. %, (b) dielectric TiO_2 , 5 vol. %, and (c) conductive Ag-coated acrylic fibers 0.5 vol. %, aligned with alternating electric field of 1 kV/mm at 10 Hz. All the results obtained show there is a wide range of materials capable of fibril alignment in certain uncured polymer matrices. Particle morphology is also important with the alignment process. Both needle-shaped Ag-coated fibers and SiC fibers align their axis parallel to the electric field direction; these may be a consideration if we wish to maximize the anisotropy of composite properties.

B. Anisotropy of ER-aligned composites

The anisotropy of the ER-formed composites is demonstrated in Fig. 5. This figure shows the difference in the transparency of aligned aluminum metal powder, 0.5 vol. % in silicone elastomers. The composite is cut to the same thickness, 2 mm, parallel and perpendicular to the fibrils. The light scattering along the aligned fibril direction is reduced compared to fibrils perpendicular to the viewing direction.

C. Patterning a composite with ER-alignment methods

With ER fibril formation, it is possible to align powder between patterned electrode arrays. Figure 6 shows photomicrographs of aligned BaTiO_3 fibrils between discontinuous parallel electrodes. These results demonstrate that possibility of manipulating a uniformly dispersed uncured mixture to one that has nonuniform mixing of volume fraction and connectivity. There is a reduction of the local volume fraction in the regions between the electrodes. Of course, this also corresponds to an increase in the local volume fraction in the vicinity between the electrodes. This redistribution of the local volume fraction is owing to dielectrophoretic forces from the electric fringing fields attracting dielectric media

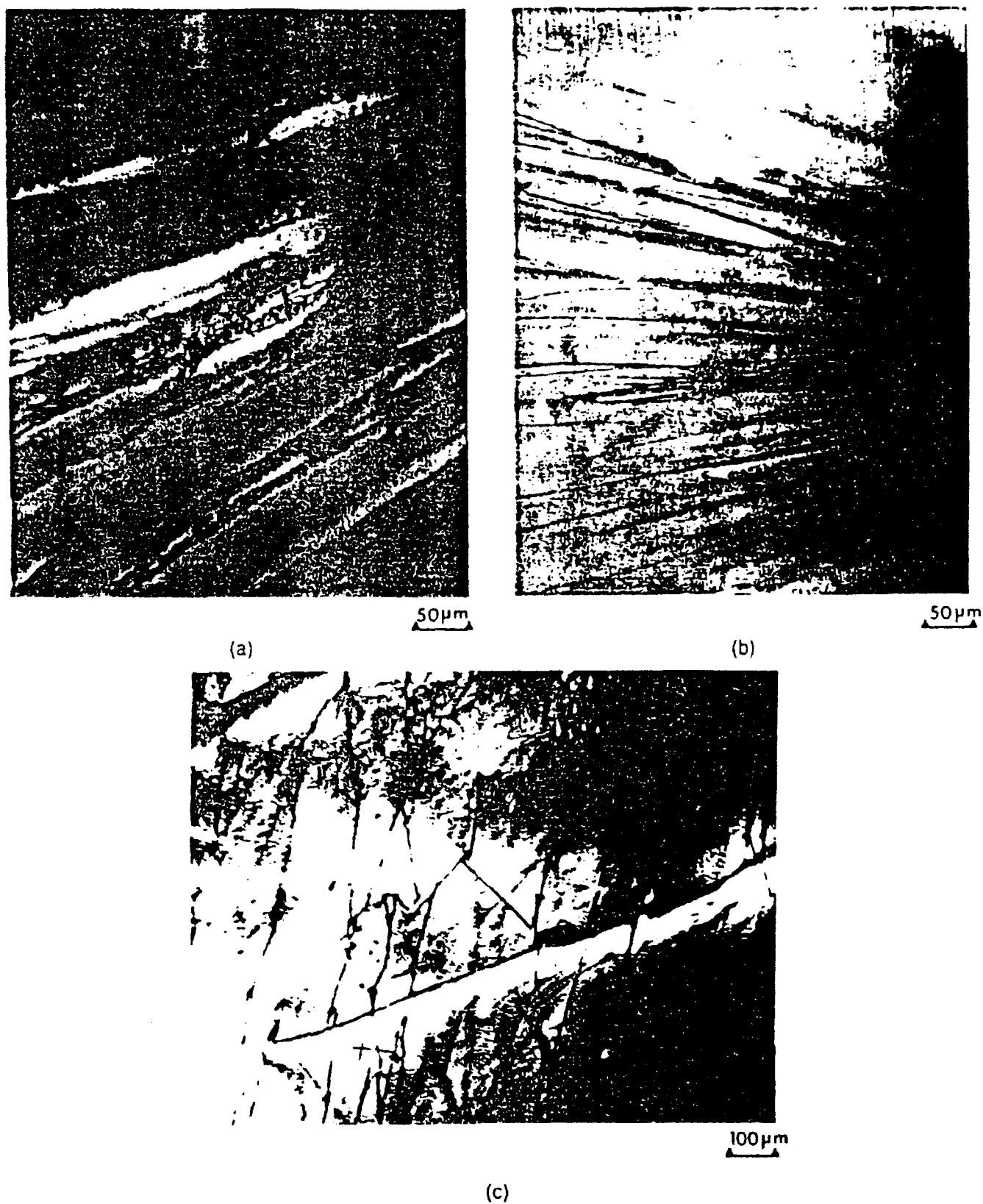
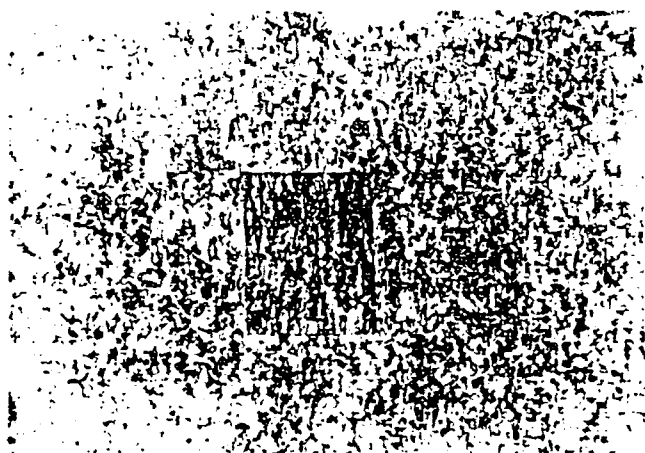


FIG. 4. Fibril formation induced with alternating electric fields of 1 kV/cm and 10 Hz with (a) $\text{Pb}(\text{Zr,Ti})\text{O}_3$, (b) TiO_2 , and (c) Ag-coated acrylic fibers.



(a)



(b)

FIG. 5. (a) Difference in the transparency for an electrorheologically aligned 0.5 vol % aluminum filler in silicone elastomer matrix cut parallel and perpendicular to the fibrils. (b) Alignment of 0.1 vol % of Ag-coated acrylic fibers in silicone elastomer composite.

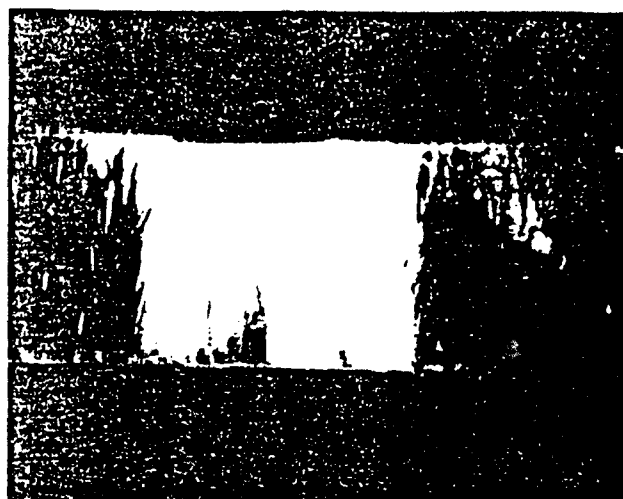
to a lower energy state between the electrodes where uniform electric field lies.^{20,21} Figure 7 shows a poorly patterned composite using unaligned electrodes. In this case, fringing fields dominated the electrorheological alignment and resulted in ill-defined connectivities and non-uniform distribution of connectivities.

III. SUMMARY AND CONCLUSIONS

(1) ER effect using alternating electric fields was shown to align powder fillers in uncured thermoset polymers.

(2) The alignment conditions vary from polymer to polymer; a universal understanding of properties necessary to exhibit this effect is undetermined at this time.

(3) Strong anisotropy is demonstrated with optical scattering with fibril alignment.



(a)



(b)

FIG. 6. Examples of aligned BaTiO₃ powder with patterned stripped electrodes.

(4) In polymers that allowed ER effect to occur, a wide variety of electroceramic fillers were found to align during the curing process. From this diverse group of fillers, applications of ER-induced anisotropies for conductive connectors, nonlinear I-V varistors, piezoelectric transducers, pyroelectric sensors, positive temperature coefficient resistors, and superconductor composites are all possible.

(5) Patterning of filler connectivities with discontinuous electrodes is demonstrated within polymer-ceramic composites.

This novel approach can be applied to a number of electroceramic composites in order to improve various properties. One limitation to this approach is that a universal understanding of the interparticle forces



FIG. 7. Nonuniform alignment of aluminum metal powder resulting from unaligned electrodes resulting in strong fringing fields.

responsible for the electrorheological phenomena does not exist, although working with alternating fields and polymer materials should expand the data base of the electrorheological phenomena. Another exciting possibility of this approach is its application to composites. Nanocomposites can be fabricated to have connectivities using the ER effect if there is good dispersion of the nanoscale filler particles within the uncured polymer.

ACKNOWLEDGMENTS

We wish to thank DARPA and ONR for supporting research related to this discovery. We also wish to thank L. E. Cross and R. E. Newnham for many useful discussions, and also J. Mantz for typing this manuscript.

REFERENCES

1. R. E. Newnham, *Annu. Rev. Mater. Sci.* **16**, 47-68 (1986).
2. R. E. Newnham, *Rep. Prog. Phys.* **52**, 123-156 (1989).
3. R. E. Newnham, *Ferroelec.* **68**, 1-32 (1986).
4. F. M. A. Carpay and W. A. Tiller, *J. Cryst. Growth*, **24**, 551-554 (1974).
5. A. Halliyal, Ph.D. Thesis, Penn State University, University Park, PA 16802.
6. V. S. Stubican and R. C. Bradt, *Annu. Rev. Mater. Sci.* **11**, 267-297 (1981).
7. E. Corcoran, *Sci. Am.* **263**, 122-131 (1990).
8. P. Calvert and S. Mann, *J. Mater. Sci.* **23**, 3801-3815 (1988).
9. C. Rosenblatt, P. Yager, and P. E. Schoen, *J. Bio. Phys.* **52**, 295 (1987).
10. F. Behvoozi, M. Orman, R. Reese, W. Stockton, J. Calvert, F. Rochford, and P. Schoen, *Sub. J. Appl. Phys.* (1990).
11. W. M. Winslow, *J. Appl. Phys.* **20**, 1137 (1949).
12. R. W. Brien, *Adv. Colloid Interface Sci.* **16**, 281-320 (1982).
13. A. J. Hurd, S. Graden, and R. B. Meyer, *Science of Ceramic Chemical Processing*, edited by L. L. Hench and D. R. Ulrich (John Wiley and Sons, New York, Chichester, Brisbane, Toronto, and Singapore, 1986), Chap. 58, pp. 555-560.
14. D. V. Miller, C. A. Randall, J. H. Adair, and A. S. Bhalla, (unpublished research).
15. T. B. Jones, *Proc. 2nd Int. Conf. ER Fluids*, edited by J. D. Carlson, A. F. Sprecher, and H. Conrad (Technomic Publishing Company, 1989), pp. 14-26.
16. N. Webb, *Chemistry in Britain* **4**, 338-340 (1990).
17. Y. F. Deinaga and G. V. Vinogradov, *Rheologica Acta* **23**, 636-651 (1984).
18. P. M. Adriani and A. P. Gast, *Phys. Fluids* **31** (10), 2757-2768 (1988).
19. R. T. Bonnecaze and J. F. Brady, *Proc. 2nd Int. Conf. ER Fluids*, edited by J. D. Carlson, A. F. Sprecher, and M. Conrad (Technomic Publishing Company, 1989), pp. 27-40.
20. H. A. Pohl, *J. Appl. Phys.* **29**, 1182-1189 (1958).
21. H. A. Pohl and J. P. Schwar, *J. Appl. Phys.* **30**, 69-73 (1959).

APPENDIX 21

Structural-property relationships in dielectrophoretically assembled BaTiO₃ nanocomposites

C.A. Randall ^a, S. Miyazaki ^b, K.L. More ^c, A.S. Bhalla ^a and R.E. Newnham ^a

^a Materials Research Laboratory, Pennsylvania State University, University Park, PA 16802, USA

^b Tsukuba Research Laboratory, Sumitomo Chemical Co. Ltd., 6 Kitahara, Tsukuba, Ibaraki 300-32, Japan

^c High Temperature Materials Laboratory, Oak Ridge National Laboratory, Oak Ridge, TN, USA

Received 30 June 1992

Using the dielectrophoretic effect, submicron BaTiO₃ powders dispersed in an uncured silicone elastomer could be redispersed into an aligned composite. The cured and aligned composites were microtomed into thin sections and characterized using electron and optical microscopy. Dielectric characterizations of the aligned composites were also studied and modelled using the conventional dielectric mixing rules. Both the microscopy and dielectric characterization suggested the alignment of BaTiO₃ particles in a quasi 1-3 connectivity pattern parallel to the direction of the applied electric field.

1. Introduction

Dielectrophoretic or electrorheological effects are usually associated with an electrically induced yield stress and viscosity variations and used in active damping control and also fluid clutch applications [1,2]. However, recently we reported that the dielectrophoretic alignment could be used to assemble composites by changing the connectivity of dispersed filler phases in some uncured polymers before curing [3,4]. Connectivity is the dimensional relationship between the phases confined within a composite, and connectivity directly influences the physical properties of the composite. Application of an electric field creates a mutual dielectrophoretic attraction of neighboring filler particles to form fibril chains; if the fibrils are continuous in one dimension throughout the thickness of the composite, we have

a so-called 1-3 composite [5].

The aim of this study was to demonstrate the possibility of processing of a nanocomposite using the dielectrophoretic fibril assembly of submicron crystals in a polymer. The associated microstructure and dielectric properties were measured and modelled.

2. Experimental

2.1. Raw materials

The raw materials used in this experiment are all commercially available. The BaTiO₃ powders from three suppliers were used for this study and listed along with associated powder properties in table 1.

Table 1
Sources and related characteristics of BaTiO₃ powders

Name	Powder processing	Particle size (μm)	Specific surface area SSA (m ² /g)
Saiki BT01	hydrothermal	0.1	12.7
Saiki BT05	hydrothermal	0.5	2.4
BaTiO ₃ TAM HPB	coprecipitation	0.2-0.3	1.0

The polymer used was 184 Sylgard silicone elastomer, supplied by Dow Corning Ltd.

2.2. Preparation of slurry

The silicone elastomer is a thermoset polymer with part A monomers and oligomers and part B being the catalyst for the polymerization reaction. The key to making homogeneous and uniform nanocomposites is with the dispersion of powders within the polymer. This was achieved by gradually mixing the BaTiO₃ powders into part A under high shear mixing with the pestle and mortar. After all the BaTiO₃ powder was dispersed in part A, the part B catalyst was added and the shear mixing process repeated. Air was removed from the slurry under a vacuum rotary pump for approximately 20–30 min. The slurry was then poured into the teflon alignment chamber, similar to one shown in fig. 1. A second evacuation of the slurry is performed in the alignment chamber for 30 min.

2.3. Alignment under electric field

An alternating electric field was applied to the slurry at curing temperatures of ≈ 60 – 80°C . An elec-

tric field angular frequency of ≈ 40 Hz with the root mean square electric field strength being ≈ 1 kV/cm was applied across the curing composite. Curing time takes approximately 1 h for the sample volumes $\approx 2.5\text{ cm} \times 1\text{ cm} \times 0.8\text{ cm}$ made in the study.

2.4. Characterization

For both microscopy and dielectric characterization large area and thin sections are required. To obtain these, microtomed sections were sliced (50–100 μm thick) from the composites. This allowed optical transmission microscopy to be performed on thin samples and also reliable dielectric measurements on thin and large area samples using a HP 4790A impedance bridge. For dielectric measurements, gold electrodes were sputtered on the surfaces of the composite sections.

3. Results and discussion

Fig. 2 shows homogeneous dispersion of the typical alignment of BaTiO₃ powders in silicone elastomer polymer as observed using transmission optical microscopy. The scanning electron microscopy (SEM) analysis demonstrated that the dispersion was such that individual submicron BaTiO₃ crystals could be aligned into fibrils. This phenomenon can be seen

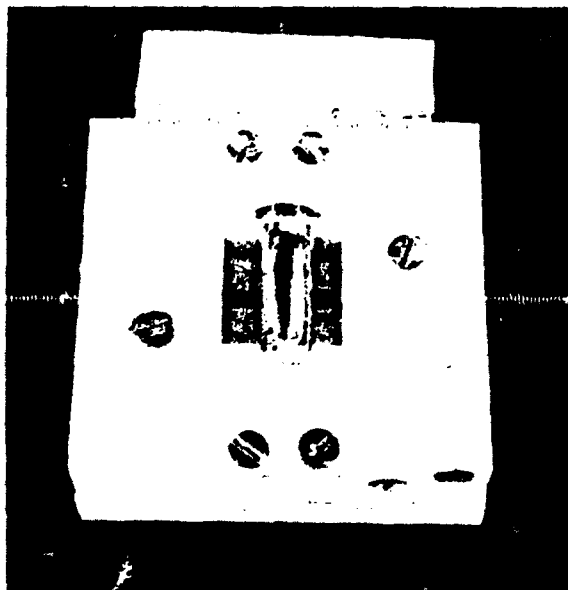


Fig. 1. Teflon holder used for polymerization under application of an electric field.



Fig. 2. Homogeneous dispersion of aligned BaTiO₃ in silicone elastomer. Magnification 100 \times .

in figs. 3a and 3b. The fibrils are discontinuous as revealed in SEM studies.

The room-temperature (1 kHz) dielectric constant and $\tan \delta$ data for these composites are listed in table 2. The theoretical estimates of dielectric constant based on using series, parallel, and logarithmic mixing laws are also listed [5,6]. The relations used for the estimates are as follows:

$$1/\bar{K} = V_1/K_1 + V_2/K_2 \quad (\text{series law}), \quad (1)$$

$$\bar{K} = V_1 K_1 + V_2 K_2 \quad (\text{parallel law}), \quad (2)$$

and

$$\log \bar{K} = V_1 \log K_1 + V_2 \log K_2 \quad (\text{logarithmic law}). \quad (3)$$

Here \bar{K} is the average dielectric constant of the composite, V_1 and V_2 are the respective volume fractions, and K_1 and K_2 are the respective dielectric constants of phase 1 and 2. Dielectric constant of $K \approx 300$ (1 kHz and at room temperature) was measured experimentally. The silicone elastomer has a dielectric constant of 2.8 at 1 kHz as determined on pure silicone elastomer samples. The experimentally determined dielectric constant of BaTiO_3 powder is lower than bulk values. This is due to the fact that the nature of the dielectric polarization mechanisms in nanoscale ferroelectric powder has size effects as discussed by Ishikawa [7] and Uchino et al. [8]. In addition to this observation, we noted from table 2 that there is a dielectric anisotropy induced by the dielectrophoretic alignment within the composites.

Using the dielectric constant $K_1 = 300$ for BaTiO_3 and $K_2 = 2.8$ for silicone elastomer for the calculation of the composite \bar{K} there appears to be a good agreement, in the case of unaligned dispersed BaTiO_3 composites, with the logarithmic mixing rule. For the composites prepared under electric field, both series and parallel contributions are important. With the aligned composite sections microtomed longitudinally to the fibril alignment, dielectric constant measurement agrees with a series mixing. Transverse microtomed sections of composites possess fibrils normal to the capacitor electrodes and hence a high parallel mixing component becomes important. From table 2 the measured dielectric constants are smaller than the theoretical parallel mixing predicts. This infers that the connectivity being quasi 1-3, that is to say, discontinuous fibrils exist within the composite thickness. Using the predicted parallel dielectric constant and the measured dielectric constant in the series mixing model it is possible to estimate the relative parallel contribution to be $\approx 90\%$. These dielectric measurements suggest a quasi 1-3 composite and this is consistent with the SEM microstructure observations, figs. 3a and 3b.

4. Conclusions

Alignment of submicron powders loaded in a sil-

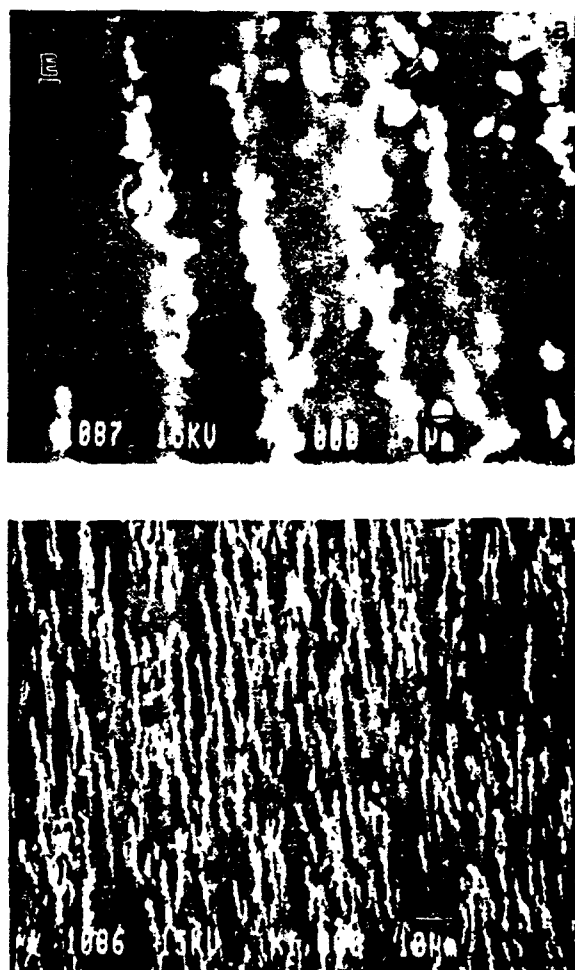

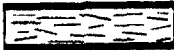




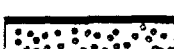
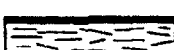

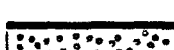
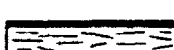



Fig. 3. SEM micrographs of aligned composites with 10 vol% of BaTiO_3 (Saiki BT05). (a) Low magnification. (b) high magnification.

Table 2

Estimated dielectric constants for the series, logarithmic and parallel connectivity models and for various volume fractions of BaTiO₃ powders using dielectric constant values $K_1 = 300$ (for BaTiO₃ (TAM, Sakai)) and $K_2 = 2.8$ (for silicone elastomer)

Volume (%)	Electric field (connectivity)	Series	Logarithmic	Parallel	Measured K (kHz)
20 ^{a,b)}		3.5	7.1	62	8.0
20 ^{c)}		3.5	7.1	62	3.1
20 ^{d)}		3.5	7.1	62	20
10 ^{a,b)}		3.1	4.5	32	3.3
10 ^{c)}		3.1	4.5	32	3.3
10 ^{d)}		3.1	4.5	32	11.5
20 ^{b,c)}		3.5	7.1	62	3.2
20 ^{c)}		3.5	7.1	62	3.0
20 ^{d)}		3.5	7.1	62	18
10 ^{b,c)}		3.1	4.5	32	4.0
10 ^{c)}		3.1	4.5	32	3.7
10 ^{d)}		3.1	4.5	32	11.5

^{a)} TAM Ceramics. ^{b)} Unaligned dispersion $E \approx 0$. ^{c)} Section perpendicular to the applied field.

^{d)} Section parallel to the applied field. ^{e)} Sakai Chemical BT05 (0.5 μm).

silicone elastomer polymer can be achieved by using dielectrophoretic effect. Quasi 1-3 composite connectivity is induced and is verified from electron microscopy observations and the estimated and measured dielectric constant values.

Acknowledgement

This work was possible thanks to the funding DARPA Nanocomposite Program NEDO International Joint Research Program No. 3-1203. The SEM characterization was performed under DOE contract. Many thanks to personnel at the High Temperatures Materials Laboratory at Oak Ridge National Laboratories, especially Drs. V. Tennery, T.

Nolan, and L. Allard. Thanks also to Brigitte Stumberger for technical assistance in microtoming composites and JoAnn Mantz for typing this manuscript.

References

- [1] N. Webb, *Chem. Britan* 4 (1990) 438.
- [2] T.D. Jones, *Proceedings of 2nd Intern. Conference on E.R. Fluids*, Technomic Publishing Company (1989) pp. 14-26.
- [3] C.A. Randall, D.V. Miller, J.H. Adair and A.S. Bhalla, *American Ceramic Society 93rd Meeting*, Cincinnati (1991).
- [4] C.A. Randall, D.V. Miller, J.H. Adair and A.S. Bhalla, *J. Mater. Res.*, submitted for publication.
- [5] R.E. Newnham, *Ann. Rev. Mater. Sci.* 16 (1986) 47.
- [6] J.D. Kingsley, H.K. Bowen and D.R. Uhlmann, *Introduction to Ceramics* (Wiley, New York, 1976) pp. 917-919.
- [7] J. Ishikawa, *Phys. Rev. B* 37 (1988) 5552.
- [8] K. Uchimo, E. Sadahaga and T. Minrose, *J. Am. Ceram. Soc.* 72 (1989) 1555.

APPENDIX 22.

Structure Property Relationships in Core-Shell BaTiO₃-LiF Ceramics

C. A. Randall, S.F. Wang, D. Laubscher, J.P. Dougherty, and W. Huebner

Materials Research Laboratory

Pennsylvania State University

University Park, PA 16802

Abstract

A sintering, microstructural development and dielectric property study of BaTiO₃-LiF ceramics was performed to assess the potential application for low-fired multilayer capacitors. Not only does LiF allow for sintering below 1000°C, it also allows for the manipulation of dielectric properties and interfaces within BaTiO₃-LiF ceramics. Using mixing laws, a model of the dielectric properties of the core-shell microstructures is presented that agrees well with the observed experimental data.

Introduction

Ceramic multilayer capacitor (MLC) formulations based on BaTiO₃ can be either chemically or physically modified to exhibit the required temperature-stable dielectric behavior. The so-called intermediate dielectric constant capacitor compositions, X7R, require less than ±15% deviation from the 25°C dielectric constant ~4000 over a temperature range of -55°C to 125°C. This stability can result either from chemical substitution in the ceramics or from the presence of core-shell grains in fine-grained microstructures as reviewed by Kahn et al.¹

The core-shell microstructures are the result of a specific type of chemically inhomogeneous BaTiO₃ grains as discussed by Kahn¹ and Hennings et al.² In general, additives and dopants soluble to the perovskite structure are incorporated during grain growth and densification processes. This is especially true when recrystallization of the liquid phase occurs during sintering and grain growth is inhibited. These additives are nonuniformly distributed over grains. Owing to the small amount of additives, many BaTiO₃ grains remain undissolved. After saturation of the liquid phase melt with BaTiO₃, a solution-precipitation process starts whereupon smaller particles dissolve and larger ones grow by epitaxially seeding the liquid phase reprecipitation of perovskite from the melt. Larger particles are rounded because of the dissolving

process and contain only pure BaTiO_3 . These are embedded into a perovskite shell that contains a non-uniform chemical distribution of doping.

As this process progresses, more and more additives from the liquid phase are absorbed into the solid-shells. This depletes the additive concentration in the liquid phase that leads to an increase in the melting temperature. Eventually, this can lead to a freezing of the liquid phase to a glassy grain boundary phase. Figure 1 shows a schematic representation of a typical core-shell microstructure observed in BaTiO_3 compositions.

The core-shell chemical distribution is a thermodynamically unstable state. The large chemical gradients within the core-shell microstructure are driving forces for diffusion. High sintering temperatures and/or long sintering times promote a more homogeneous distribution of additives that eventually cause the core-shell microstructure to disappear. This has been clearly verified by Lu et al. in the $\text{BaTiO}_3\text{-ZrO}_2$ system with up to 60 hours of sintering.³

The formation of a core-shell microstructure not only requires liquid phase sintering, solubility of BaTiO_3 into the glass, and reprecipitation of BaTiO_3 including additives into the perovskite structure. There also has to be a limited grain-growth process and limited interdiffusion to a homogeneous distribution of dopants. Given the correct kinetic balance of these conditions during processing, the core-shell microstructures can be formed.

In terms of the dielectric properties, another important criterion is that additives must be Curie shifters.⁴ A Curie shifter is a dopant, that upon entering the perovskite BaTiO_3 causes the paraelectric \rightarrow ferroelectric and also ferroelectric \rightarrow ferroelectric transition temperatures to change. The concentration of the shifter is approximately proportional to the degree of shift in Curie temperature. In the case of non-uniform distributions of dopant shifters, there will be a distribution of local Curie temperatures; this then generally lowers and broadens the peak transition permittivity of pure BaTiO_3 ceramics. The dielectric mixing of these various doped transitions can be tailored under the processing conditions to form X7R capacitor materials.

The aim of this paper is to report the variety of microstructures developed and the corresponding dielectric properties in the low-fired LiF- BaTiO_3 system. Qualitative and quantitative descriptions of dielectric behavior, defect chemistry, and microstructural development is presented and correlated.

2.0. Experimental Procedure

High purity TAM-HPB BaTiO₃ powders were used with a reagent grade LiF and BaCO₃ powders for liquid phase sintering. Calcination of powders were performed in a platinum crucible at 850°C for 1 hour. These calcined powders were milled and mixed with binder (DuPont 5400) to form green ceramic disks. Binder was removed by heating to 500°C for 2 hours. Sintering followed in a closed crucible for 2 hours with temperatures ranging from 800°C to 1150°C. Phase purity of ceramics was characterized using Scintag x-ray diffraction analysis. Additionally, chemical analyses of ceramics were made on bulk samples using a d.c. plasma-emission spectrometer (Spectrametrics, Inc.) and a Dionex Ion Chromatographer. Microstructural analysis is made on ion-beam thinned samples with a Phillips 420 transmission electron microscope.

Dielectric property analysis was measured as a function of temperature and frequency using an HP 4274 Bridge. Measurements were taken on platinum sputtered electroded disks on cooling from 200°C to -150°C over a frequency range from 10-10,000 Hz at a cooling rate of 1°C/min.

3.0 Results

Dielectric Properties:

Dielectric constant and dielectric loss ($\tan\delta = \epsilon''/\epsilon'$) were studied over a temperature range between -150°C and +200°C for a variety of LiF-BaTiO₃ compositions and sintering conditions. Figure 2 shows a series of dielectric constant temperature curves for LiF-BaTiO₃ ceramics sintered at 850°C for 2 hours. The LiF-BaTiO₃ composition range was limited between 0.1 wt% to 2.0 wt %, corresponding to mole fractions between 1 mole % and 18 mole %. Important features to be noted from these curves are the following:

- (a) Small dielectric anomalies exist at the pure BaTiO₃ transition temperature ~125°C for all LiF-concentrations studied at 850°C.
- (b) The large dielectric constant peak maximum shifts to lower temperatures with higher LiF concentrations.
- (c) A broadening and lowering of the dielectric constant maximum occurs with higher LiF concentrations.

- (d) There is also a broadening of the dielectric constant anomalies associated with all phase transitions, cubic→tetragonal, tetragonal→orthorhombic, and orthorhombic→rhombohedral, with higher LiF concentrations.
- (e) With increased LiF content there is a major shifting of the cubic→tetragonal and orthorhombic→rhombohedral phase transitions to lower and higher temperatures, respectively.

Replotting the above data to give temperature dependence of the inverse dielectric constant ($1/K$), classic Curie-Weiss behaviour can be observed above 125°C for all LiF concentrations, Figure 4. This is consistent with an anomaly observed at 125°C (See Figure 2). The parallel Curie-Weiss curves imply the transitions at 125°C have similar Curie constants and are consistent with those of pure BaTiO₃. This suggests a pure BaTiO₃ phase existing within the LiF-BaTiO₃ ceramic.

The dielectric loss temperature dependence is shown in Figure 5 for various LiF-BaTiO₃ compositions sintered at 850°C for 2 hours. The dielectric loss shows anomalies corresponding to phase transitions observed in the temperature dependence of the dielectric constant. The dielectric losses are low (≈ 0.01 at room temperature) and are very suitable for X7R capacitor applications.

The variation of dielectric constant with LiF content in BaTiO₃ ceramics sintered at 1000°C for 2 hours is shown in Figure 6. The important features to be noted are:

- (a) Decrease of the cubic to tetragonal phase transition temperature with LiF content up to 1.0 wt %.
- (b) Increase in dielectric constant maxima with LiF content up to 1.0 wt %.
- (c) Decrease of dielectric constant maxima with LiF in excess of 1.0 wt %.
- (d) Slight decrease in tetragonal→orthorhombic phase transition temperature and a large increase in the orthorhombic→rhombohedral transition temperature with increasing LiF content up to 1.0 wt %.
- (e) Relatively little broadening of dielectric maximum with LiF content compared to 850°C LiF-BaTiO₃ ceramics.

Replotting these data as inverse dielectric constant versus temperature reveals Curie-Weiss behavior, Figure 7. However, the Curie-Weiss behavior departs slightly from linearity. This is the result of Curie-Weiss behavior from lower temperatures superimposing on the overall dielectric characteristics of the ceramic. Note that the Curie-Weiss behaviour is very similar for 1.0 wt % and above. This suggests that a solubility limit has been reached. Also, distinct Curie-Weiss behavior for the tetragonal→orthorhombic transitions can be seen for 0.25 and 0.5 wt % LiF. All of the above dielectric data and the corresponding X-ray diffraction patterns suggest a more homogeneous LiF distribution exists. The dopants appear to be pinching the three ferroelectric transitions towards a cubic→rhombohedral phase transition similar to Ba(Sn,Ti)O₃ systems, as studied by Isupov et al.⁵

With the higher sintering temperature (1100°C) of LiF-BaTiO₃ ceramics, the corresponding dielectric properties are very different. Figure 8 shows the variety of dielectric behaviour for compositions in the range of 0.25 wt % to 2.0 wt % LiF. Important features to be noted with the 1100°C and 2-hour soak time sintered ceramics are:

- (a) Increasing of the dielectric constant maximum with increasing LiF content.
- (b) Lowering of the cubic→tetragonal Curie transition temperature with increasing LiF content.
- (c) Broadening of the dielectric constant peaks with increasing LiF content.
- (d) No evidence of a dielectric constant anomaly corresponding to a pure BaTiO₃ phase within the ceramic.
- (e) Broad and high dielectric constant (~8000) close to room temperature for 1.0 and 1.5 wt% LiF compositions. These compositions are potentially useful for various capacitor applications.

Figure 9 shows the temperature dependence of the dielectric loss for the 1100°C - 2-hour sintered LiF-BaTiO₃ ceramics. These ceramics also show low dielectric loss behaviour. However, with x-ray diffraction and dielectric constant temperature dependence in the 1000°C sintered samples, there is an increase in the chemical inhomogeneity at 1100°C. We believe that there is an inhomogeneous loss of Li from the ceramic. These chemical inhomogeneities give rise to a broad dielectric maximum.

The general trends of the dielectric behaviour with compositions and sintering conditions in LiF-BaTiO₃ systems are discussed in greater detail in Section 4.0.

3.2. Microstructural Studies of LiF-BaTiO₃ Core-Shell Structure.

Transmission electron microscopy (TEM) studies revealed a wide variety of microstructural features in the 2 wt % LiF-BaTiO₃ ceramics. These microstructural features allow us to understand the dielectric properties in more detail, explained later in this paper.

Samples sintered at temperatures 850°C and 1100°C reveals that grains exist with (111) growth twins. This is to be expected in BaTiO₃ when fired below the BaTiO₃-TiO₂ peritectic temperature of 1320°C, as suggested by Schmelz et al.⁶ Typical (111) twins are shown in Figure 10(a) from a LiF-BaTiO₃ ceramic sintered @ 850°C for 2 hours; the corresponding [110] zone axis diffraction pattern is shown in 10(b). The origin of the (111) twins is believed to be the intergrowth of topotaxial Ba₆Ti₁₇O₄₀ planes according to the work of Krasevec et al.⁷

The grain boundaries on both 850°C and 1100°C sintered ceramics reveal glassy phases at the triple junctions and along the grain boundary and is believed to be based on the BaO-Li₂O-TiO₂ system. These glassy phase distributions are typical of liquid phase sintered microstructures. Figure 11 shows a micrograph revealing the glassy phase distribution in LiF-BaTiO₃ ceramics sintered at 850°C. An additional crystalline second phase of LiTiO₂ was identified using both TEM and X-ray diffraction. These findings agree with previous reported studies by Wu et al. (1989).⁸

No evidence for a core-shell structure exists in LiF-BaTiO₃ ceramics sintered @ 1100°C. As can be noted from X-ray diffraction peak broadening and dielectric properties, chemical inhomogeneity of Li and/or F still exists but not on a scale comparable to the core-shell ceramics. A direct chemical analysis using energy-dispersive spectroscopy could not be applied to the LiF-BaTiO₃ ceramics. The BaL_α and TiK_α X-ray peaks overlapped and Li and F characteristic X-rays were not detectable, owing to absorption of low energy X-rays by the detector window.

For low-temperature (850°C) sintered LiF-BaTiO₃ ceramics, core-shell structures are clearly observed. Figure 12 shows a core-shell grain structure in a 2 wt % LiF-BaTiO₃ ceramic sintered at 850°C. The cores have a high density of 90° twin domain configurations corresponding to the tetragonal (4mm) ferroelectric symmetry of BaTiO₃. In the core-shell grains there is often an

associated high density of growth dislocations. Lu et al. suggests that these dislocations may aid in diffusion and hence aid homogenization of the composition.³ Heating the grains above the Curie temperature within the TEM causes the ferroelectric domains to disappear. The structure of the interface between the shell and core is revealed to be semi-coherent with associated dislocations.

An estimate of misfit, δ , can be obtained from the Burger vector, b , and interspacing of the dislocations using equation (9)

$$\delta = \frac{|b|}{D}$$

Where D is the interspacing between dislocations $\approx 3 \times 10^{-8} \text{m}$ and $|b|$ is the Burger's vector magnitude. The Burger's vector being $b \wedge a(100)$ predicts for the LiF-BaTiO₃ core-shell structures a misfit strain, $\delta \approx 1.3\%$ in the high temperature phases. The misfit parameter, δ , is described by:

$$\delta = \frac{a_s - a_c}{a_c}$$

where a_s is cubic phase lattice parameter of the shell region and a_c is cubic phase lattice parameter of core region BaTiO₃.¹⁰ Armstrong et al. point out that the strain mismatch between the core and shell will tend to give a compressive stress to the core regions, which will in turn affect the dielectric properties.¹⁰ Note that a number of previous authors estimate the strains directly from selected area measurements of the TEM foils. The validity of such a method is doubtful because the stress is relieved when producing TEM thin foils. However, estimating the strain from the misfit dislocations is believed to be free of any stress relaxation effects and may be more representative of the stress from a three-dimensional ceramic in its high temperature phase, i.e. above 130°C.

3.4. Chemical Distribution of LiF in BaTiO₃.

Although a direct Energy Dispersive Spectroscopy method to determine compositional variations was not possible, owing to the Ba and Ti X-ray peaks overlapping and the absorption of low energy of Li and F characteristic X-rays. There are still a number of conclusions to be inferred regarding the compositional distribution throughout the microstructure, including the crystal-chemistry of the structure described below.

From the dielectric studies presented in Section 3.0, we can infer that either Li or F is entering the perovskite BaTiO_3 and causing the shift in paraelectric \rightarrow ferroelectric phase transition temperatures. This, of course, is also confirmed with the formation of core shell microstructure as discussed in Section 2.1. The question now arises about which additive, Li and/or F, causes the dramatic changes in microstructure and dielectric properties. An analytical chemical analysis of the sintered BaTiO_3 -LiF ceramics is given in Table I. This analysis demonstrates that there has been a volatilization of F gas, and Li has predominantly been absorbed and remains in the BaTiO_3 perovskite structure. This is not consistent with the earlier predictions which suggested that both Li and F are soluble in BaTiO_3 to give a compositional formula, $\text{Ba}(\text{Ti}_{1-x}\text{Li}_x)(\text{O}_{3-3x}\text{F}_{3x})$.^{8,11} Additionally, there does exist indirect evidence that at high pressure, processed $\text{BaTi}(\text{O}_{3-x}\text{F}_x)$ perovskites decompose to BaTiO_3 and F gas at 650°C ¹¹. This implies that at temperatures used to sinter BaTiO_3 -LiF ceramics, F would be given off as a gas. Hence, all the evidence suggests Li is the important dopant in modifying the BaTiO_3 dielectric properties.

Table I.
Chemical Analysis of LiF- BaTiO_3 Ceramics

Sintering Temperature	BaTiO ₃ (HPB) +0.5 wt % LiF	
	wt % Li	wt % F
700°C/2 hr.	0.11	0.03
800°C/2 hr.	0.10	0.02
900°C/2hr.	0.09	0.02
1000°C/2 hr.	0.07	0.006
1100°C/2 hr.	0.06	0.003

4.0 Discussion

Assuming lithium to be the important soluble cation in BaTiO₃ perovskite, we have to consider its occupancy in the crystal structure. The possibility of an interstitial lithium is an extremely unlikely situation, owing to the high packing density and the defect energy calculations by Lewis and Catlow (1983).¹² In this study only substitutional solid solutions are debated.

The substitution of Li-cations onto the perovskite A-site is unlikely as there is no required evidence of Li in a twelve-fold coordinated site.

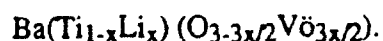
The most likely occupancy for Li with the perovskite structure is the six-fold octahedral B-site. It is noteworthy that the (Shannon and Prewitt) ionic radii for six-fold coordinated lithium is 0.74 Å, which fits into stable perovskite structures as discussed by Megaw.¹³ Since Li ions have a different valence than that of the titanium ion, substitution by lithium produces a charge imbalance, that has to be compensated through defect chemistry processes. The occupancy of Li on the Ti⁴⁺ site constitutes an acceptor doping. These acceptors can be compensated electronically or ionically. Electronic compensation involves the formation of holes in the valence band and may result in p-type behavior. Ionic compensation occurs when the acceptor dopant fixes the doubly ionized oxygen vacancies concentration as shown by Hagemann and Ihrig.¹⁴ In BaTiO₃, the latter is nearly always the case. The net effect of the Li ion substitution is to change the electro-neutrality condition of the defect chemistry, i.e.:

$2[V_{Ba}'] + 4[V_{Ti}'''] + p + 3[Li_{Ti}'''] = n + 2[V\ddot{O}]$ is expressed using standard Kröger-Vink notation.

For ionic compensation at intermediate oxygen pressures and close to stoichiometry, the electro-neutrality condition reduces to:

$$3[Li_{Ti}'''] = 2[V\ddot{O}].$$

The $[Li_{Ti}''']$ acceptor doping fixes the oxygen vacancy concentration with ionic compensation. This corresponds to a perovskite compositional formulation:



For every Li cation substituting a titanium cation there is an equivalent of one and a half oxygen vacancies per unit cell. Hence, if Li substitutionally occupies the perovskite B-site there is a corresponding loss of titania. This is consistent with the discovery of a LiTiO_2 second phase being produced during the sintering process. In addition, the low dielectric losses measured in the LiF-BaTiO_3 ceramics indirectly suggests that the intrinsic electronic conductivity of the ceramic remains largely unchanged. The frequency dispersion in Figure 6(b) suggests an ionic conductivity relaxation mechanism or ionic dipole relaxation. So both structural and electrical properties support the assumption of ionic compensation of the lithium substitution for titanium.

Although the chemical analysis suggests that Li is the dominant soluble additive there exists a possibility of F occupying the anion sublattice. Hence, for completeness we consider the substitution of F in addition to Li. We recall a donor has an effective positive charge with respect to the lattice. In this specific case, the F occupies oxygen sites as a singly ionized donor, $\text{F}_\text{O}^\bullet$ in Kröger-Vink notation.

Considering the electro-neutrality condition with acceptor Li occupancy of the B-site and F-donor occupancy of the anion sublattice we obtain:

$$n + 2[\text{V}_{\text{Ba}}''] + 3[\text{Li}_{\text{Ti}}'''] = p + 2[\text{V}_\text{O}] + [\text{F}_\text{O}^\bullet].$$

When ionically compensated the electro-neutrality condition reduces to :

$$3[\text{Li}_{\text{Ti}}'''] = 2[\text{V}_\text{O}] + [\text{F}_\text{O}^\bullet].$$

The corresponding general substitutional formula for Li and F in BaTiO_3 is then given by:

$$\text{Ba}(\text{Ti}_{1-x}(\text{Li}_{\text{Ti}}''')_x)((\text{O}_{3-1/2(3x+z)})(\text{F}_\text{O}^\bullet)^{\frac{z}{2}}(\text{V}_\text{O})_{(3x/2-z/2)}).$$

It may be that this is self consistent with the previous formula when assuming the trivial case of $[\text{Li}] \gg [\text{F}]$ i.e. $x \gg z$, as was experimentally determined in the chemical analysis (Table I).

The two major influences to be considered for explaining the dielectric behaviour in BaTiO₃ ceramics are traditionally chemical inhomogeneity and internal stresses. Chemical inhomogeneity has often been regarded as the major source of broad or diffuse phase transitions in ferroelectrics.

This chemical inhomogeneity can be on a macroscopic scale, demonstrated by growth striations ~10 to ~100µm in ferroelectric tungsten bronze crystals. Microscopic compositional inhomogeneities are on a submicron scale. This causes the phase transition temperature and spontaneous polarization to vary from one region or "microvolume" to another. Traditionally, this type of description has been linked with the relaxor-like ferroelectrics, e.g. Pb(Mg_{1/3}Nb_{2/3})O₃, after the work of Smolenskii et al.¹⁵ Recently work has shown that the original Smolenskii postulates proposed to explain relaxor behaviors are not valid.^{16,17} Despite the shortcomings of the Smolenskii model for relaxor ferroelectrics, we believe the description to be valid for chemical inhomogeneities in systems such as Ba(Zr,Ti)O₃, (Ba,Sr)TiO₃.^{18,19} These are broad phase transition ferroelectrics that do not have the characteristic dispersive behaviour of dielectric constant and tanδ, which determines a relaxor ferroelectric as described by Cross.²⁰ Below we show the Smolenskii compositional inhomogeneity model can be successfully applied to the dielectric properties of LiF-BaTiO₃ ceramic with core-shell structures.

Owing to the connectivity of the respective phases in core-shell ceramics, the dielectric properties are expected to be dominated by the continuous or semicontinuous shell region volume fraction. The surrounding shell is believed to have microvolumes of various compositions and hence various paraelectric→ferroelectric transition temperatures. Based upon the observed microstructural and dielectric behaviour, we developed the following model. The volume fraction of the core can be described with the following dielectric temperature dependence:

$$\begin{aligned} \langle K(T) \rangle_{\text{core}} &= K_{av} \quad \text{for } 10^\circ\text{C} \leq T \leq T_c \\ &= \frac{4\pi C}{T - T_c} \quad \text{for } T \geq T_c \approx 125^\circ\text{C} \end{aligned}$$

The K_{av} is expected to be similar to that of fine-grain BaTiO₃, owing to the compressive stresses, i.e. $K_{av} \approx 4000$. We assume the core to be elastically clamped, which causes the transition to be second order. Therefore, Curie-Weiss temperature coincides with transition temperature.

The shell volume fraction is comprised of an inhomogenous distribution of phase transitions. The general expression for the average dielectric constant of the shell volume fraction is given by:²⁵

$$\langle K(T) \rangle_{\text{shell}} = \frac{\int_{-\infty}^{+\infty} K(T-T_c') f(T_c') dT_c'}{\int_{-\infty}^{+\infty} f(T_c') dT_c'}$$

Where $f(T_c')$ is a general distribution function describing the spread of microvolume Curie points. This is simply taken to be a Gaussian distribution, i.e.:

$$f(T_c') = \exp [-(T_c' - T_m)^2 / \alpha^2]$$

which is centered on Curie maximum temperature, T_m with a width α . The dielectric temperature dependence $K(T; T_c')$ of the individual microvolumes is regarded as a second order phase transition with transition temperature T_c' , such that:

$$K(T, T_c') = \begin{cases} K'_{av} & \text{for } T < T_c' \\ \frac{4\pi C}{T - T_c'} & \text{for } T > T_c' \end{cases}$$

where C is the Curie constant and T_c' is the local Curie temperature of a ferroelectric microvolume.

These core and shell regions are regarded as the two major contributors to the dielectric properties of 850°C LiF-BaTiO₃ ceramics. With the core-shell structures, there are both substitutional series and parallel components to be considered for dielectric mixing. Hence, the most appropriate mixing law to use is the semi-empirical logarithmic law. The logarithmic expression for the core-shell ceramic is given by:

$$\log \langle K(T) \rangle = V_{\text{shell}} \log \langle K(T) \rangle_{\text{shell}} + V_{\text{core}} \log \langle K(T) \rangle_{\text{core}}.$$

Computer generated dielectric temperature dependence is based on the above model, as seen in Figure 14. Good agreement is obtained with the experimentally determined dielectric dependence found within core-shell structures.

The dielectric behaviour of the 1000°C LiF-BaTiO₃ is the result of an almost homogeneous compositional substitution. Although there is still some finite diffuseness, this is very much reduced compared to the core-shell ceramics. The transition temperatures of the various ferroelectric phases converge at a common temperature with LiF contents up to 1.0% wt%. This gives rise to an enhancement of the dielectric constant. Beyond this, the solubility limit appears to have been approached within the grains. Further addition of LiF contributes to a larger volume fraction of grain boundary phase. This glassy phase has a dielectric constant many orders of magnitude below the BaTiO₃; hence the series mixing of the grain boundary and grain phases reduces the average the dielectric constant of the ceramic.

As can be inferred from the chemical analysis X-ray diffraction and dielectric studies, the 1100°C LiF-BaTiO₃ ceramic sintered samples have an inhomogeneous decomposition of the $\text{Ba}(\text{Ti}_{1-x}\text{Li}_x)(\text{O}_{3-3x/2}\text{V}\ddot{\text{O}}_{3x/2})$ composition. This additional inhomogeneity accounts for the corresponding increase in diffusions in the 1100°C LiF-BaTiO₃ ceramics.

4.0. Summary and Conclusions

The dielectric and microstructural properties have been studied over a wide range of sintering conditions. A wide range of properties are found to occur owing to a variety of chemical inhomogeneities present within the ceramic processing.

A shifting of the Curie temperatures is owing to the solubility of lithium on BaTiO₃ to form $\text{Ba}(\text{Ti}_{1-x}\text{Li}_x)\text{O}_{\frac{3-3x}{2}}\text{V}\ddot{\text{O}}_{\frac{3x}{2}}$. The corresponding dielectric properties were accounted for by using a statistical distribution of ferroelectric transitions. A semi-quantitative analysis was made for LiF-BaTiO₃ sintered at 850°C which possessed a core-shell microstructure. The low firing temperature of 750°C and the dielectric temperature dependence are very attractive for X7R capacitor applications.

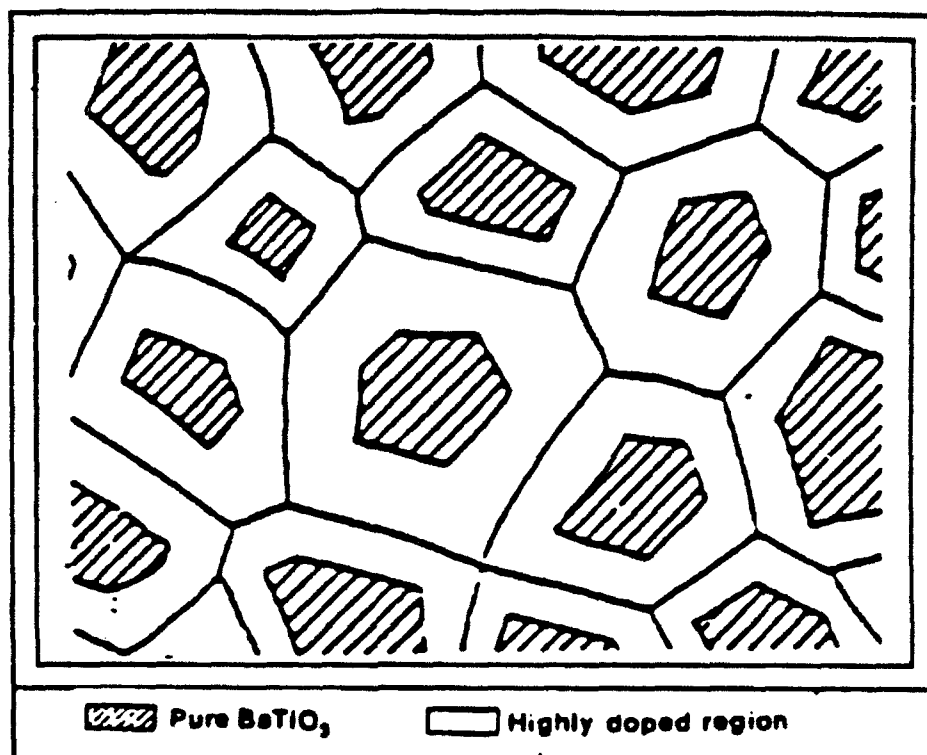


Figure 1. Schematic representation of a typical core-shell microstructure observed in BaTiO₃ composition.

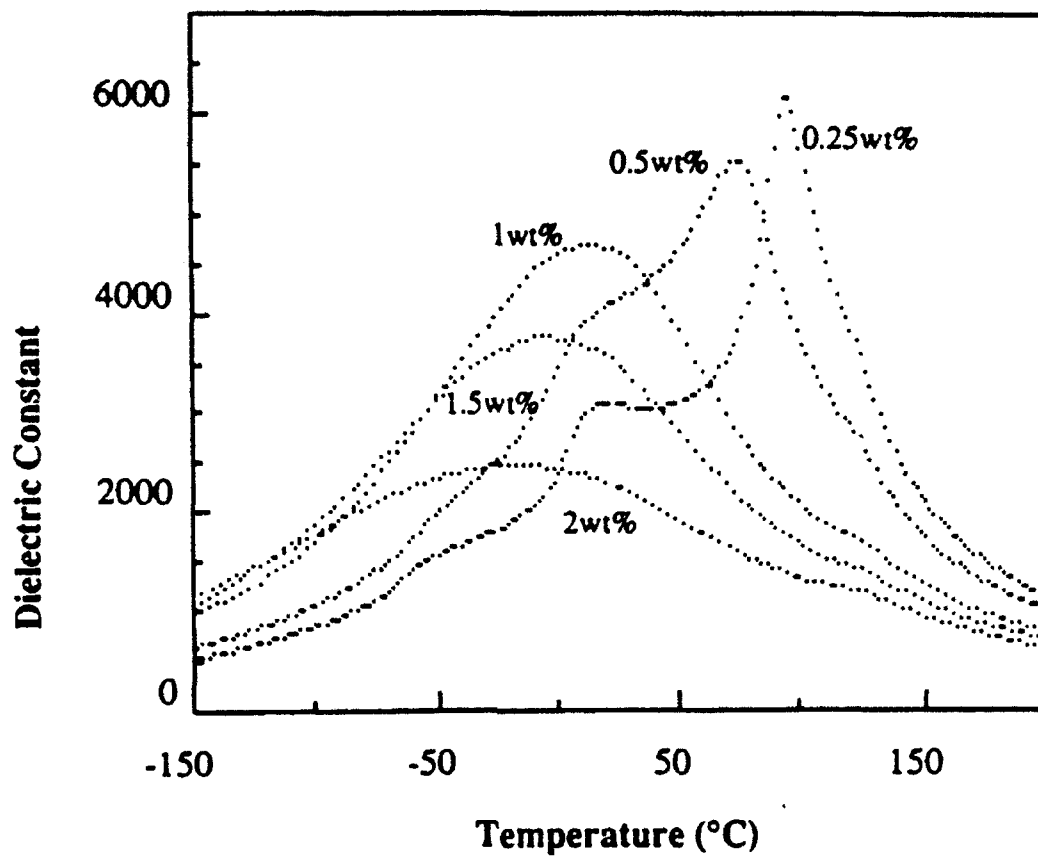


Figure 2. Dielectric constant of BaTiO_3 with various amount of LiF sintered at 850°C for 2 hours.

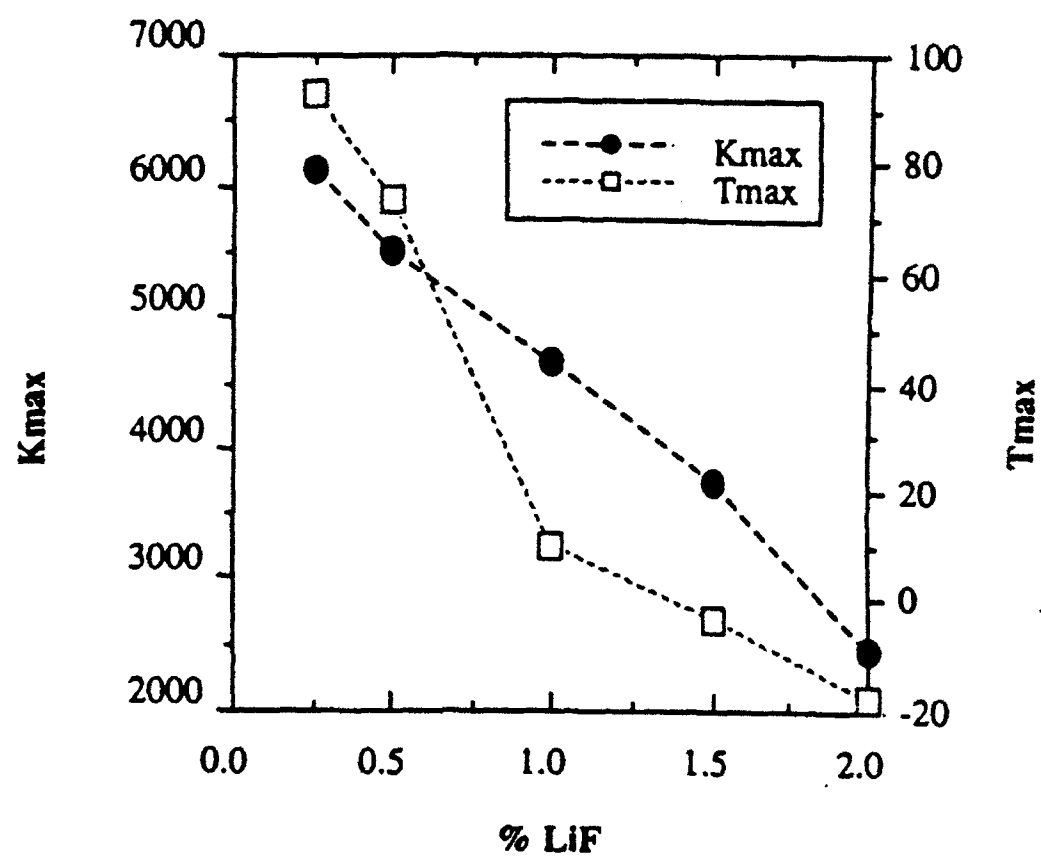


Figure 3. Plot of K_{max} and T_{max} vs. wt% of LiF from Figure 2.

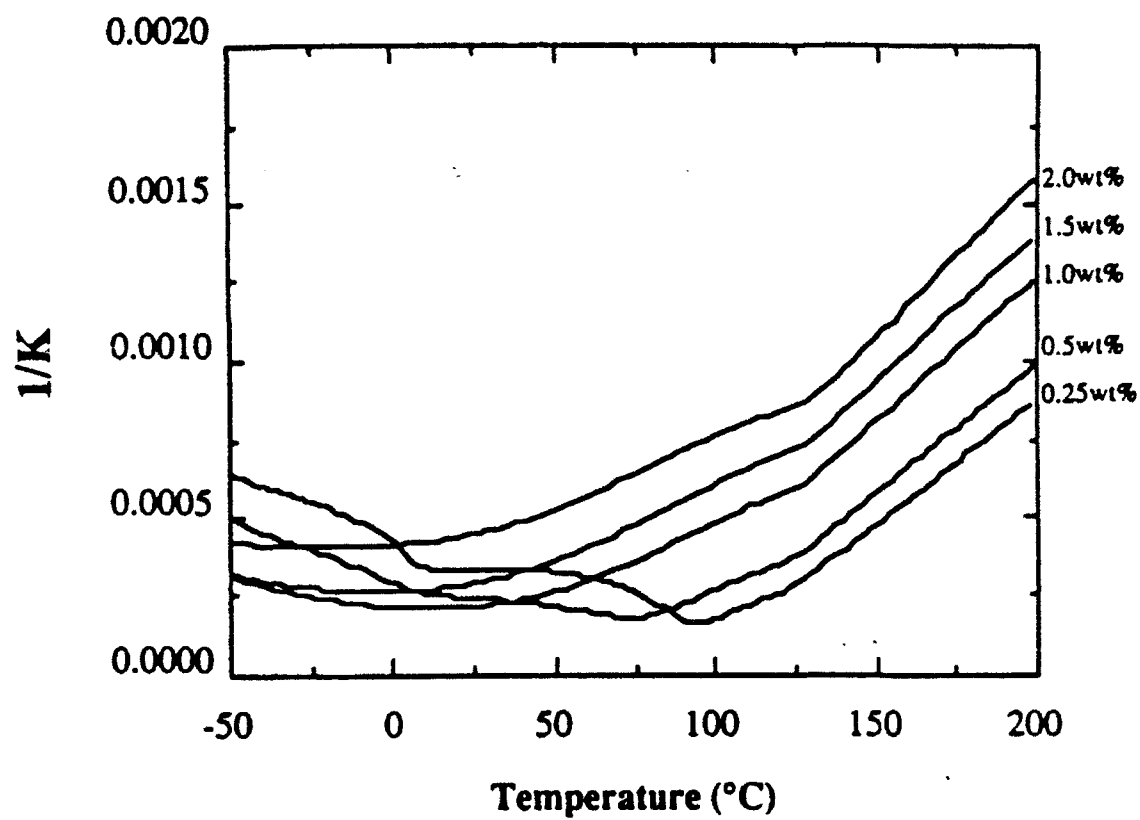


Figure 4. Curie-Weiss plot of the dielectric behavior exhibited in Figure 2

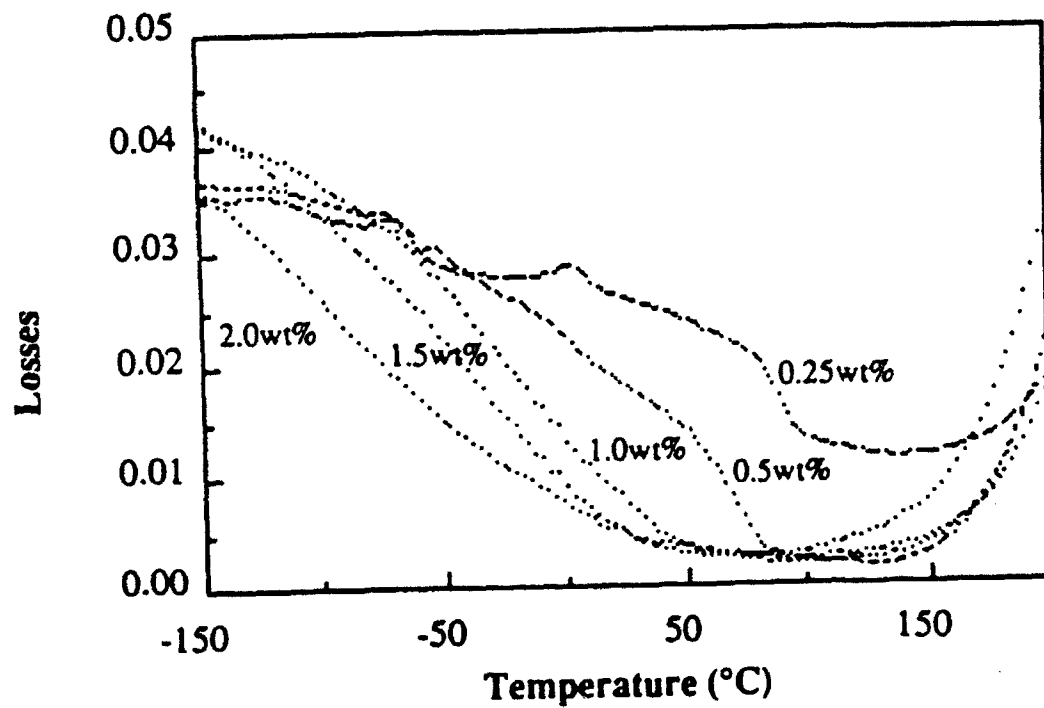


Figure 5. Dielectric loss with temperature for various LiF-fluxed BaTiO₃ sintered at 850°C for 2 hours.

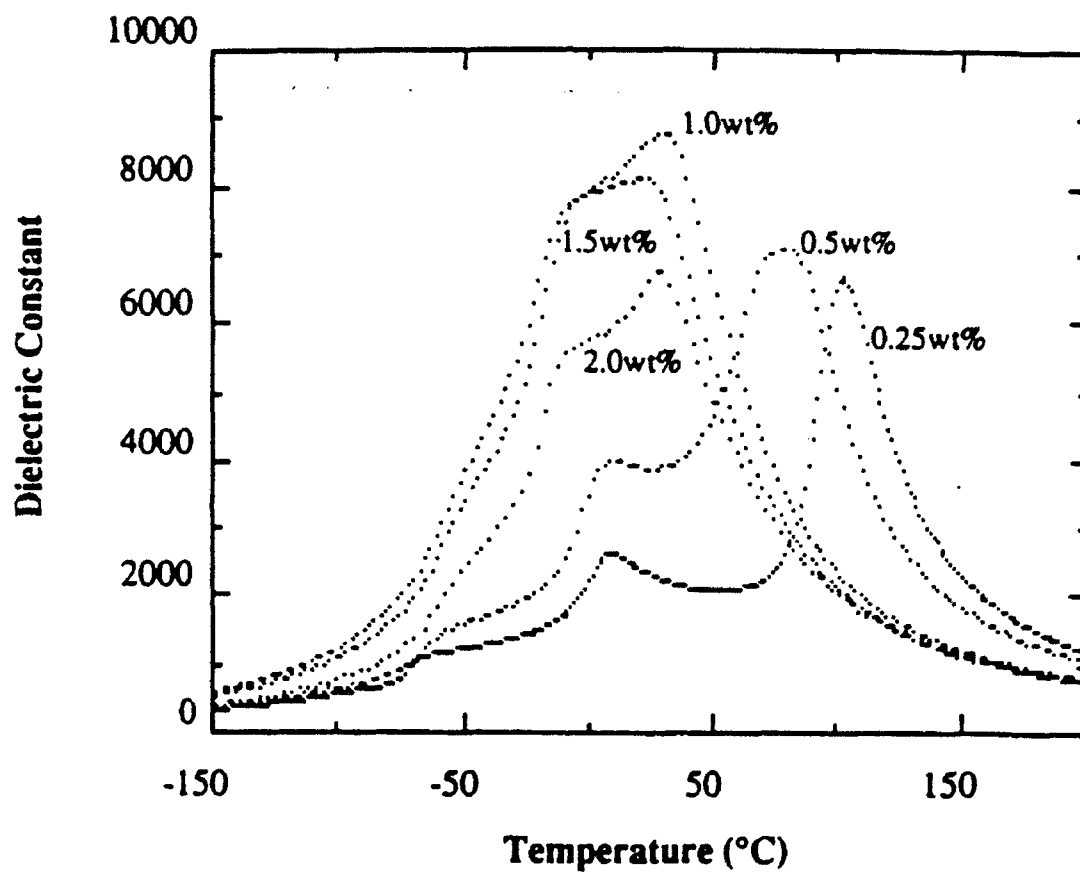


Figure 6. Dielectric constant of BaTiO_3 with various amount of LiF sintered at 1000°C .

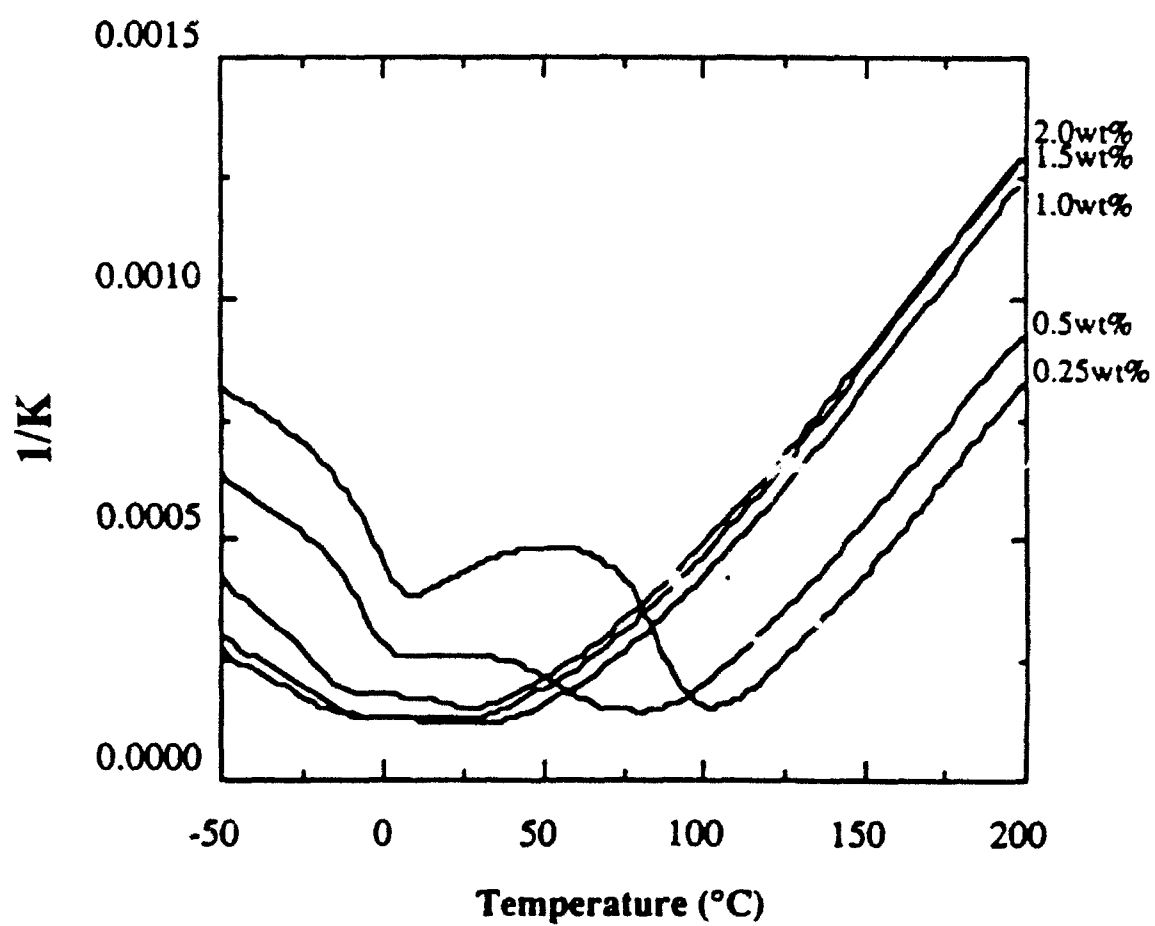


Figure 7. Curie-Weiss plot of dielectric behavior exhibited in Figure 6.

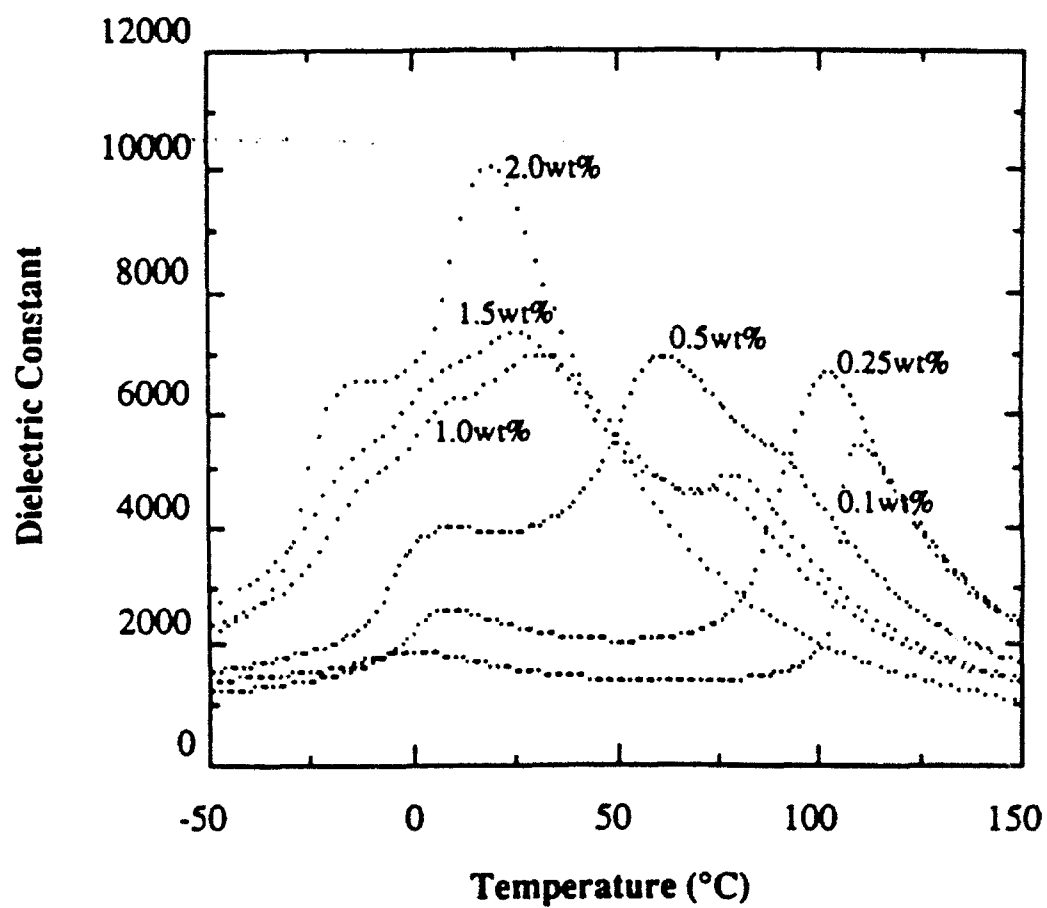


Figure 8. Dielectric constant of BaTiO_3 with various amount of LiF sintered at 1100°C for 2 hours.

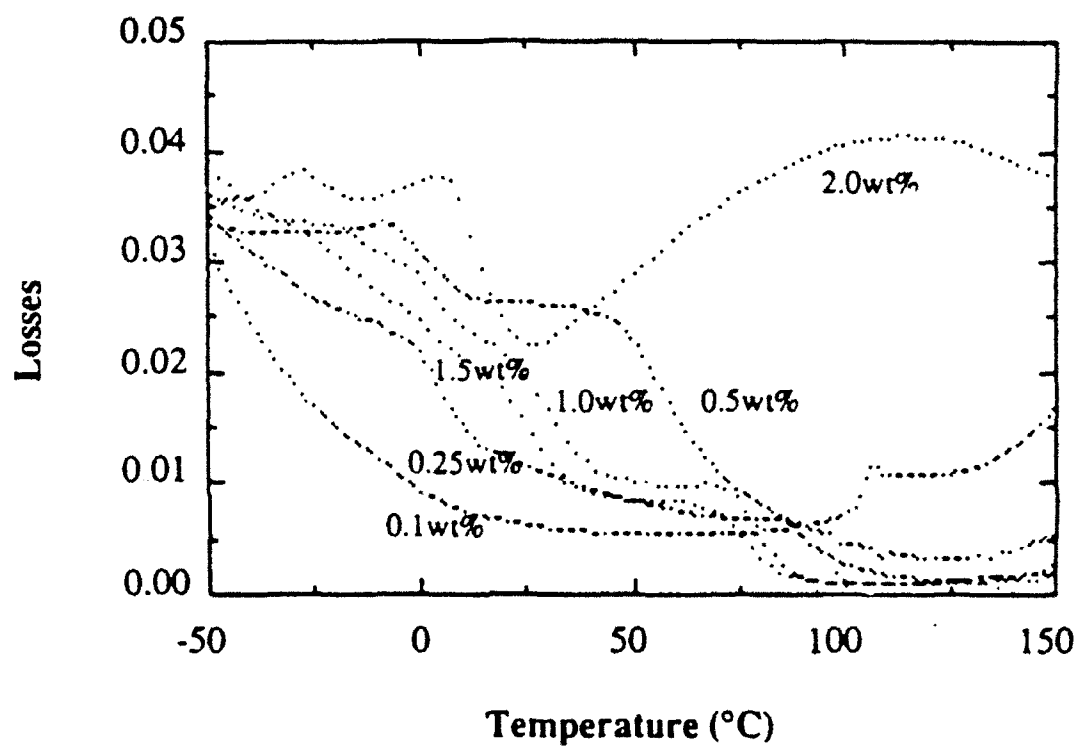


Figure 9. Dielectric loss with temperature for various LiF-fluxed BaTiO₃ sintered at 1100°C for 2 hours.

(a)



(b)

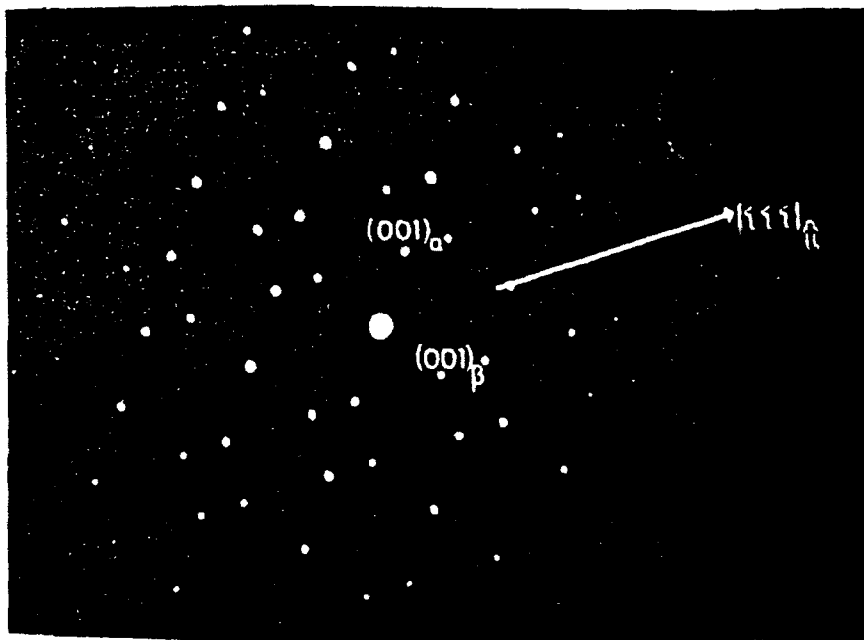


Figure 10. (a) TEM micrograph of (111) growth twin presence in the BaTiO_3 with 2wt% LiF sintered at 850°C for 2 hours. (b) The corresponding [110] selected area diffraction pattern of (a).



Figure 11. TEM micrograph of BaTiO₃ sintered with 2wt% LiF at 850°C for 2 hours, showing glassy phases in the grain boundary regions.

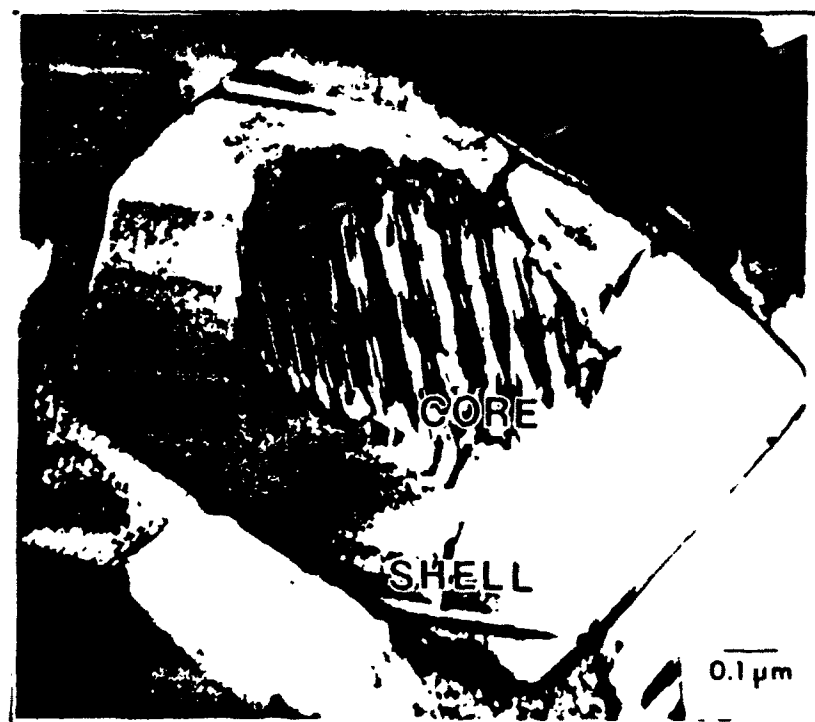


Figure 12. TEM micrograph showing grain core shell structure of LiF-fluxed BaTiO_3 sintered at 850°C.

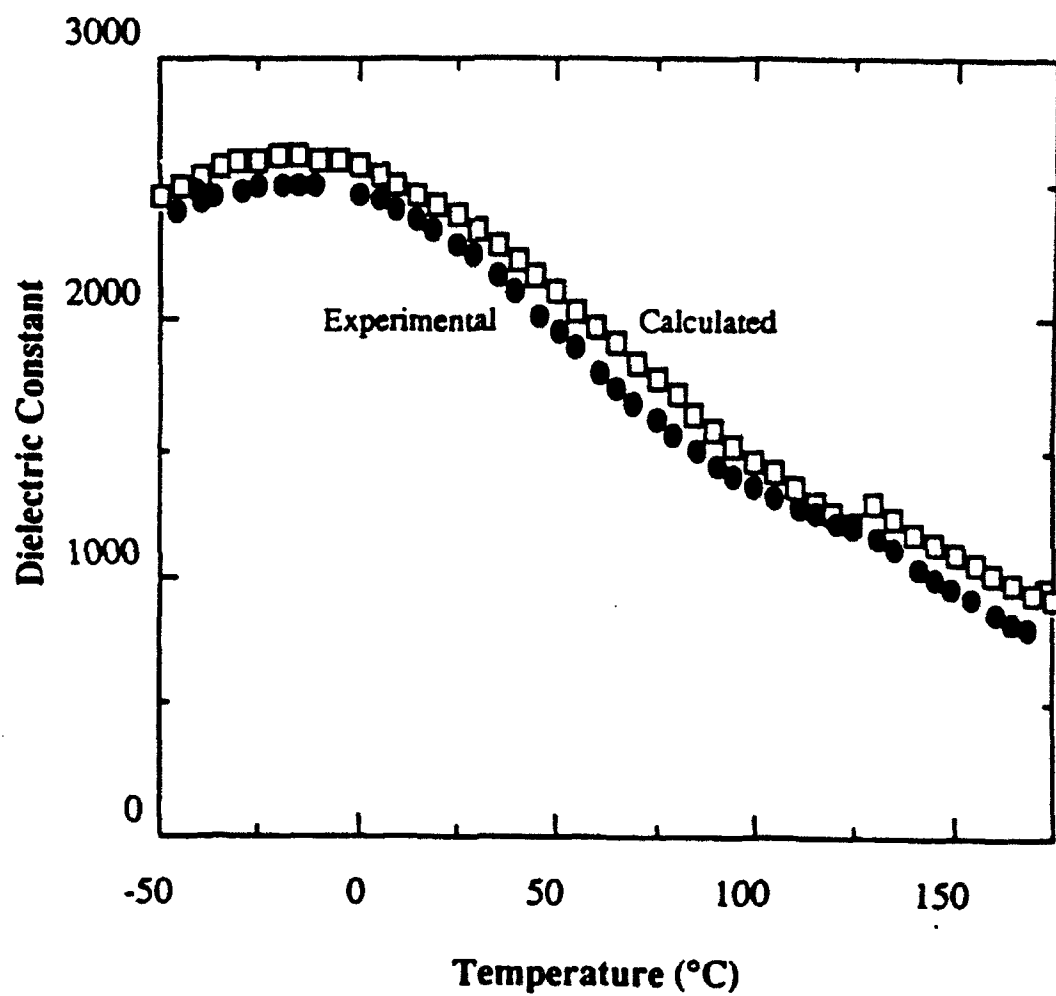


Figure 13. Calculated and experimental dielectric constant with temperature for BaTiO₃ sintered with 2wt% LiF at 850°C.

THIS
PAGE
IS
MISSING
IN
ORIGINAL
DOCUMENT

References

1. B.S. Rawal, M. Kahn, and W.R. Buessem, "Grain Core-Grain Shell Structures in BaTiO₃ Based Dielectrics" in *Advances in Ceramics*, Vol. 1, Grain Boundary Phenomena in Electronic Ceramics, Edited by L.M. Levinson. American Ceramic Society, Columbus, OH, 1981.
2. D. Hennings and G. Rosenstein, "Temperature-Stable Dielectrics Based on Chemically Inhomogeneous BaTiO₃," *J. Am. Ceram. Soc.*, Vol. 67, No.4, 249-255 (1985).
3. H.Y. Lu, J.S. Bow, and W.H. Deng, "Core-Shell Structures in ZrO₂-Modified BaTiO₃ Ceramic," *J. Am. Ceram.*, Vol. 73, No. 12, 3562-68 (1990).
4. B. Jaffe, W.R. Cook, H. Jaffe, *Piezoelectric Ceramic*, Academic Press, New York, 1971.
5. G.H. Smolenski and V.A. Isupov, *Sov. Phys. Tech. Phys.*, Vol. 24, 1375 (1954).
6. H. Schmelz and A. Meyer, "The Evidence of Abnormalous Grain Growth Below the Eutectic Temperature in BaTiO₃ Ceramic," *Dtsch. Keram. Ges.* 59, No. 8/9, 436-440 (1982).
7. V. Krasevec, M. Drofenik, and D. Kolar, "Genesis of (111) Twin in Barium Titanate," *J. Am. Ceram. Soc.*, Vol. 73, No. 4, 856-860 (1990).
8. J.N. Lin and T.B. Wu, "Wetting Reaction Between Lithium Fluoride and Barium Titanate," *J. Am. Ceram. Soc.*, Vol. 72, No. 9, 1709-12 (1989).
9. D.A. Porter and K.E. Easterling, "Phase Transformations in Metals and Alloys," Van Nostrand Reinhold, Inc., 1981.
10. T.R. Armstrong and R.C. Buchanan, "Influence of Core-Shell Grains on the Internal Stress State and Permittivity Response of Zirconia-Modified barium Titanate," *J. Am. Ceram. Soc.*, Vol. 73, No. 5, 1268-73 (1990).
11. T. Endo, T. Kobayashi, T. Sato, and M. Shimada, "High Pressure Synthesis and Electrical Properties of BaTiO_{3-x}F_x," *J Mater. Sci.*, Vol. 25, 619-621 (1990).
12. G.V. Lewis and C.R.N.A. Catlow, "Computer Modeling of Barium Titanate," *Rad. Effects*, Vol. 73, 307-14 (1983).
13. H.D. Megaw, "Temperature Changes in the Crystal Structure of Barium Titanate Oxide," *Proc. Phys. Soc. London*, Vol. A189, 261-83 (1947).
14. H.J. Hagemann and H. Ihrig, "Valence Change and Phase Stability of 3d-doped BaTiO₃," *Phys. Rev.* Vol. B20, 3871-3878 (1979).
15. G.A. Smolenski, "Physical Phenomena in Ferroelectrics with Diffuse Phase Transitions," *J. Phys. Soc. Jap. Suppl.*, Vol. 28, 26 (1970).
16. D.D. Viehland, Ph.D. Dissertation, Pennsylvania State University, 1991.

17. C.A. Randall and A.S. Bhalla, "Nanostructural-Property Relations in Complex Lead Perovskites," Jap. J. Appl. Phys., Vol. 29, No. 2, No. 2, 327-333 (1990).
18. I.C. Ho and S.L. Fu, "Effects of Zirconium on the Structural and Dielectric Properties of (Ba, Sr)TiO₃ Solid Solution," J. Mater. Sci., Vol. 25, 4699-4703 (1990).
19. D. Hennings and A. Schnell, "Diffuse Ferroelectric Phase Transitions in Ba(Ti_{1-y}Zr_y)O₃ Ceramic," J. Am. Ceram. Soc., Vol. 65 No. 22, 539-544 (1982).
20. N. Setter and L.E. Cross, "The Role of B-Site Cation Disorder in Diffuse Phase Transition Behavior of Perovskite Ferroelectrics," J. Appl. Phys. Vol. 51, No 8, 4356-4360 (1980).
21. H. Diamond, "Variation of Permittivity with Electric Field in the Perovskite-Like Ferroelectrics," J. Appl. Phys., Vol 32, No. 5, 909-915 (1961).

APPENDIX 23

Spatial Variations of Polarization in Ferroelectrics and Related Materials

C.A.Randall, G.A. Rossetti, Jr., and W. Cao
Materials Research Laboratory
The Pennsylvania State University
University Park, PA 16802

Abstract

Electron microscopy studies in lanthanum doped lead titanate reveals the evolution of a spatial modulation in the magnitude of the spontaneous polarization with the increase of the lanthanum dopant. On the incorporation of ~ 25 atom percent lanthanum, the conventional domain structure becomes ill-defined, and tweed microstructures are observed. The structural information can be associated with the change from normal ferroelectric to diffuse ferroelectric phase transition behavior. Different from twin structures, these modulated structures represent a new type of polarization variation existing within a single domain. Further understanding of the observed spatial variation in polarization requires structural analysis at the atomic scale. Holographic electron microscopy is proposed as a potential tool to study various polarization gradients in ferroelectric materials. Understanding the spatial variations in polarization is essential to more fully comprehend the extrinsic contributions to the elasto-dielectric properties in ferroelectrics.

Introduction

Mesoscopic structures within ferroelectrics and related materials have important consequences with respect to the macroscopic elasto-dielectric properties. These structures exist on a scale of a few tens to a few thousands of angstroms and include defect structures within the lattice as well as the polarization domain structures associated with the ferroic phase transition. In general, there are two contributions to the elasto-dielectric properties: the intrinsic contribution, which is related to the ferroelectric (antiferroelectric) atomic structure, and the extrinsic contribution, which is associated with domains and defects.^{1,2} In technologically important materials, such as $\text{Pb}(\text{Zr,Ti})\text{O}_3$, the extrinsic factors can contribute as much as 70% to the total elasto-dielectric response (see Figure 1). Therefore, it is necessary to develop a greater understanding of all the possible defect and polarization mechanisms which could contribute to the extrinsic elasto-dielectric properties. However, a comprehensive theoretical description of the extrinsic contributions is currently not in place.

The most common mesoscopic structures associated with ferroelectric and related materials are domains and domain walls. Domains form at the phase transition and relate the low temperature phase to the high temperature prototype phase via certain symmetry constraints. In the example of "normal" first- or second-order ferroelectric transitions, each domain is an area of uniform polarization, and the boundary which divides two domains (i.e. a twin structure) is known as the domain wall. The domain wall is a region of distorted crystal structure in which there exists a spatial transition of the polarization from one orientation state to another.

There are two main types of twin structures. One type is a twin with inversion symmetry of the polarization but in which the strain is the same in both variants. The second type is a twin of two variants with different orientation for both polarization and strain. Ferroelectric twins are typically of the head to tail configuration. There are reports of other domain configurations, such as head-to-head types, but these have not been extensively investigated.^{3,4}

The fine structure of the ferroelectric domain walls depends on a number of inter-related parameters: including the symmetry, temperature, order of the phase transition, spontaneous polarization, and the electrostrictive and elastic compliances. A number of analytical descriptions now exist to describe the spatial variation of the order parameter in a ferroelectric domain wall.^{5,6,7} However, some of the parameters required by the theory cannot be easily acquired with current experimental techniques, and so there is a need to develop new experimental methods to study polarization variations in these materials.

Defects and dopants are known to have a strong influence on the elasto-dielectric properties of ferroelectrics and related materials. Theoretical treatments of the role of defects near structural phase transitions are usually restricted to defect densities that are much less than the reciprocal correlation volume ($\sim 10^{18} \text{ cm}^{-3}$).⁸ In the perovskite ferroelectrics of commercial interest, such a situation is almost never realized.

This article outlines some of the results observed by diffraction contrast electron microscopy in perovskite-based ferroelectrics.¹⁰ From these results, and requirements of the theoretical developments, there is an urgent need to experimentally investigate the polarization gradients, both within the domain region and in the region of the domain wall. Electron holography is discussed as a technique potentially capable of quantifying the polarization gradients in these materials.

Results and Discussion

La-doping in PZT-based Perovskites

Doping in $\text{Pb}(\text{Zr,Ti})\text{O}_3$ -based materials by lanthanum is used as a means to soften the switching characteristics of piezoelectric materials.¹¹ Additionally, the incorporation of lanthanum facilitates the fabrication of transparent ceramics for an optoelectronic applications¹² In general, doping with lanthanum has a significant influence on many of the elasto-dielectric properties. For sufficiently high levels of doping in Zr-rich PZT compositions, this leads to the observation of diffuse phase transition behavior having strong dielectric dispersion. Ferroelectrics with this behavior are generally referred to as relaxors, and are of technological importance owing to their unique electrostrictive, capacitive, and optoelectronic properties. The domain structures of relaxor $(\text{Pb,L a})(\text{Zr,Ti})\text{O}_3$ (PLZT) ceramics are difficult to study using transmission electron microscopy. However, by carefully cooling a 8.2/70/30 composition, a microdomain contrast could be detected, as shown in Figure 2(a). Under the irradiation of the electron beam, the domain structure is unstable. By agitating the structure through focusing/defocusing the beam, the domain configuration transforms to a more stable ordered structure, Figure 2(b). It is believed that thermally induced stresses switch the microdomain structure to a new domain configuration.¹³

The end-member of the PZT solid solution, PbTiO_3 , has the highest transition temperature ($T_c = 490^\circ\text{C}$) and the largest strain ($c/a - 1 \sim 6.5\%$) within the perovskite family. This makes PbTiO_3 an ideal material to study by transmission electron microscopy. Doping PbTiO_3 with lanthanum (PLT) reduces both the phase transition temperature and the characteristic discontinuity of the first-order transition. A systematic study of the structural effect of lanthanum on the polar domain structure in PLT ceramics reveals the development of a strain texture within the normal domains, Figure 3(a),(b),(c). Using diffraction contrast invisibility conditions, we were able to deduce that the texture is the result of a non-uniform spontaneous deformation along the c -axis within the domain. As shown in Figure 3(a), for a sample doped with 1 atom % La, there is no evidence of a texture. As the lanthanum concentration is increased from between 5 and 10 atom %, texturing appears, and this becomes progressively more pronounced with increasing dopant concentration. When the dopant concentration reaches 25 atom %, a normal domain structure is

not identified, and a full cross-hatched or "tweed" domain structure is observed below the transition temperature, Fig. 3d. Similar structures have been observed in ferroelastic systems such as $\text{YBa}_2(\text{Cu}_{0.9}\text{Fe}_{0.03})_3\text{O}_{7-\delta}$ and Mg-Cordierite.^{14,15} Inhomogeneous polarization distributions are not unique to the PLZT system, but also exist in the complex lead $\text{Pb}(\text{B}''\text{B}''')\text{O}_3$ perovskite systems. In these systems, the intermediate scale B-site cation ordering is the source of the polarization modulation.¹⁶ In order to further our understanding of the polarization variation in these materials, we need to develop a technique to quantify the polarization gradients and defect structures. In this regard, the potential of the electron holography technique is discussed below.

Electron Holography

The idea of using coherent electrons in electron microscopy was proposed in 1949 by Gabor in an attempt to extend the limits of electron microscope resolution.¹⁷ However, the realization of electron holography was achieved only in the 1980's owing to the development of a coherent field-emission electron beam. Commercial instruments for electron holography have been developed by Hitachi Ltd. and Philips but have only recently become available. The principle of electron holography is similar to that of optical holography, in which the the phase and amplitude of the electron beam are recorded simultaneously. Because the phase change is much more sensitive than the amplitude variation, more information can be gathered from holographic images as compared with conventional and high resolution electron microscopy. There have been a variety of applications for this new technique starting since 1980, especially in the study of magnetic domains and fluxons in superconducting materials.¹⁸

Recently the possibility of using the holography technique to study ferroelectric domain walls and other defect structures in ferroelectrics was recognized. Some encouraging results have been reported on the profiles of domain walls, as shown in Figure 4.¹⁹ The kink-like electron interference fringe pattern closely resembles the space profile of the polarization vector across a domain wall as predicted by the Landau-Ginzburg model.^{5,6} Although a complete theoretical description of the fringe profile in Ref. 18 is not currently available, the fact that the electric field variation can be probed on a scale less than 1 Å is both exciting and promising.

It has been demonstrated that the electron holography technique may also be used to study the location of aliovalent dopants inside crystal structures through the perturbed local electric fields. As shown in Fig. 4a the fringe bifurcations occurred across the domain wall. Potential contour reveals there are charge centers attracted to the domain wall (see Figure 4b).²⁰ This information may lead to a significant advance in the understanding of the effect of dopants, and may shed new light on the study of interactions between the dopants and domain walls and other polarization modulations as described above.

Quantitative study of the polarization profiles can have a significant impact on the fundamental understanding of ferroelectrics. Once the relationship between the fringe variation and the polarization space profile is established, one can obtain the polarization gradient coefficients through back fitting the observed domain profiles to the theoretical results on domain walls.⁷ These gradient coefficients are a measure of the nonlocal coupling strength. Using lattice dynamics, one may correlate these gradient coefficients to the dispersion surface near the soft mode of the paraelectric-ferroelectric phase transition.²¹ Hence, the electron holography technique, together with the continuum model described in Ref. 6, can potentially provide a methodology to study the characteristics of the over damped soft mode in systems such as BaTiO₃, which could not be directly probed through inelastic neutron scattering.

As a new technique, many problems still exist in the electron holography, especially with regard to the interpretation of the observed fringes. In principle, the total phase shift of high energy coherent electrons passing through a ferroelectric thin sample may be calculated from the following equation²²

$$\phi(x_0, y_0) = \frac{\pi}{\lambda \Sigma} \int V(x_0, y_0, z) dz$$

where λ is the electron wavelength, x_0 and y_0 define the point on the thin sample, Σ is the electron energy, and $V(x_0, y_0, z)$ represents the electrical potential experienced by the traveling electrons. However, $V(x_0, y_0, z)$ represents the total potential, and it is quite difficult to delineate contributions from the "bound" charges (relevant to the polarization) and the "free" charges (relevant to compensation). We believe this is the main reason for the inconsistencies encountered in the current studies of ferroelectrics using electron holography. More theoretical analysis of the interpretation of the holography results is in order.

Conclusions

Observations by conventional transmission electron microscopy techniques on ferroelectric and related materials reveal a variety of polarization modulations which can be induced when there exists coupling of the primary order parameter to symmetry breaking defects. From the evolution of the modulated structures and domain structures, one can see some link between these mesoscopic structures and the extrinsic elasto-dielectric properties.

A new electron-microscopy technique using coherent electrons known as electron holography opens up opportunities in the study of domain walls and defect structures. In this technique, phase shifts can be correlated to local variations of the electrostatic fields within materials. Further development of this new technique in the study of ferroelectrics may help us to

gain new insight into the mechanisms of extrinsic contributions to the macroscopic elasto-dielectric properties.

Acknowledgements

We wish to thank ONR Grant No. N00014-89-J-1689 and AFOSR-91-0433 for partly funding this program. We also wish to thank Drs. D. C. Joy, Xiao Zhang, and Larry Allard for many useful conversations regarding electron holography and Dr. L.E. Cross for discussions on ferroelectrics in general.

References:

- 1 M. Marutake, J. Phys. Soc. Japan, 11, 807 (1956).
- 2 A. G. Luchaninov, L. Z. Potikha and V. A. Rogozin, Zh. Tekh. Fiz., 50, 616 (1980).
- 3 S. I. Yakunin, V.V. Shakmanov, G. V. Spivak and N. V. Vasileva, Sov. Phys. Solid State, 14, 310 (1972).
- 4 C. A. Randall, D. J. Barber, and R. W. Whatmore, J. Mat. Sci., 22, 925 (1987).
- 5 V.A. Zimov, Sov. Phys. JETP 35, 822 (1959).
- 6 W. Cao and L. E. Cross, Phys. Rev. B 44, 5 (1990).
- 7 W. Cao and G. R. Barsch, Phys. Rev. B 41, 4334 (1990).
- 8 A. P. Levanyuk and A. S. Sigov, in "Defects and Structural Phase Transitions" Gordon and Breach Science Publisher, New York (1987).
- 9 E. K. H. Salje, Acta Cryst., A47, 453 (1991).
- 10 P. Hirsch, A. Howie, R. B. Nicholson, D. W. Pashley, M. J. Whelan "Electron Microscopy of Thin Crystals" Robert Krieger Publishing Co. New York (1965).
- 11 B. Jaffe, W. R. Cook and H. Jaffe, in "Piezoelectric Ceramics" Academic Press Inc., New York (1971).
- 12 G. H. Haertling and C. E. Land, Am. Cer. Soc., 54, 1 (1971).
- 13 C. A. Randall, D. J. Barber, and R. W. Whatmore, J. Microsc., 145, 275 (1987).
- 14 Y. Zhu, J. Jaffe and M. Suenagan, MRS Bul., 54 (1991).
- 15 E. K. H. Salje, Phase Transitions, 34, 25 (1991).
- 16 C. A. Randall, A. S. Bhalla, T. R. Shrout and L. E. Cross, J. Mat. Res., 5, 829 (1990).
- 17 D. Gabor, Proc. R. Soc. London, Ser. A. 197, 454 (1949).
- 18 see the review article by A. Tonomura, Rev. of Mod. Phys., 59, 639 (1987) and the references thereafter.
- 19 X. Zhang, T. Hashimoto, and D.C. Joy, Appl. Phys. Lett. 60, 784 (1992).
- 20 X. Zhang and D. C. Joy, Presentation in Materials society Meeting, Boston, Massachusetts, 1992.
- 21 W. Cao, to be published.
- 22 G.F. Missiroli, G. Pozzi, and U. Valdré, J. Phys. E 14, 549 (1981).

Figure Captions

- Figure 1. Temperature dependence of the dielectric permittivity of doped-PZT ceramics. The theoretical value from the Landau-Devonshire theory is also shown.
- Figure 2. (a) Bright field image of liquid nitrogen cooled PLZT 8.2/70/30 relaxor ferroelectric revealing a microdomain structure. (b) An *in situ* switched pseudo-domain structure of (a).
- Figure 3. Bright field image of domain structures in a solid solution series $(\text{Pb}_{1-3x/2}\text{La}_x)\text{TiO}_3$ with four different La contents.
- Figure 4. An electron hologram of a 90° domain wall in BaTiO_3 , the fringe bending is related to the polarization difference across the domain wall (ref. 19).
- Figure 5. (a) An electron hologram showing anomalous fringe bifurcations in a 90° domain wall in BaTiO_3 . (b) Electron interferogram of the same area of (a) shows charge defect centers within the wall (courtesy of Drs. D. Joy and X. Zhang).²⁰

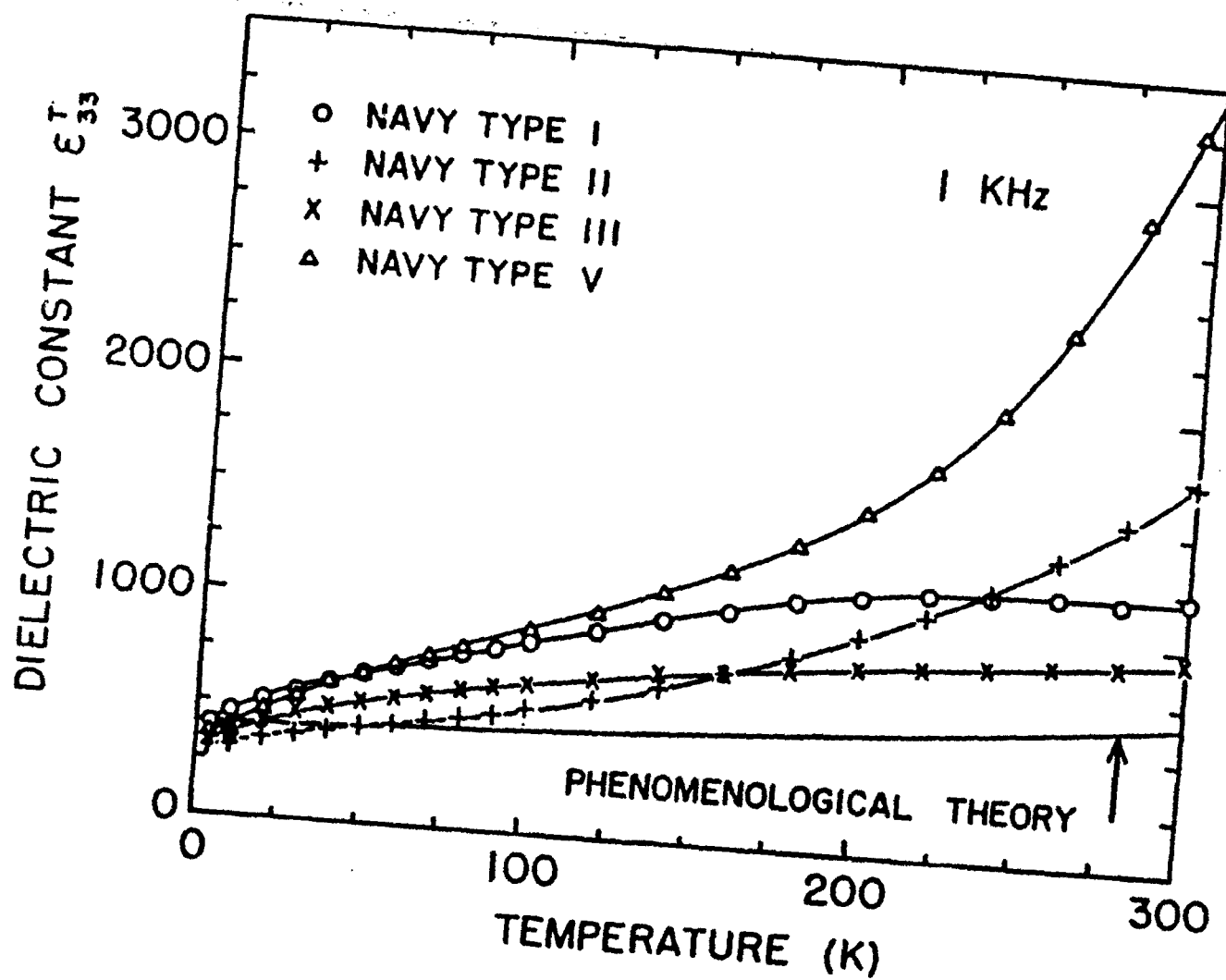
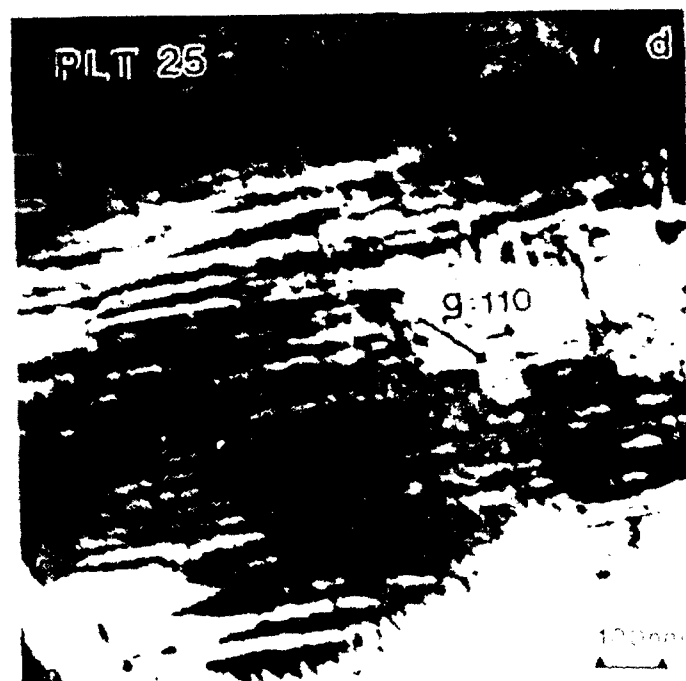
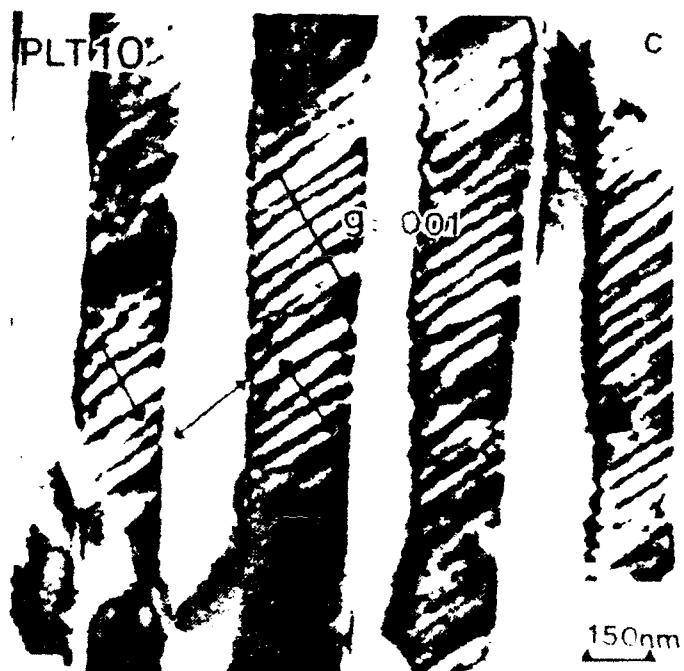
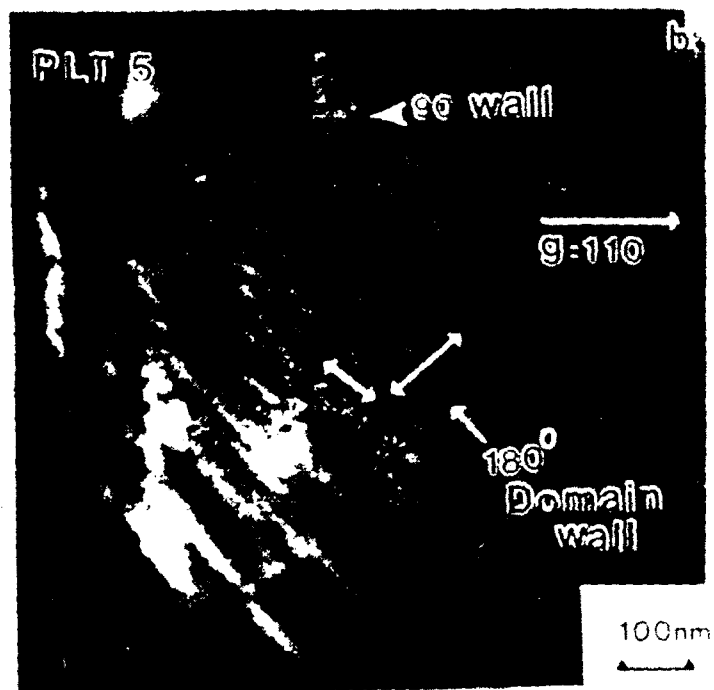
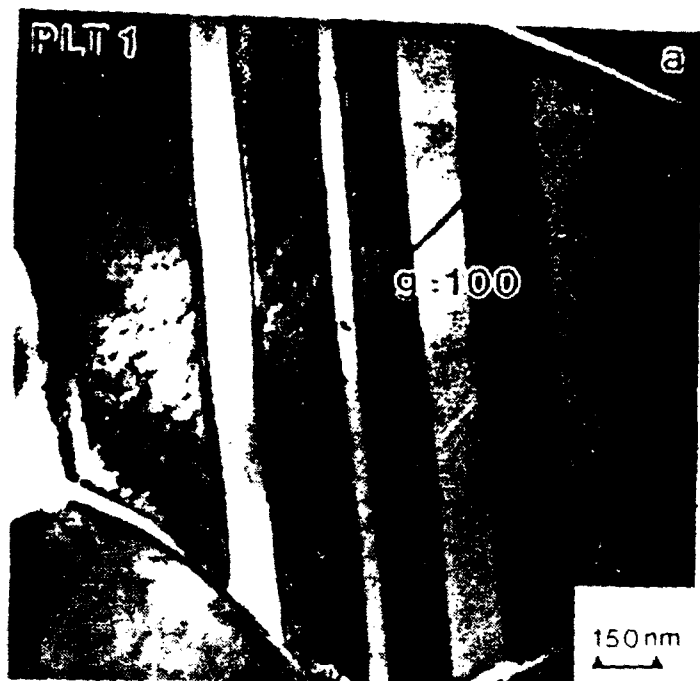




Figure 2



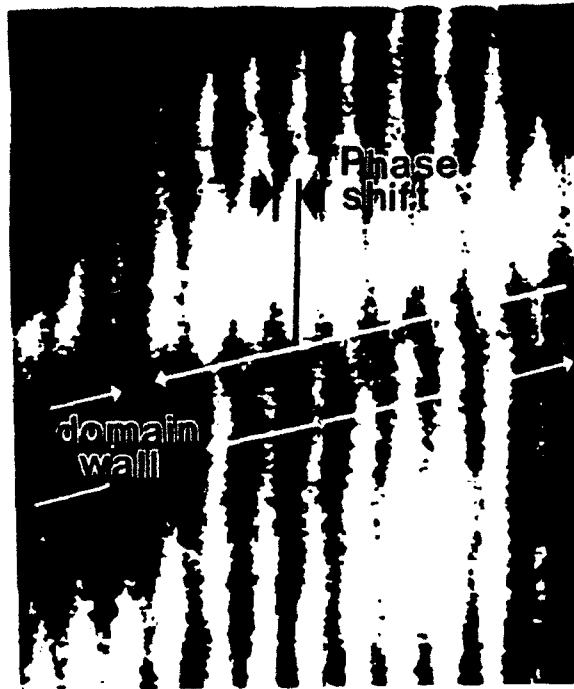


Figure 11

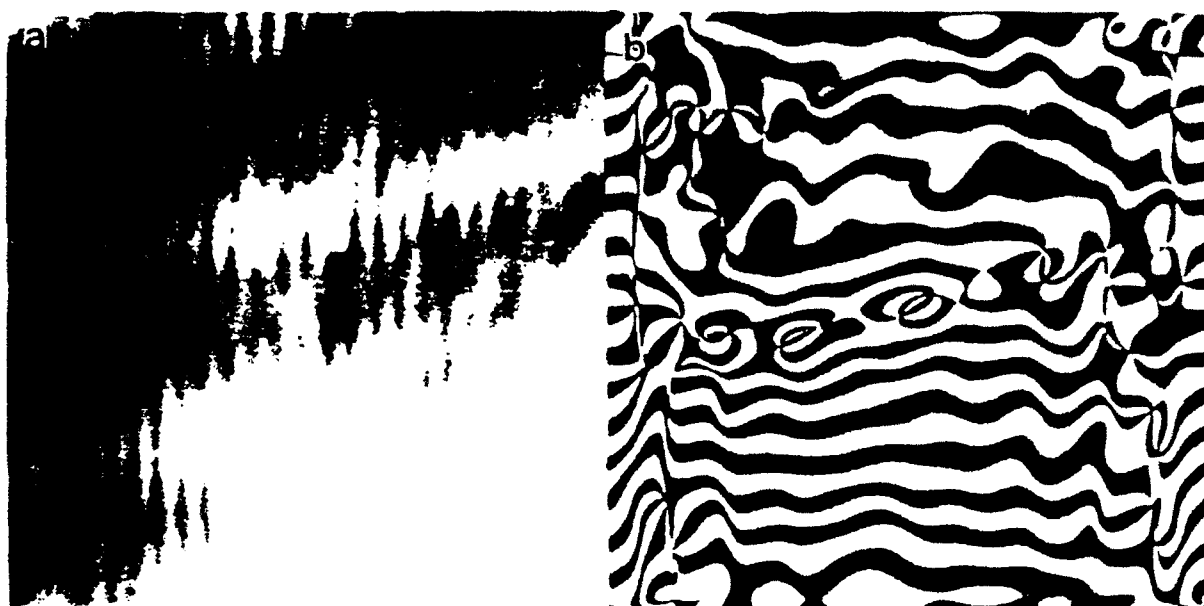


Figure 5

APPENDIX 24

Lead Zirconate Titanate Films on Nickel-Titanium Shape Memory Alloys: SMARTIES

Jayu Chen, Qi Chang Xu, Michael Blaszkiewicz, Richard Meyer, Jr.,* and Robert E. Newnham*

Materials Research Laboratory, The Pennsylvania State University, University Park, Pennsylvania 16802

Thin films of 52/48 PZT have been deposited on Ni-Ti shape memory alloys using a sol-gel spin-on method. Micrometer-thick PZT films adhere well to the alloy for strains as large as 0.4%, and they retain their ferroelectric properties during repeated cycling through the shape memory transformation.

I. Introduction

SMART MATERIALS have the ability to perform both sensing and actuating functions.¹ *Passively* smart materials, such as varistors and positive temperature coefficient thermistors, respond to external change in a useful manner without assistance, whereas *actively* smart materials have a feedback loop which allows them to recognize the change and initiate an appropriate response through an actuator circuit. Applications of actively smart materials include vibration-damping systems for outer-space platforms² and electrically controlled automobile suspension systems using a multilayer piezoelectric ceramic as both sensor and actuator.³

Poled PZT ($\text{PbZr}_{1-x}\text{Ti}_x\text{O}_3$) ceramics are natural candidates for applications as smart materials because of their sensitive response to weak stresses through the direct piezoelectric effect and their ability to generate powerful forces by means of the converse piezoelectric effect. An important advantage of piezoelectric actuators is that the strain response to an applied electric field is very fast, often on the order of microseconds. Their principal disadvantage is that the magnitude of the strain is quite small ($<10^{-3}$), generating displacements of only a few micrometers.⁴

Shape memory alloys,⁵ on the other hand, develop very substantial forces and strains of several percent or more, but they are very slow because of the long thermal time constants.

By combining shape memory alloys with piezoelectric ceramics we intend to fabricate a family of smart materials which retain the best characteristics of both types of actuators. We call these composites "SMARTIES," an acronym for "Shape Memory Actuators and Regulating Transducers for Intelligent Electronic Systems." There are a number of ways in which the alloys and ceramics can be assembled in different connectivity patterns⁶ to optimize the actuating and sensing functions. In this report, we describe a simple 2-2 composite in which sol-gel films of PZT are laid down on ribbons of Ni-Ti shape memory alloy. Subsequent papers will describe SMARTIES with 1-3 connectivity⁶ and strain-amplifying mechanisms similar to the moonie.^{7,8}

II. Preparation and Characterization

Thin films of PZT (52/48) were coated on a shape memory alloy foil using a sol-gel spin-on technique. Preparation of the films involved the following processing steps. Lead acetate trihydrate was dissolved in 2-methoxyethanol at 70°C and refluxed. The water of hydration from this lead precursor was distilled through a reflux condenser to facilitate the addition of moisture-sensitive alkoxides of titanium and zirconium. The byproducts of the reaction were expelled, following prolonged refluxing, at 125°C. The solution was partially hydrolyzed, and a controlled amount of acid or base was added as catalyst. Films were fabricated by a multistep spin-on technique, with pyrolysis at 400°C after each step to remove the organics. Films were built up to the desired thickness and then crystallized to obtain the perovskite phase by annealing at temperatures above 500°C.

The Ni-Ti shape memory alloys were commercially supplied (Shape Memory Applications, Inc., Sunnyvale, CA). Square foils, 25 mm \times 25 mm \times 0.1 mm, were used in the initial experiments. The martensite-austenite phase transformation was at 82°C. Prior to coating with PZT, the foils were cleaned using consecutive washes of acetone, NH_4OH , and HCl .

The fired PZT films were characterized by X-ray diffraction. All lines were indexed on the perovskite unit cell, consistent with single-phase behavior. Scanning electron microscopy images indicated a grain size of less than 1 μm .

The dielectric properties of the PZT thin film were assessed in terms of the dielectric constant ϵ , and loss factor $\tan \delta$. Dielectric measurements were conducted using an impedance analyzer (Model 4192A, Hewlett-Packard Co., Palo Alto, CA) at room temperature. Gold electrodes, 0.6 mm in diameter, were sputtered on the top of the film. The Ni-Ti alloy was used as the counter electrode. The capacitance spots varied by less than 5%, indicating a satisfactory degree of homogeneity in the properties of the film. The permittivity and loss factor of a 0.6- μm film were measured over a frequency range from 10 kHz to 10 MHz. The relaxation frequency of the film was about 2 MHz, which implies that the film has a thin interfacial layer but can be used at moderately high frequencies. The dielectric constant and loss factor at 100 kHz were about 700 and 0.03, respectively, comparable to that of the bulk ceramics.⁹

Ferroelectric hysteresis was examined using a loop tracer to follow the polarization reversal behavior of the films. The saturation field of a 0.6- μm PZT film on Nitinol (Nickel-Titanium Naval Ordnance Laboratory alloy) was about 100 kV/cm with a remanent polarization value of 15 $\mu\text{C}/\text{cm}^2$.

III. Shape Memory Experiments

Mechanical- and electrical-testing experiments were conducted on a second specimen consisting of a PLZT film deposited on Nitinol using the same sol-gel spin-on method. A rhombohedral 6/65/35 PLZT film was fired on Ni-Ti alloy at 700°C for 15 s to a final thickness of 1.4 μm . A number of gold spot electrodes 0.6 mm in diameter were again sputtered on the upper surface of the PLZT. The substrate was a Ni-Ti alloy ribbon 23 mm long, 3 mm wide, and 0.1 mm thick.

G. H. Haertling—contributing editor

Manuscript No. 195566 Received June 24, 1992; approved August 5, 1992.
Supported by the Electronics Technology and Devices Laboratory under the auspices of the U.S. Army Research Office's Scientific Services Program.
*Member, American Ceramic Society

The objective of this study was to assess the dielectric behavior of the ferroelectric film as the metal substrate underwent its shape memory cycle. First, the SMARTIE composite film was examined under an optical microscope and its electrical properties measured. The dielectric constant at 500 Hz was 1160 and the loss tangent was 0.02. The hysteresis loop obtained with a Sawyer-Tower circuit gave a remnant polarization of $36.7 \mu\text{C}/\text{cm}^2$, very close to the bulk value of $34.8 \mu\text{C}/\text{cm}^2$. The coercive field of 9.7 kV/cm was only slightly larger than the reported bulk value of 8.7 kV/cm.

Next, the composite film was bent around a 2.5-cm-diameter mandrel corresponding to an elongation of 0.4%. The SMARTIE film was then heated on a hot plate to a temperature above the 82°C martensitic-austenitic phase transformation of the shape memory alloy, causing it to revert back to the original flat shape. No change in the adhering PLZT film was observed under microscopic examination. The electrical properties were remeasured and remained unchanged.

Considerable cracking was observed when the bilayer composite was bent around a 1.9-cm-diameter mandrel, equivalent to a strain of 0.5%. Numerous fractures caused the electrode to lift off the surface, and even after the substrate was heated back to its original shape, cracking was still evident and the open-circuit condition remained.

Similar mechanical behavior was observed for the PZT films deposited on the shape memory alloy. Both types of films were deposited on films in which the major axis of the ribbon was perpendicular to the rolling direction of the shape memory alloy. The texture of the Ni-Ti alloy surfaces adversely affected the mechanical strength of the ferroelectric films.

IV. Summary

Thin films of PZT and PLZT have been successfully grown on shape memory alloy substrates with both the ferroelectric and the shape memory alloy retaining their useful properties. Measurements of the piezoelectric properties are in progress and we expect to develop a family of smart composites, two-stage actuators, and tunable transducers from these bilayer SMARTIES.

Acknowledgments: We wish to thank Ms. Shoko Yoshikawa and Drs. L. E. Cross and Arthur Ballato for helpful discussions.

References

- *R. E. Newham and G. R. Ruchau, "Smart Electroceramics," *J. Am. Ceram. Soc.*, **74**(3), 467-80 (1991).
- *S. Burke and J. E. Hubbard, "Active Vibration Control of a Simply Supported Beam Using a Spatially Distributed Actuator," *IEEE Control Systems Magazine*, **7**, 25-30 (1987).
- *H. Tsuka, J. Nakomo, and Y. Yokoyama, "A New Electronic Controlled Suspension Using Piezoelectric Ceramics," presented at IEEE Workshop on Electronic Applications in Transportation, 1990.
- *K. Uchino, *Piezoelectric/Electrostrictive Actuators*, Monikita Publishers, Tokyo, Japan, 1986.
- *L. Scheer, "Shape Memory Alloys," *Sci. Am.*, **241**, 74-82 (1979).
- *R. E. Newham, D. P. Skinner, and L. E. Cross, "Connectivity and Piezoelectric Composites," *Mater. Res. Bull.*, **13**, 525-36 (1978).
- *Q. C. Xu, S. Yoshikawa, J. R. Bellick, and R. E. Newham, "Piezoelectric Composites with High Sensitivity and High Capacitance for Use at High Pressures," *IEEE Trans. Ultrason. Ferroelectr. Freq. Control*, **UFFC-38** [6], 634-39 (1991).
- *Y. Sugawara, K. Onitsuka, S. Yoshikawa, Q. Xu, R. E. Newham, and K. Uchino, "Metal-Ceramic Composite Actuators," *J. Am. Ceram. Soc.*, **75**[4], 946-48 (1992).
- *R. Buchanan (Ed.), *Ceramic Materials for Electronics*, p. 184, Marcel Dekker, New York, 1986.
- *R. E. Newham, "Tunable Transducers: Nonlinear Phenomena in Electroceramics," *NIST Spec. Publ.*, **804**, 39-52 (1991).

ACTUATOR STUDIES

APPENDIX 25

Electrostrictive and Piezoelectric Materials for Actuator Applications

D. DAMJANOVIC AND R. E. NEWMHAM
*Materials Research Laboratory
The Pennsylvania State University
University Park, PA 16802*

ABSTRACT: The piezoelectric and electrostrictive effects in ferroelectric ceramics are reviewed with an emphasis on those properties that are relevant for applications in actuators. Various contributions to the piezoelectric effect in ferroelectric ceramics, especially lead zirconate titanate ceramics, are discussed in some detail. Relaxor ferroelectrics such as lead magnesium niobate are shown to be a unique family of materials with very attractive electrostrictive effects as well as piezoelectric properties. Finally, several actuator systems that employ piezoelectric and electrostrictive ceramics are briefly discussed.

INTRODUCTION

PIEZOELECTRIC AND ELECTROSTRICTIVE materials are a natural choice for precision displacement transducers or actuators. They utilize the strain induced by an electric field, an external parameter which can be easily controlled. Achievable strains are on the order of 10^{-4} – 10^{-3} for realizable fields ($\sim 10^6$ V/m), which for samples with dimensions on the order of 1 cm, translates into 10 μm displacements. At the same time, the expected accuracy may be as good as 0.01 μm . This, together with high speeds (1–10 μs), low power requirements, relatively high generative forces and the possibility of miniaturization makes electrostrictive and piezoelectric actuators far superior to the conventional electromagnetic methods, as well as to the newer types of actuators that are controlled by temperature (shape memory effect) or magnetic field (magnetostrictive effect) [22].

Formally, the relationship between the induced strain and electric field is simple, even in highly anisotropic piezoelectric and electrostrictive materials. The coupling coefficients (piezoelectric and electrostrictive coefficients), however, depend on the impurities present in the material, on the preparation procedure, on the size and frequency of applied electric and mechanical fields, on the temperature, and on aging time. Thus, a materials engineer has a challenging task when designing a material that will deliver the reproducible displacements required by the new generation of ultraprecise actuators. This paper deals with some of the properties of piezoelectric and electrostrictive ceramics that are important in the successful performance of an actuator assemblage.

FUNDAMENTAL RELATIONS

Piezoelectric Effect

Piezoelectricity describes the first order (linear) coupling between dielectric and elastic phenomena. For an anisotropic, homogeneous solid, under isothermal conditions and neglecting the magnetic field effects, the components of the elastic strain tensor x_{ij} are given by the following relation [16]:

$$x_{ij} = s_{ijkl}^E X_k + d_{ijk} E_k + \text{higher order terms} \quad (1)$$

where X_k and E_k are the components of the stress tensor and the electric field vector, respectively. The s_{ijkl}^E coefficients are the components of the elastic compliance tensor measured at constant electric field. The components d_{ijk} of the piezoelectric tensor define the linear electromechanical coupling. In the first approximation, all the higher order terms in Equation (1) are considered to be negligible. If a static electric field is applied to a piezoelectric material that is free to change its shape, the total stress X is zero and Equation (1) reduces to $x_{ij} = d_{ijk} E_k$. The piezoelectric term thus relates the mechanical strain developed in a material as a consequence of the electric field applied to the material. For this reason d is called the piezoelectric strain coefficient and the effect is known as the converse piezoelectric effect. Alternatively, for a linear, anisotropic, homogeneous, polarizable solid the components of the dielectric displacement vector D_i are given by the relation:

$$D_i = d_{ijk} X_k + \epsilon_{ij}^E E_j + \text{higher order terms} \quad (2)$$

where ϵ_{ij}^E are the components of the dielectric permittivity tensor measured at constant stress. As before, the higher order terms are neglected. If an elastic field (stress) is applied to a piezoelectric material that is short-circuited, the total electric field across the material is zero, and Equation (2) becomes $D_i = d_{ijk} X_k$. In this case, the piezoelectric term relates the charge developed on the material's surface upon application of stress. The d coefficient is now called the piezoelectric charge coefficient and the corresponding electromechanical coupling is known as the direct piezoelectric effect. It can be shown that the components of the piezoelectric tensors for the direct and converse effects are equivalent. In matrix form one can write $d_{ijk} = (d_{ijm})_k^T$, where i denotes the transpose matrix.

The piezoelectric coupling between the elastic and dielectric parameters of a material can be readily introduced using the thermodynamic approach. One can arbitrarily choose a set of the independent variables in the appropriate thermodynamic potential to derive the so-called constitutive piezoelectric equations. In addition to Equations (1) and (2), the other three sets of constitutive equations are [3]

$$X = e^T \epsilon - e^T E \quad (3a)$$

EDITOR-IN-CHIEF

Craig A. Rogers

Department of Mechanical Engineering

Virginia Polytechnic Institute and State University

Blacksburg, VA 24061-0238

USA

EDITORIAL ADVISORY BOARD

Masuo Aizawa

Tokyo Institute of Technology

Tokyo, Japan

Richard Claus

Virginia Polytechnic Institute & State University

Blacksburg, VA, USA

Leon N. Cooper

Brown University

Providence, RI, USA

Ed Crawley

Massachusetts Institute of Technology

Cambridge, MA, USA

Daniilo DeRossi

University of Pisa

Pisa, Italy

Michael Geoghegan

E. I. du Pont de Nemours & Co

Wilmington, DE, USA

K.-H. Hoffmann

Institut für Mathematik der Universität

Augsburg

Augsburg, FRG

Richard D. James

University of Minnesota

Minneapolis, MN, USA

Raymond M. Measures

University of Toronto

Downsview, Ontario, Canada

Koryo Miura

The Institute of Space and Astronautical Science

Kanagawa, Japan

A. V. Srinivasan

United Technologies Research Ctr.

East Hartford, CT, USA

Toshinori Takagi

Ion Engineering Research Institute Corp.

Osaka, Japan

Kiyoshi Takahashi

Tokyo Institute of Technology

Tokyo, Japan

Eric Udd

McDonnell Douglas

Huntington Beach, CA, USA

Julian FV Vincent

University of Reading

Reading, Berkshire, UK

Ben K. Wada

Jet Propulsion Laboratory

Pasadena, CA, USA

Nabil Zahlan

ICI Wilton Materials Research Centre

Cleveland, UK

$$D = \epsilon \tau + \epsilon' E \quad (3b)$$

$$X = c^p x - h' D \quad (4a)$$

$$E = -h x + \beta' D \quad (4b)$$

$$x = s^p X + g' D \quad (5a)$$

$$E = -g X + \beta' D \quad (5b)$$

In these equations the indices for the tensorial components are dropped for simplicity. The piezoelectric tensors ϵ , g and h are respectively known as the stress (or charge), voltage (or strain) and stress (or voltage) piezoelectric coefficients. ϵ is the elastic stiffness tensor, and the superscript denotes whether it is measured at constant field E or constant displacement D . s^p is the elastic compliance at constant electric displacement. The difference between the two types of coefficients will be discussed in a subsequent section. ϵ' is the dielectric permittivity at constant strain. β' and β'' are the dielectric impermeabilities at constant strain and constant stress, respectively. Matrices of the dielectric impermeability tensors are defined as $\beta' = (\epsilon')^{-1}$ and $\beta'' = (\epsilon'')^{-1}$. Relationships between the four piezoelectric coefficients are as follows:

$$d_{ijk} = \epsilon_{ijm} s_{lmk}^p = g_{ijk} \epsilon_{lm}^p \quad (6a)$$

$$\epsilon_{ijk} = d_{ilm} \epsilon_{lmk}^p = h_{ijk} \epsilon_{lm}^p \quad (6b)$$

$$g_{ijk} = d_{ilm} \beta_{lm}^p = h_{ilm} s_{lmk}^p \quad (6c)$$

$$h_{ijk} = \epsilon_{ilm} \beta_{lm}^p = g_{ilm} c_{lmk}^p \quad (6d)$$

The choice of which of Equations (1-5) is to be used in the particular problem depends on the elastic and electric boundary conditions. Furthermore, the constitutive equations may be derived for isothermal or adiabatic conditions. For non-polar materials, the isothermal and adiabatic coefficients are equal. For the polar materials (pyroelectric and ferroelectric) the difference between the isothermal and adiabatic coefficients is usually negligible [3].

Symmetry Arguments

Because of the symmetry of the stress and strain tensors the third rank tensor of the piezoelectric coefficients d_{ijk} (as well as ϵ , g and h) is also symmetrical in indices j and k . This leaves only 18 independent piezoelectric coefficients. To convert the tensor coefficients to matrix form, the pair of indices jk is replaced with a single index $m = 1, 2, 3$ if $j = k$ and $jj = 11, 22$, or 33 , respectively. If $j \neq k$ then $jk = 23$ or 32 , 13 or 31 and 12 or 21 is replaced with $m = 4, 5, 6$, respectively. In matrix notation [16], d_{ijk} are written as $d_{im} = d_{im}$ when $m = 1, 2, 3$

and $d_{im} = 1/2 d_{im}$ when $m = 4, 5, 6$. Hence, the direct and converse piezoelectric effects may be written in the following matrix form:

$$D_i = d_{im} X_m \quad (7a)$$

$$x_m = d_{im} E_i \quad (7b)$$

where a corresponding reduction is made in the subscripts of the components of the stress and strain tensors [16].

Neumann's principle states that the symmetry elements of a physical property of a crystal must include the symmetry elements of the point group of the crystal [16]. The principle can be extended to include not only the 32 crystallographic point groups but also the Curie point groups which contain the infinite symmetry axes [19]. The most important consequence of Neumann's principle is that certain physical properties may be absent in a material because of its symmetry. Thus, in the eleven centrosymmetric point groups and in point group 432 all the components of the piezoelectric tensor (and all odd-rank tensors) are equal to zero. The remaining 20 point groups are potentially piezoelectric. Neumann's principle, however, gives only necessary conditions for a material to exhibit the piezoelectric effect. Whether a material that belongs to one of the piezoelectric point groups exhibits measurable piezoelectricity has to be verified experimentally. Of the 20 piezoelectric point groups, 10 are polar. These are 1, m , 2, $mm2$, 3, $3m$, 4, $4mm$, 6, and $6mm$. Crystals that belong to these point groups possess spontaneous electrical polarization P_s and exhibit a pyroelectric effect. If there is more than one equilibrium direction along which the vector of the spontaneous polarization may be oriented the material is also ferroelectric, provided that switching between states can be achieved by a realizable electric field.

Among the polycrystalline materials only ferroelectric materials and polar glass ceramics show piezoelectricity. The polycrystalline materials with a random orientation of grains belong to the Curie point group $\infty\infty m$ which has spherical symmetry [14]. This point group has a center of symmetry and all odd-rank tensor properties of polycrystalline materials with random distribution of grains are equal to zero. In ferroelectric materials, however, a strong electric field can permanently reverse the directions of the polarization vector P_s within many of the domains inside each grain, leading to a nonzero macroscopic polarization. Polarized or poled polycrystalline ferroelectric materials possess conical symmetry ∞m . This symmetry has the same nonzero components of the dielectric, elastic and piezoelectric tensors as the point group $6mm$. Therefore, poled ferroelectric ceramics exhibit the piezoelectric effect. The polycrystalline ferroelectric piezoelectrics are by far the largest and the most important group of the piezoelectric materials. Matrices for the elastic compliance s , the dielectric permittivity ϵ , and the piezoelectric coefficient d are given in Table 1 for poled ceramics.

Electrostrictive Effect

In the section on piezoelectricity the relationships between strain and electric field (converse piezoelectricity) and between electric displacement and stress

Table 1. Matrices of the elastic compliance s , dielectric permittivity ϵ and piezoelectric coefficient d for poled ceramics.

s_{11}	s_{12}	s_{13}	0	0	0	0	0	d_{31}	schematic $= \begin{pmatrix} s & d' \\ d & \epsilon \end{pmatrix}$
s_{12}	s_{11}	s_{13}	0	0	0	0	0	d_{31}	
s_{13}	s_{13}	s_{33}	0	0	0	0	0	d_{33}	
0	0	0	s_{44}	0	0	0	0	d_{15}	
0	0	0	0	0	s_{44}	0	d_{15}	0	
0	0	0	0	0	0	s_{44}	0	0	
0	0	0	0	0	0	0	0	0	
0	0	0	0	d_{15}	0	0	0	0	
0	0	0	d_{15}	0	0	0	0	0	
d_{31}	d_{31}	d_{33}	0	0	0	0	0	0	
$s_{44} = 2(s_{11} - s_{12})$									ϵ_{33}

(direct piezoelectricity) are developed assuming a linear dependence of strain on electric field and electric displacement on stress. This assumption is valid only if the applied stress or electric field is small. Otherwise, higher order terms in the expansion of the corresponding thermodynamic functions must be taken into account [16]. Thus, for a nonlinear solid one may write the following expression for the total strain:

$$\epsilon_{ij} = s_{ij}^0 X_{ij} + d_{ijk} E_k + M_{ijkl} E_k E_l + \text{higher order terms} \quad (8)$$

As before, the first term in Equation (8) describes Hooke's law, the second term is the converse piezoelectric effect and the third term is called the electrostrictive effect. The components M_{ijkl} of the fourth rank tensor M are the electrostrictive coefficients and the corresponding matrix has the same nonzero elements as that of the elastic compliance (see Table 1). For a zero stress ($X = 0$) and neglecting the higher order terms, Equation (8) reduces to [16]:

$$\epsilon_{ij} = d_{kij} E_k + M_{ijkl} E_k E_l = (d_{kij} + M_{ijkl} E_l) E_k \quad (9)$$

The electrostrictive effect can therefore be classified as an electric-field dependent contribution to the linear piezoelectric effect. In principle, however, the two effects are separable because the piezoelectric effect is possible only in noncentrosymmetric materials. Being described by an even rank tensor, the electrostrictive effect is not limited by symmetry and is in fact present in all materials, even those that are amorphous. Hence, the electrostrictive effect describes the nonlinear (second order or quadratic) dependence of the strain on the applied electric field.

If the strain in Equation (8) is expressed in terms of the components of the polarization vector P , one obtains another commonly used set of electrostrictive coefficients Q_{ijkl} :

$$\epsilon_{ij} = g_{ijk} \epsilon_{lm}^0 P_k + Q_{ijkl} P_k P_l \quad M_{ijkl} = \epsilon_{lm}^0 \epsilon_{lm}^0 Q_{ijkl} \quad (10)$$

In addition to the direct electrostrictive effect, the second order coupling between stress and polarization leads to a converse electrostrictive effect. The direct and converse effects are thermodynamically equivalent. However, in materials with non-zero spontaneous polarization there is an additional coupling term caused by the dependence of the dielectric permittivity on the spontaneous polarization, which in turn is dependent on pressure. For this reason the interpretation of the experimentally determined values of the electrostrictive coefficients in ferroelectric materials is not always straightforward [24]. Similarly, the equivalence between the direct and converse piezoelectric coefficients as derived thermodynamically breaks down in materials with nonzero spontaneous polarization [12,13]. A unique piezoelectric tensor can still be defined if there is an external surface charge compensation of the internal polarization. In the absence of such charge compensation new piezoelectric relations ought to be used.

Electromechanical Coupling Factors

The constitutive piezoelectric Equations (1-5) show that the elastic or dielectric response of a piezoelectric material depends not only on its piezoelectric properties but also on its elastic and dielectric parameters. Therefore, a figure of merit of a piezoelectric material must include its elastic, dielectric and piezoelectric coefficients and at the same time should be independent of external forces. Clearly such a figure of merit or, as it is most often called, a coupling factor, is not uniquely defined. Berlincourt et al. [3] define the piezoelectric coupling factor as "the ratio of the mutual elastic and dielectric energy density to the geometric mean of the elastic and dielectric self-energy density". For a linear system the internal energy is given by:

$$U = 1/2(\epsilon_{ij} X_{ij} + D_i E_i) \quad (11)$$

which together with Equation (1) gives

$$\begin{aligned} U &= 1/2(X_{ij} s_{ij} X_{ij} + X_{ij} d_{ijk} E_k + E_i d_{ij} X_{ij} + E_i \epsilon_{ij} E_j) \\ &= U_e + 2U_m + U_d \end{aligned} \quad (12)$$

where U_e is elastic contribution to the internal energy, U_d is dielectric and U_m is the mutual or coupled contribution to the internal energy U . According to this definition, the electromechanical coupling factor k is given by the absolute value of the following expression:

$$k = U_m / (U_e U_d)^{1/2} \quad (13)$$

Each term in Equation (11) involves generally a summation over six stress and three electric field components. Equations (11) and (13) depend on the constitutive

piezoelectric relationships used, i.e., they depend on boundary conditions of the particular problem.

For a one-dimensional ceramic bar (point group ∞m) with electric field perpendicular to its length, Equation (II) becomes

$$U = 1/2(X_1^2 s_{11}^E) + E_3 X_1 d_{31} + 1/2(\epsilon_{33}^E E_3^2) \quad (14)$$

and the corresponding coupling factor is

$$k_{31} = d_{31}/(\epsilon_{33}^E s_{11}^E)^{1/2} \quad (15)$$

For a ceramic bar with electric field along its length the coupling factor is

$$k_{11} = d_{11}/(\epsilon_{11}^E s_{11}^E)^{1/2} \quad (16)$$

Similarly, coupling factors can be obtained for other configurations of stress and electric field or any other set of independent variables and for all piezoelectric point groups.

As defined by Equation (13), coupling factors are, however, meaningful only in the static limit. In a dynamic case, for example near a resonant frequency, the coupling factor is dependent on stress and strain, which show spatial variations [20]. Furthermore, for two- or three-dimensional cases, the distribution of strains and stresses is usually more complicated, and the stress components in the numerator and denominator in Equation (13) do not always cancel even in a static situation. Hence, the coupling coefficients are dependent on external variables and often do not describe intrinsic properties of the material. Despite these drawbacks, the concept of electromechanical coupling factors as defined by Berlincourt is very widely used.

The factor $k^2 = d^2/(\epsilon\epsilon')$ involving the piezoelectric, elastic, and dielectric constants that is found in all the coupling factors is a fundamental characteristic of a piezoelectric material and appears in many piezoelectric relations independent of Equation (13). Thus, if a static electric field E is applied to a clamped piezoelectric material the strain x is zero and Equation (1) gives $Xs^E = -dE$. Replacing the stress X in Equation (2) with $X = -dE/s^E$, the following expression for the dielectric displacement D is obtained:

$$D = -d^2 E/\Delta s^E + \epsilon^E E = \epsilon^E [1 - d^2/(s^E \epsilon^E)] E \quad (17)$$

The dielectric permittivity $\epsilon^E = \epsilon^E [1 - d^2/(s^E \epsilon^E)]$ is called the clamped dielectric constant. Similarly, under open-circuit conditions, the dielectric displacement D in Equation (2) is zero, and $dX = -\epsilon^E E$. Replacing the electric field E in Equation (1) with $E = -dX/\epsilon^E$, the strain x becomes

$$x = s^E X - d^2 X/\epsilon^E = s^E [1 - d^2/(s^E \epsilon^E)] X \quad (18)$$

and the elastic compliance $s^D = s^E [1 - d^2/(s^E \epsilon^E)]$ at constant (zero) displace-

ment D is obtained. It follows that the velocity of acoustic waves, $v = (q_s)^{1/2}$ where q is density, in a piezoelectric material depends on electric boundary conditions. The velocity of elastic waves at constant electric field E (short-circuit condition) and constant electric displacement D (open-circuit condition) are thus related to each other through the electromechanical coupling factors. For materials such as PZT with electromechanical coupling factor k close to 0.7, the difference between clamped and free dielectric constant or between the short- and open-circuit elastic compliances may be as high as 50%.

PIEZOELECTRIC AND ELECTROSTRICTIVE CERAMIC MATERIALS

The only requirement for a nonconductive material to exhibit the piezoelectric effect is that the material belongs to one of the 20 piezoelectric point groups. It is not surprising then that piezoelectricity is often encountered in nature. It is found in many organic materials, single crystals and ceramics, but also in hybrid materials such as polymer/ceramic composites and polar glass ceramics. Clearly then, an answer to the question of what mechanisms contribute to piezoelectricity is not a simple one.

Contributions to the Piezoelectric Effect

SINGLE CRYSTAL VS. CERAMIC PROPERTIES: FERROELECTRIC DOMAINS

The complexity of the coupling between the electric and elastic properties can be comprehended when ferroelectric materials are considered. The origin of the intrinsic piezoelectricity in most ferroelectric materials can be explained in terms of the electrostriction of the paraelectric phase using thermodynamic phenomenological theory [8]. In principle then, it is possible to predict a complete set of the values of the piezoelectric coefficients of, for example, single crystal BaTiO₃, knowing the corresponding electrostrictive coefficients and the value of the spontaneous polarization at the temperature of interest.

In practice, however, ferroelectric materials are usually used in polycrystalline or ceramic form. Each grain consists of domains which are oriented along the directions dictated by the symmetry of the parent phase. Ferroelectric domains form as the ferroelectric material is cooled through its Curie temperature. In ceramics, the individual grains tend to assume anisotropic shapes determined by the orientation of the crystallographic axes. The shape change of each grain induces large stresses upon adjacent grains. In order to minimize the total elastic energy, a complex domain structure forms within each grain adjusting its shape to the immediate environment. Thus, all the tensor properties of a ceramic material are averages of the corresponding single crystal values represented by the individual grains and domains [11].

The poling process required to induce piezoelectricity only partly aligns the polar vectors of the domains and the resulting property values are always different than those for the single crystal. The averaging procedure used to calculate the components of a tensor property of a poled ferroelectric ceramic must include not only the degree of the orientation of the domains, and the structure, size, and

shape of grains, but also the boundary conditions on the grains and domains. For coupled properties such as piezoelectricity this means that the elastic and dielectric boundary conditions on the grains and domains must be known. Furthermore, when the response of a piezoelectric ceramic is examined under weak alternating electric fields or mechanical stress, the domain walls will move in a reversible fashion. The effect of the domain wall dynamics on the dielectric, elastic and piezoelectric properties may be considerable and must be taken into account [2].

ROLE OF DEFECTS

The spontaneous polarization P_s carried by the domains interacts with polar defects (point defects) present in the crystal structure. The defects may be induced in the material either accidentally during preparation, or may be purposely added with the aim of controlling the conductivity and the poling behavior of material. Defects also influence the domain wall mobility, the diffusion properties and the sintering of the ceramic. The interaction of the domains and defects leads to so-called "soft" and "hard" piezoelectric compositions. Piezoelectrically soft materials are characterized by relatively mobile domain walls and high piezoelectric constants. In the hard compositions the domain wall motion is more inhibited resulting in lower piezoelectric constants but a more stable remnant polarization [15]. Some examples of the mechanisms which lead to soft and hard compositions will be given in the section on PZT piezoelectric ceramics.

PIEZOELECTRIC RELAXATION

Recently, there has been an increasing evidence that the piezoelectric constants of ferroelectric ceramics exhibit nonzero phase angle, i.e., they may be described as complex quantities. This should be expected since the piezoelectricity represents a coupling between the elastic and dielectric properties of a material, both of which are known to be major sources of energy dissipation. Although the piezoelectric relaxation in ferroelectric ceramics is not yet fully understood, it is clear that it does not originate from an independent loss mechanism in the material but is a result of an electromechanical coupling between the dielectric and mechanical losses operating in the material. The loss mechanisms may lead to a large and unwanted dependence of piezoelectric coefficients on frequency often characterized as relaxation-type behavior [1].

Summing up, the piezoelectric constants of a ferroelectric ceramic may be written in the following form:

$$d = d[d_{ij}(s.c.), \theta] + \Sigma \Delta d' - i \Sigma \Delta d'' + \Sigma \text{other} \quad (19)$$

where $d[d_{ij}(s.c.), \theta]$ is a function of intrinsic single crystal piezoelectric coefficients, $d_{ij}(s.c.)$, and also a function of the degree of polarization of ceramic, described by an orientation parameter θ . $\Sigma \Delta d'$ - $i \Sigma \Delta d''$ describes the sum of all relaxation contributions, and Σother is a sum of all nonrelaxational extrinsic contributions to the total piezoelectric coefficients of ceramics. The various competing mechanisms to piezoelectricity in ferroelectric ceramics are sometimes of

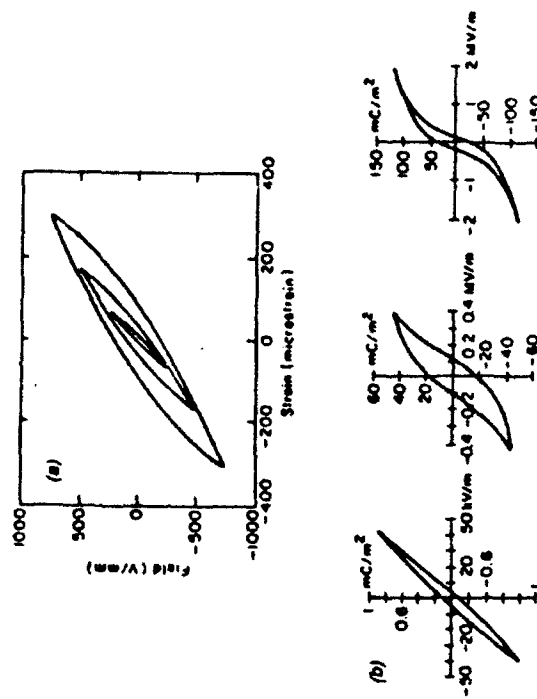


Figure 1. (a) Strain-electric field and (b) polarization-electric field hysteresis loops for typical ceramic ferroelectrics.

comparable strength and may even lead to a change of sign of the piezoelectric constant with temperature or frequency [7,10].

HYSTERESIS

The complex changes in the configuration of domain walls in ferroelectric materials under an AC electric field lead to the characteristic hysteresis relationships between polarization and electric field and between electric field and strain (Figure 1). Those domains that do not return to their initial random configuration after the electric field is removed, but remain oriented to a certain degree, are responsible for the remnant (residual) strain and polarization. Since the remnant strain and polarization are functions of the maximum applied field, it is clear that there is a range of possible strain and polarization states for zero field (Figure 1) [4,9].

AGING

One of the most complex properties of the ferroelectric ceramics is the time dependence of their elastic, dielectric and piezoelectric coefficients. This phenomenon, known as aging, follows the poling of ceramics, even in the absence of external forces or temperature changes. Aging occurs in all ferroelectric ceramics although its degree varies greatly from one composition to another. The effect is closely related to the mobility of the domain walls. An important contribution to the aging is the slow relaxation of the high stresses that are introduced into ceramic during poling at elevated temperatures. The poling is accompanied by

anisotropic shape changes of the grains, which are caused by the reorientation of domains under the poling field. When the external field is removed and the ceramic is cooled to room temperature, the domain configuration will tend to reach a new equilibrium state relieving some of the stresses [11].

Aging is affected by the internal fields created by defect dipoles which, under certain conditions, may stabilize the domain configuration by interacting with the spontaneous polarization within domains. Thus, the aging in for example PZT ceramics, may be controlled by doping the ceramics with suitable aliovalent cations [15]. In relaxor ferroelectrics, such as lead magnesium niobate (PMN), aging seems to be fully controlled by the impurities and may be completely absent in pure, stoichiometric material [17].

Lead Zirconate Titanate (PZT) Ceramics

The phase diagram of the lead zirconate titanate $[\text{Pb}(\text{Zr}_x\text{Ti}_{1-x})\text{O}_3]$ or PZT system is shown in Figure 2(a). A complete solid solution forms at high temperature with Zr and Ti randomly distributed over the octahedral sites of the cubic perovskite structure. On cooling, the structure undergoes a displacive phase transformation into a distorted perovskite structure. Titanium-rich compositions favor a tetragonal modification with a sizeable elongation along [001] and a large spontaneous polarization in the same direction. There are six equivalent polar axes in the tetragonal state corresponding to the [100], [100], [010], [010], [001] and [001] directions of the cubic paraelectric state. A rhombohedral ferroelectric state is favored for zirconium-rich compositions. Here the distortion and polarization are along [111] directions, giving rise to eight possible domain states: [111], [111], [111], [111], [111], [111], [111] and [111].

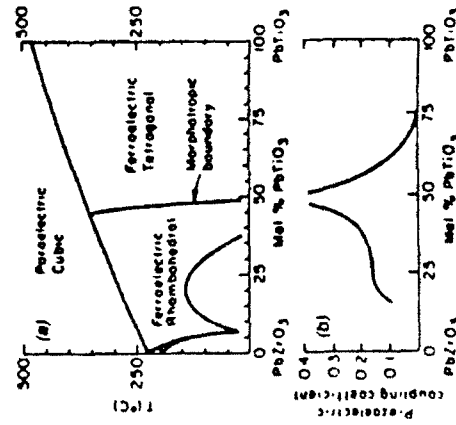
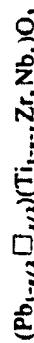


Figure 2. (a) Binary phase diagram of the lead zirconate-titanate ceramics (b) Large piezoelectric coefficients are obtained for poled ceramics with compositions near the morphotropic phase boundary

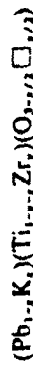
The compositions which pole best lie near the morphotropic boundary between the rhombohedral and tetragonal ferroelectric phases. For these compositions there are fourteen possible poling directions over a very wide temperature range. This explains why the piezoelectric coefficients are the largest near the morphotropic boundary [Figure 2(b)]. Typical values are $d_{33} \approx 400$, $d_{31} \approx -170$ and $d_{15} \approx 500$ pC/N. The magnitudes depend markedly on dopants and defect structure because of their influence on domain wall motion.

Donor ions create Pb vacancies in the PZT structure. As an example, when Nb^{5+} is substituted for Ti^{4+} , vacancies on the lead site result:



Donor doping is not effective in pinning domain walls. Pinning is believed to result from the alignment of defect dipoles with the spontaneous polarization within a domain. The defect dipoles come from the negatively charged Pb vacancies paired with dopant Nb^{5+} ions. Since the defect dipoles are formed at high temperature, the dipoles are not aligned with P_r initially because the spontaneous polarization is zero in the cubic paraelectric state. Alignment can only take place below the Curie temperature ($\sim 350^\circ\text{C}$ for PZT) where diffusion rates are low. Such is the case for donor-doped PZT, a so-called "soft" PZT. In a soft PZT, the main wall motion contributes to the size of the dielectric and piezoelectric coefficients. Adversely, however, soft PZT ceramics are easily depoled because the domain walls are not pinned.

Acceptor doping with lower valent ions such as K^+ (for Pb^{2+}) or Fe^{3+} (for Ti^{4+}) is employed to produce "hard" PZT. Oxygen vacancies are generated by acceptor doping:



Domain walls are pinned in hard PZT because the defect dipoles are able to align in accordance with the domain structure. Dipoles consisting of oxygen vacancies and associated dopant ions are able to reorient more easily in a hard PZT. The explanation lies in the ease with which oxygen vacancies diffuse at temperatures below T_c .

Examination of the perovskite structure makes it clear why oxygen vacancies diffuse faster than cation vacancies. Cations are completely surrounded by oxygens and are separated from the nearest cation site by an entire unit cell (~ 4 Å) making diffusion very difficult. Oxygen sites, on the other hand, are adjacent to one another, only 2.8 Å apart. Hence oxygens can easily move into nearby oxygen vacancies, realigning defect dipoles and pinning domain walls.

Since their discovery in the 1950s, PZT based ceramics have become, along with quartz, the most widely studied and used piezoelectric material. Because of its high piezoelectric coefficients, simple preparation, ease of poling and low cost the PZT family is used more than any other piezoelectric material for transducer, sensor, and actuator applications. The only exception is quartz which, owing to the excellent stability of its piezoelectric properties with time and temperature has not been surpassed by PZT in the field of frequency control.

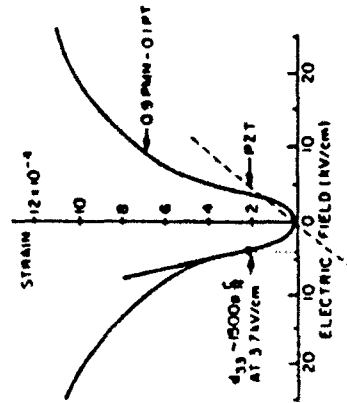


Figure 3. Electromechanical coupling in electrostrictive (PMN-PT) and piezoelectric (PZT) ceramics.

Electric Field Induced Piezoelectricity in Relaxor Ferroelectrics

The relaxor-type ferroelectrics are discussed in detail in this section. For the present purpose, it is sufficient to say that relaxor ferroelectrics cannot be poled, even at temperatures considerably below the so-called diffuse phase transition. However, in this temperature range, relaxor materials show high dielectric constants and very large electrostrictive effects (Figure 3) [5,6]. The piezoelectric d_{33} coefficient is the slope of strain-electric field curve [Equation (8)]. The nonlinearity between strain and electric field in a relaxor ferroelectric can be used to tune the piezoelectric coefficient. From Figure 3, the value of d_{33} for lead magnesium niobate ($\text{Pb}(\text{Mg}_{1-x}\text{Nb}_x)_2\text{O}_6$), or PMN) with 10-mole % lead titanate (PbTiO_3 or PT) (0.9PMN-0.1PT) at room temperature is zero at zero field and increases to a maximum value of ~ 1500 pC/N (about three times larger than PZT) under a bias field of about 3.7 kV/cm. Recent measurements with a laser interferometer show that transverse piezoelectric coefficient (d_{31}) in 0.9PMN-0.1PT ceramics also exhibits very high values under bias field, with a maximum of about -400 pC/N at bias field of ~ 3 kV/cm (Figure 4) [21].

Electrostrictive Materials

The electrostrictive effect is often believed to be too small for exploitation in devices. This is indeed true for most conventional nonferroelectric materials as well as for many ferroelectrics. The magnitude of the polarization related electrostrictive coefficients Q in nonferroelectric materials is on the order of $10 \text{ m}^2/\text{C}^2$ and in most "normal" ferroelectrics $Q \sim 10^{-1} \text{ m}^2/\text{C}^2$. Equation (10) however indicates that the electrostrictive strain x is equal to QP , where $P = \epsilon_0 \epsilon_r E$ is the induced polarization, ϵ_r is the dielectric constant of the material and ϵ_0 permittivity of free space. Thus, for a given electric field E , the materials with a very large dielectric constants exhibit large electrostrictive strains, even though their electrostrictive coefficients are relatively small. In most nonferroelectric mate-

rials dielectric constant is about 10 and for a typical field, say $E = 10^6 \text{ V/m}$, achievable strain is only 10^{-7} . In normal ferroelectric materials near the ferroelectric-paraelectric phase transition dielectric constant may reach high values (10^3) but the electrostrictive strain ($\sim 10^{-3}$) is still smaller than that in piezoelectric ceramics.

Over the past 20 years, however, the development of high permittivity capacitor dielectrics have led to the discovery of many partially disordered structures such as the relaxor ferroelectrics, with extremely large dielectric constants. The values of electrostrictive coefficients in relaxor ferroelectrics are relatively small on the order of $10^{-1} \text{ m}^2/\text{C}^2$, but dielectric constants on the order of 10^4 are observed over a wide range of temperatures near the diffuse phase transition. The electrostrictive strains in a typical relaxor material are on the order of 10^{-4} , and are comparable in size to those in piezoelectric ceramics.

RELAXOR FERROELECTRICS

Relaxor ferroelectrics are characterized by a strong dispersion of the dielectric permittivity with frequency (Figure 5) and the absence of macroscopic polarization even at temperatures much below the temperature of the maximum dielectric constant [5]. This unusual dielectric response of relaxor ferroelectrics is explained by a statistical inhomogeneity in the distribution of the B_1 and B_2 cations in the B sites of the $A(\text{B}_1\text{B}_2)\text{O}_3$ perovskite structure. This chemical disorder is responsible for formation of microregions (microdomains) within the material which have widely different Curie temperatures. Relaxor ferroelectrics thus do not have a well-defined Curie temperature but rather exhibit a Curie range over which the material is a statistical mixture of paraelectric and ferroelectric regions. As temperature decreases from the high-temperature paraelectric state the microdomains gradually coalesce to macrodomains giving rise to a diffuse phase transformation. The polarization fluctuations associated with the polar microregions are dependent on the electric bias field and measurement frequency. The

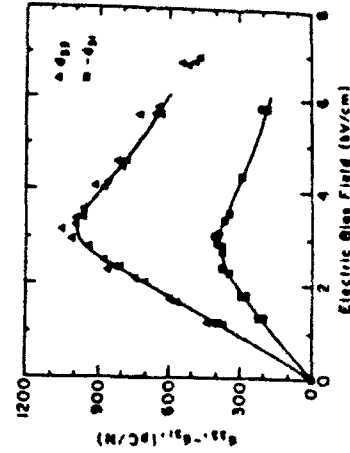


Figure 4. Piezoelectric coefficients d_{33} and d_{31} of 0.9PMN-0.1PT as a function of DC electric bias field, measured at 500 Hz using a laser interferometer.

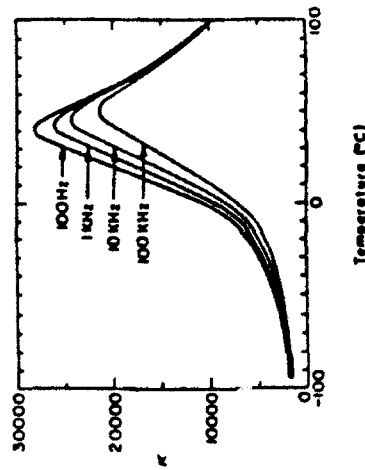


Figure 5. Dielectric constant of 0.9PMN-0.1PT as a function of temperature for selected frequencies.

dielectric constant drops off rapidly with frequency (hence the name "relaxor") because it takes time for the polarization fluctuations to respond. DC bias fields favor coalescence, having the same effect as lowering the temperature. This classical interpretation of the relaxor behavior is not completely successful in explaining all the complex properties of relaxor ferroelectrics, as several recent studies suggest [5,23]. Relaxor behavior is very common among Pb-based perovskites, suggesting that Pb^{2+} and its "lone-pair" electrons play a role in the microdomain process, possibly by adjusting the orientation of the lone pair.

LEAD MAGNESIUM NIOBATE - LEAD TITANATE RELAXOR FERROELECTRICS

Lead magnesium niobate [$\text{Pb}(\text{Mg}_{1/3}\text{Nb}_{2/3})\text{O}_3$ or PMN] is a typical relaxor ferroelectric and perhaps the most studied. Its solid solution with lead titanate (PT) has a morphotropic phase boundary near 35-mole% PT. All compositions on the PMN rich side of the morphotropic phase boundary exhibit relaxor behavior. The most recent studies of this system suggest that the relaxor ferroelectric is a polar-glassy system, analogous to a spin-glass rather than being "superparaelectric" as suggested in the past [23].

It has been pointed out that for temperatures within the Curie range, the relaxor ferroelectric may be driven into polar form by an electric bias field. The induced piezoelectric effect is thus tunable by the bias field. On removal of the field the relaxor reverts back to a random arrangement of microregions with no net remnant polarization or strain [6]. The absence of hysteresis in the field-strain curve on the high-temperature side of the Curie range is another advantageous feature of relaxor ferroelectrics.

PMN-PT relaxor ferroelectrics are a unique family of materials with a remarkable set of properties: (1) electrostrictive strains are comparable to that of the best conventional piezoelectric ceramics, (2) nonhysteretic behavior is responsible for

Table 2. Actuator applications.

Tracking Optical and Magnetic Heads
Drivers for Relays and Switches
Wire-Dot Printers and Via Punches
Fuel Injection Valves
Adaptive Optic Systems
Micropositioners for Robots and Machine Tools
Cone Vibrators for Speakers
Fans and Conical Air Movers
Ink Jet Printers

excellent positional reproducibility (3) no poling is required, and (4) the magnitude of piezoelectric coefficients may be adjusted by electric bias field, and the maxima values of the piezoelectric coefficients are 2-3 times higher than those in PZT ceramics.

PIEZOELECTRIC AND ELECTROSTRICTIVE ACTUATORS

There are presently more than 20 practical devices that employ piezoelectric and electrostrictive actuators [22] and it seems likely that the range of applications for solid state displacement transducers will continue to grow in the future. Table 2 lists some of the applications of piezoelectric/electrostrictive actuators. Properties that are essential for the performance of one type of actuator, for instance a linear response, are often irrelevant for others. Thus, each application demands carefully defined figure of merit for the actuator material.

Classification of Electrostrictive and Piezoelectric Actuators

The strain of a displacement transducer may be controlled by an electric field in different ways [17,22] (Figure 6). In the first case, the strain of the actuator is

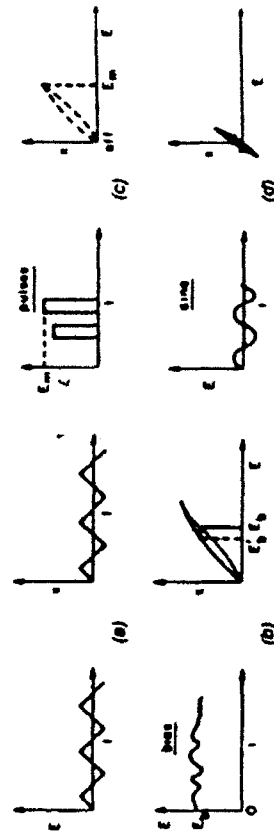


Figure 6. Classification of piezoelectric and electrostrictive actuators according to the modes of driving. (a) Strain is controlled directly by electric field. (b) Displacement is controlled by a feedback system and electric bias field. (c) Strain is controlled by electric field in an on/off manner. (d) Resonating strain in ultrasonic motors.

controlled directly by electric field, as illustrated in Figure 6(a). The waveform of the electric field depends on the required waveform of the displacement. The displacement will follow the field only with a linear relationship between strain and electric field. This type of actuator requires a transducer material with a reproducible, nonhysteretic, field-independent relationship between strain and field. The second type [Figure 6(b)] of displacement transducer is used in the situations in which the displacement is affected by an external parameter, such as a mechanical disturbance or temperature change. A feedback system is then necessary to adjust the magnitude of the electric bias field and bring the displacement to the desired value. In this type of transducer nonlinearities between strain and electric field are tolerable, but the hysteretic behavior is still detrimental. If the displacement drifts away from the desired value, longer times and large variations in bias field are required to bring the displacement back to the desired value for an actuator with hysteresis.

In the third type [Figure 6(c)] strain is controlled by electric field in an on/off manner. There are two variations of this type of actuators: in one, the field induced displacement disappears as soon as the field is switched off; in the other, the induced strain may remain, but its level has to be controlled in some other way after the field is removed. For an actuator of this type only the reproducibility of the maximum strain induced by the electric field pulse is critical and it is not of a great importance how the strain reaches its optimum value. Since the pulses are usually very short, the response of actuator must also be very fast. The driving mechanism for ferroelectric actuators that perform in an on/off mode does not necessarily have to involve a piezoelectric or electrostrictive effect. Certain compositions in the PbZrO_3 - PbTiO_3 - PbSnO_3 ternary system undergo phase transitions from an antiferroelectric to a ferroelectric phase under applied electric field [18]. The phase transition is accompanied by a large volume change since the antiferroelectric phase has the smaller lattice volume than the ferroelectric form. Associated strains are as large as 1% but the electric fields required for switching are very high.

Finally, in ultrasonic motors, an alternating electric field is applied to the actuator with a frequency equal to the resonant frequency of the actuator. In this way, larger strains may be induced under relatively smaller fields compared to the other types of actuators. Since the actuator operates at its resonant frequency, the material properties of greatest importance are a high mechanical quality factor and a high electromechanical coupling coefficient. There are several types of ultrasonic motors. The most widely studied type uses surface acoustic waves to move an object that is in contact with the transducer surface. The surface acoustic waves are generated by superimposing two standing waves of equal amplitude but with a phase difference of 90° with respect to both time and space. The waves are caused by a combination of longitudinal and shear motions governed by the stress-free boundary conditions at the surface [11]. The particles at the surface describe elliptical motions with amplitudes that decrease with thickness and become insignificant below $\sim 1 \mu\text{m}$. The horizontal component of the elliptical motion is responsible for the force acting on an object in contact with the surface.

Applications of Electrostrictive and Piezoelectric Actuators

There are four major groups of applications of electrostrictive/piezoelectric actuators. These are briefly reviewed below [17,22].

DEFORMABLE MIRRORS

In the field of adaptive optics, a mirror surface is dynamically controlled using a feedback system to adjust the phase of the light wave and eliminate atmospheric turbulence, thermally induced stresses or gravitational forces. Applications of active optical systems include large ground-based and space telescopes, high energy lasers, laser communication systems, and highly sensitive AC interferometric dilatometers. Typical requirements for deformable mirrors are a maximum throw of $\pm 20 \mu\text{m}$, small volumes, long-term stability, good reproducibility and low thermal expansion.

MECHANICAL MICROPOSITIONERS

Precision actuators are often required to position mechanical parts very accurately and reproducibly on a micron or even submicron level. The displacement of the actuators used for these purposes is usually controlled by a feedback system. Applications are found in the fields of optical microscopy, cutting-error corrections, micropositioners for robots, and in the tracking of optical and magnetic heads. Excellent reproducibility and anhyseretic behavior of the strain-electric field relation are important requirements for actuators used in these applications.

IMPACT DEVICES

The impact type actuators are driven in an on/off manner. They move parts to a desired position by making an impact with them. Typical applications are drivers for relays and switches, via punches, wire-dot printers, and ink jet printers. Clearly, such actuators should have a quick response, large electromechanical coupling factors and large generative forces.

ULTRASONIC MOTORS

Ultrasonic motors are mainly at the development stage [22], but they have considerable potential because they are compact and light weight, with a self-locking mechanism, relatively high torque at low speeds and motion in both forward and reverse directions. Two of the problems with ultrasonic motors are the maintenance of frictional forces between the surface and the moving object at the contact points, and the need for high frequency power supplies. A typical application is the automatic focusing unit in a movie camera.

REFERENCES

1. Arlt, G. 1982. "Piezoelectric Relaxation", *Ferroelectrics*, 40:149.
2. Arlt, G., H. Dederichs and R. Herbert. 1987. " 90° Domain Wall Relaxation in Tetragonally Distorted Ferroelectric Ceramics", *Ferroelectrics*, 74:37-53.
3. Berlincourt, D., D. R. Curran and H. Jaffe. 1964. "Piezoelectric and Piezomagnetic Materials

- and Their Function in Transducers", in *Physical Acoustics*, Vol. 1, W. P. Mason, ed., New York Academic, (Part A) 169-270.
4. Crawley, E. F. and E. H. Anderson, 1990, "Detailed Models of Piezoceramic Actuation of Beams", *J. of Intell. Mater. Syst. and Struct.*, 1(1):4-23.
5. Cross, L. E. 1987 "Relaxor Ferroelectrics", *Ferroelectrics*, 76:241-267.
6. Cross, L. E., S. J. Jang, R. E. Newham, S. Nomura and K. Uchino, 1980 "Large Electrostrictive Effects in Relaxor Ferroelectrics", *Ferroelectrics*, 23:187-192.
7. Damjanovic, D., T. R. Gururaja and L. E. Cross, 1987 "Anisotropy in Piezoelectric Properties of Modified Lead Titanate Ceramics", *Am. Ceram. Soc. Bull.*, 66(4):699.
8. Devonshire, A. F. 1949 "Theory of Barium Titanate - Part I", *Phil. Mag.*, 40:1040.
9. Herbert, J. M. 1982, "Ferroelectric Transducers and Sensors", *Electromechanical Science Monographs*, Vol. 3, New York: Gordon and Breach.
10. Jimenez, B. and J. De Frutos, 1990, "Piezoelectric Relaxation Studies of Ferro-Piezoelectric Ceramics", *Ferroelectrics*, 109:107-112.
11. Moulson, A. J. and J. M. Herbert, 1990, *Electroceramics*, London: Chapman and Hall, pp 265-318.
12. Nelson, D. F. and M. Lax, 1973, "New Piezoelectric Contributions to Piezoelectricity", *Phys. Rev. Lett.*, 31:763.
13. Nelson, D. F. and M. Lax, 1976, "Linear Elasticity and Piezoelectricity in Pymelectrics", *Phys. Rev.*, B13:1785.
14. Newham, R. E. 1975, *Structure-Property Relations*, Berlin: Springer-Verlag.
15. Newham, R. E. 1989, "Electroceramics", *Rep. Prog. Phys.*, 52:123-156.
16. Nye, J. F. 1985, *Physical Properties of Crystals*, Oxford: Clarendon.
17. Pan, W. Y. 1988, "Ferroelectric Materials for Actuator Applications", Ph. D. thesis, The Pennsylvania State University, University Park, PA.
18. Pan, W. Y., Q. M. Zhang, A. Bhalla and L. E. Cross, 1989, "Field-Fired Antiferroelectric-to-Ferroelectric Switching in Modified Lead Zirconate Titanate Ceramics", *J. Am. Ceram. Soc.*, 72(4):571-578.
19. Simin, Yu. I. and M. P. Shasholskaya, 1982, *Fundamentals of Crystal Physics*, Moscow: Mir.
20. Smith, J. G. 1978, "Eigenstates of Coupling Factors and Loss Factor of Piezoelectric Ceramic", Ph. D. thesis, Twente University of Technology, Netherlands.
21. Taylor, D. J., D. Damjanovic, A. S. Bhalla and L. E. Cross, Submitted for publication, "Large Hydrostatic Piezoelectric Coefficient in Lead Magnesium Niobate-Lead Titanate Ceramics", *J. Mater. Sci. Lett.*
22. Uchino, K. 1986, "Electrostrictive Actuators: Materials and Applications", *Am. Cer. Soc. Bull.*, 65(4):647-652.
23. Viehland, D., S. J. Jang, L. E. Cross and M. Wuttig, 1990, "Freezing of the Polarization Fluctuations in Lead Magnesium Niobate Relaxors", *J. Appl. Phys.*, 68(16):2916-2921.
24. Zhang, Q. M., W. Y. Pan, S. J. Jang and L. E. Cross, 1988, "The Pressure Dependence of the Dielectric Response and Its Relation to the Electrostriction", *Ferroelectrics*, 88:147-154.

APPENDIX 26

Metal-Ceramic Composite Actuators

Yutaka Sugawara, Katsuhiko Onitsuka,* Shoko Yoshikawa,* Qichang Xu,
Robert E. Newnham,* and Kenji Uchino*

Materials Research Laboratory, The Pennsylvania State University, University Park, Pennsylvania 16802

A new type of actuator composed of metal (brass) end caps and piezoelectric ceramics has been developed as a displacement transducer. Shallow cavities positioned between the metal caps and the central ceramic disk convert and amplify the radial displacement of the piezoelectric ceramic into a large axial motion of the metal end caps. Large d_{33} coefficients exceeding 2500 pC/N are obtained with the composite actuators. The behavior of the electrically induced strain with geometric variables, such as the thickness of the metal end caps, and with pressing force and driving frequency has been evaluated. Sizeable strains are obtained with both PZT (piezoelectric lead zirconate titanate) and PMN (electrostrictive lead magnesium niobate) ceramics. [Key words: actuator, ceramic-metal systems, piezoelectric properties, strain, geometry.]

I. Introduction

IN RECENT years, piezoelectric and electrostrictive ceramics have been used as displacement transducers, precision micro-positioners, and in many other actuator applications.¹ An important drawback to these devices, however, is the fact that the magnitude of strain in piezoelectric ceramics is limited to about 0.1%. Magnification mechanisms have, therefore, been developed to produce sizeable displacements at low voltages. The two most common types are the multilayer ceramic actuator with internal electrodes and the cantilevered bimorph actuator. The multilayer actuator produces a large force at low voltages, but large displacements are not obtained. Bimorphs, on the other hand, produce large displacements up to hundreds of micrometers, but the forces are very small. Therefore, there is a need for another type of magnification giving sizeable displacement with sufficient force to conduct actuator applications.

A cross section of a newly patented ceramic-metal composite² is shown in Fig. 1. It is called the "Moonie" because of the moon-shaped spaces between the metal end caps and the piezoelectric ceramic. Originally, this composite was designed as a hydrophone, and the hydrostatic piezoelectric properties were reported elsewhere.³

Referring to Fig. 1, the radial motion of the piezoelectric ceramic is converted into a flextensional motion in the metal end caps. As a result, a large displacement is obtained in the direction perpendicular to the ceramic disk. This is the basic principle of the composite actuator described in this paper.

II. Effective Piezoelectric Coefficient

Poled PZT ($\text{Pb}(\text{Zr,Ti})\text{O}_3$) ceramics are strongly piezoelectric.⁴ Under an applied electric field, the ceramic expands longitudinally through d_{33} and contracts transversely through d_{31} .

G. H. Haertling-contributing editor

Manuscript No. 196210. Received December 19, 1991; approved February 6, 1992.

*Member, American Ceramic Society.

Therefore, in the Moonie structure, the axial displacement comes from two different sources. One is the longitudinal displacement of the ceramic itself through d_{33} ; the other is the flextensional motion of the metal arising from the radial motion of the ceramic and d_{31} . The two contributions add together to give unusually large displacements which can be described by an effective d_{33} coefficient.

The d_{33} coefficient relates strain and electric field in the poling direction and is often used to compare different piezoelectric materials. In a weak piezoelectric, such as quartz, d_{33} is approximately 1 pC/N, and is about an order of magnitude smaller than an average piezoelectric, such as poly(vinylidene fluoride). Strong piezoelectrics, such as BaTiO_3 or PZT have piezoelectric coefficients larger than 100 pC/N. Effective d_{33} values in excess of 1000 pC/N are obtained for the composite structures reported in this paper.

III. Sample Preparation and Measurement Technique

The initial objective of the research was to make an actuator capable of very large displacements, and to evaluate its performance under dc and ac drive.

The composite actuators were made from electroded PZT 5A disks (11 mm in diameter and 1 mm thick) and brass end caps (13 mm in diameter and thicknesses ranging from 0.4 to 3 mm). Shallow cavities 6 mm in diameter and 150 μm center depth were machined into the inner surface of each brass cap. The PZT disk and the end caps were bonded around the circumference, taking special care not to fill the cavity or short circuit the ceramic electrodes. Silver foil (25 μm thickness) and silver paste were used as bonding materials. The composite was heated to 600°C under stress to solidify the bond. After cooling, the actuator was encapsulated around the circumference in epoxy resin (Spurrs) followed by curing at 70°C for 12 h. Electrodes were attached to the brass end caps and the ceramic was poled at 2.5 MV/m for 15 min in an oil bath held at 120°C.

The direct piezoelectric coefficient was measured at a frequency of 100 Hz using a d_{31} meter (Berlincourt, Channel Products, Inc., Chesterland, OH). The converse piezoelectric coefficient of the ceramic was determined with a laser inter-

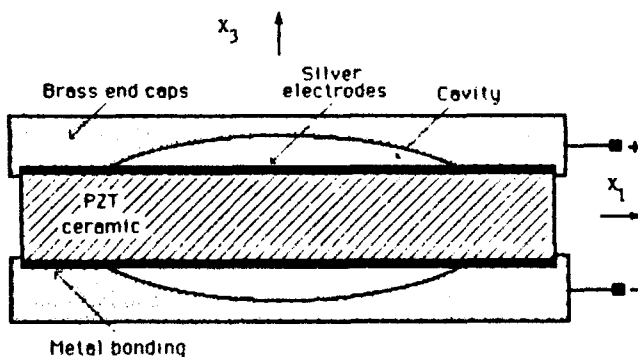


Fig. 1. Composite Moonie actuator.

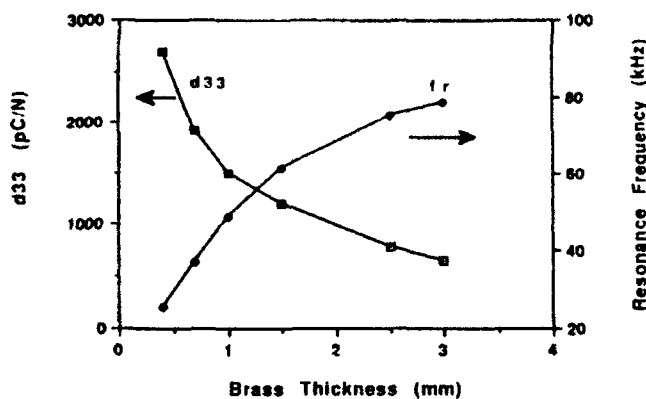


Fig. 2. Resonance frequency (f_r) and d_{33} coefficient plotted as a function of the thickness of the brass end caps.

ferometer. Displacements of the composite actuator were measured by a linear-voltage differential transducer (LVDT) having a resolution of approximately $0.05 \mu\text{m}$. The effective d_{33} coefficient of the composite was obtained by dividing the strain by the applied electric field. In comparing the resulting d_{33} with that of a ceramic, it was important to use the total thickness of the composite in calculating the field-induced strain. Resonant frequencies were obtained with a low-frequency impedance analyzer (Model No. 4192A, Hewlett-Packard Co., Palo Alto, CA).

IV. Experimental Results

Figure 2 shows the d_{33} coefficient and resonant frequency plotted as a function of the brass thickness. As expected, thinner end caps flexed easier, resulting in larger piezoelectric coefficients. The d_{33} values were measured at the center of the brass end caps using the Berlincourt d_{33} meter. Values as high as 2500 pC/N, approximately 5 times that of PZT 5A, were obtained with the Moonie actuator. A spectrum analyzer was used to measure the fundamental flextensional resonant frequency. The resonant frequency decreased rapidly with decreased brass thickness, dropping to less than 20 kHz for a thickness of 0.4 mm.

Piezoelectric effects are largest near the center of the transducer where the flexural motion is largest. The d_{33} values measured as a function of position with a Berlincourt d_{33} meter are shown in Fig. 3. Plots are shown for two brass thicknesses of 0.4 and 3.0 mm. Ample working areas of several square millimeters are obtained with the actuators.

Maximum displacements obtained with the Moonie actuators are shown in Fig. 4. The values were recorded with the LVDT system and a field of 1 MV/m, which is well below the

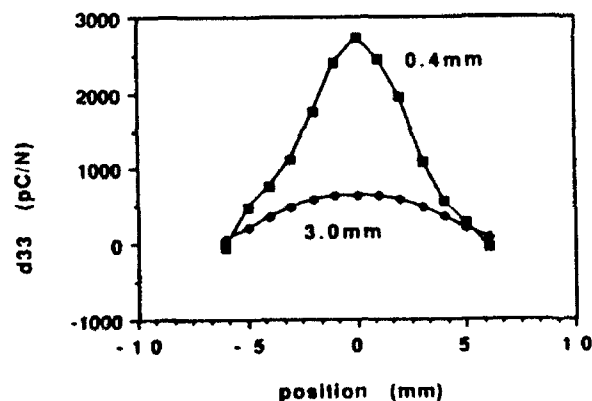


Fig. 3. Positional dependence of the d_{33} coefficient for two actuators with brass thickness of 0.4 and 3.0 mm.

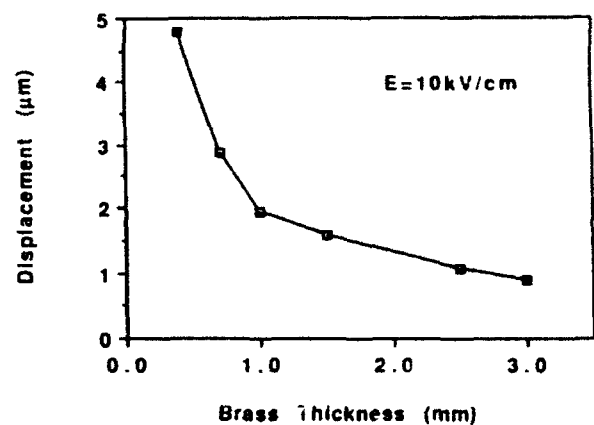


Fig. 4. Maximum displacement plotted as a function of brass thickness.

breakdown field of PZT. The largest displacements were obtained with actuators having thin end caps. By loading the actuators with weights it was demonstrated that even thin end caps are capable of exerting forces in excess of 2 kgf.

A few experiments have also been conducted with actuators incorporating PMN (lead magnesium niobate) ceramics. PMN does not need to be poled because it utilizes the electrostrictive effect rather than piezoelectricity. As shown in Fig. 5, displacements as large as $10 \mu\text{m}$ are obtained with PMN and brass end caps 0.4 mm thick. Corresponding curves for the composite containing PZT, and for the uncapped PZT and

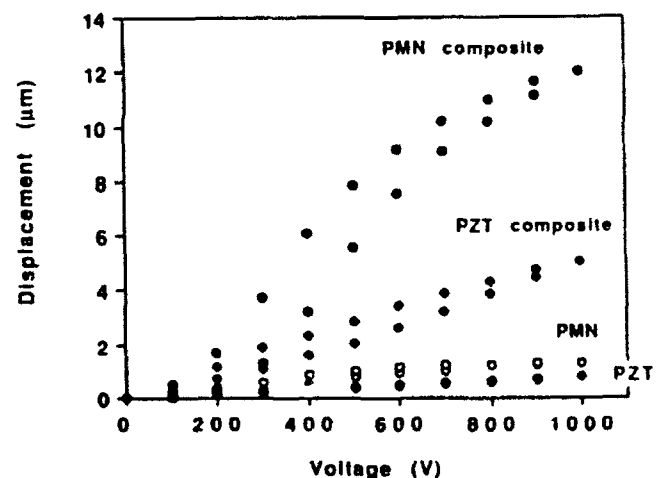


Fig. 5. Displacements measured for composite actuators driven by PZT and PMN ceramics. Displacement for the uncapped ceramics are shown for comparison.

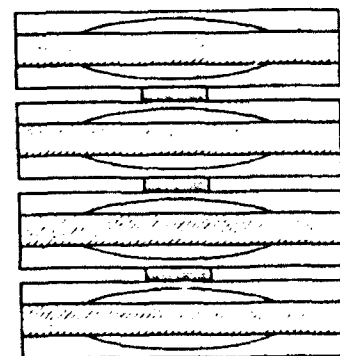


Fig. 6. Illustration of stacked composite.

PMN ceramics, are shown in Fig. 5 as well. The composites produce a strain amplification of about 5 times.

V. Conclusions

A new type of actuator has been constructed from piezoelectric PZT ceramics bonded to metal end caps. Shallow spaces under the end caps produce substantial increases in strain by combining the d_{33} and d_{31} contributions of the ceramic. Even larger displacements are obtained using PMN electrostrictive ceramics. Further improvements in actuator performance are expected using improved materials and design. Driving voltages can be reduced using multilayer ceramics, and larger

displacements can be obtained using multi-Moonie stacks (Fig. 6).

References

- ¹K. Uchino, *Piezoelectric/Electrostrictive Actuators*. Morikita Publishers, Tokyo, Japan, 1986.
- ²R. E. Newnham and Q. C. Xu, "Transformed Stress Direction Acoustic Transducer" (to The Pennsylvania Research Corporation), U.S. Pat. No. 4 999 819, March 12, 1991.
- ³Q. C. Xu, J. Belsick, S. Yoshikawa, T. T. Srinivasan, and R. E. Newnham, "Piezoelectric Composites with High Sensitivity and High Capacitance for Use at High Pressures," *IEEE Transactions on Ultrasonics, Ferroelectrics, and Frequency Control*, **38** [6] 634-39 (1991).
- ⁴H. Jaffe, W. Cook, and B. Jaffe, *Piezoelectric Ceramics*. Academic Press, New York, 1971. □

APPENDIX 27

CERAMIC-METAL COMPOSITE ACTUATOR

Q.C. XU, A. DOGAN, J. TRESSLER, S. YOSHIKAWA,
and R. E. NEWNHAM

Materials Research Laboratory
The Pennsylvania State University
University Park, PA 16802

ABSTRACT

The main objective of this work was to develop a new type of actuator. It consists of a piezoelectric ceramic disk or multilayer stack and two metal end plates with a crescent-shaped cavity on the inner surface. The plates are used as mechanical transformers for converting and amplifying the lateral displacement of the ceramic into a large axial motion in the plates. Both d_{31} and d_{33} contribute to the axial displacement. Sizeable strains were obtained with both PZT-metal and PMN-metal actuators. Displacement amplification principle, fabrication, and measurement results are presented.

INTRODUCTION

In recent years, piezoelectric and electrostrictive ceramics have been used in many actuator applications. The two most common types of actuator are a multilayer ceramic actuator with internal electrodes and a cantilevered bimorph actuator[1]. A frame structure for displacement amplifier in impact printer head has also been developed using piezoelectric multilayer actuators [2].

This paper describes a new type of ceramic-metal composite actuator which is based on the concept of a flextensional transducer[3]. The ceramic is excited in an extensional mode and the metal plates in a flexure mode. The metal plates are used as a mechanical transformer for transforming the high mechanical impedance of the ceramic to the low mechanical impedance of the load. Therefore, a large effective piezoelectric coefficient, d_{33} , exceeding 4000 pC/N as well as a hydrostatic piezoelectric coefficient d_{11} , exceeding 800 pC/N can be obtained from a single PZT disk-metal (brass) composite[4].

PRINCIPLE

The extensional mode of the piezoelectric ceramic element is characterized by a large generated force, a high electromechanical coupling, a high resonant frequency, and a small displacement. Often it is desirable to use a compact structure to magnify the displacement of the ceramic element. Figure 1 shows the basic configuration of the ceramic-metal composite actuator. The ceramic element can either be a piezoelectric ceramic or an electrostrictive ceramic with single layer or multilayer. Low driving voltages can be used for the multilayer ceramic element. The electrostrictive ceramic is expected to reduce hysteresis as well as exhibit a nonlinear relationship between the voltage and the displacement.

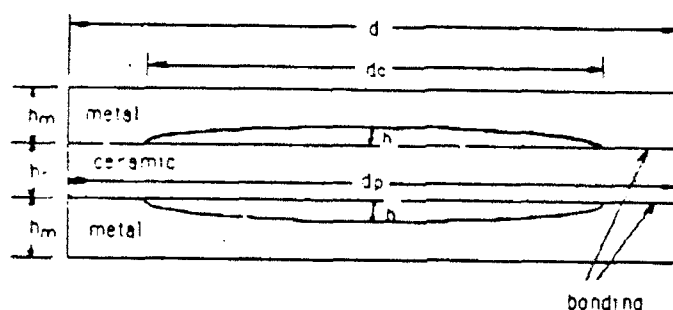


FIGURE 1. The geometry of the composite.

The "Moonie" metal plates are used as displacement magnifiers. The relationship between the displacement of the metals and the geometry of the metals and the ceramic is explained below. For simplicity, consider a curved beam with small curvature bonded to a ceramic bar (Figure 2). According to elastic theory [5], the bending moment M under an electroactive force from the ceramic is as eq. (1):

$$M = \frac{-T_d(b^2 - a^2)^2 - 4a^2b^2(\ln \frac{b}{a})}{4\left[\frac{-a^2b^2}{r^2} \ln \frac{b}{a} + b^2 \ln \frac{r}{b} + a^2 \ln \frac{a}{r} + b^2 - a^2\right]} \quad (1)$$

The electroactive force will be transmitted to the Moonie metal. The stress in the metal is:

CERAMIC-METAL COMPOSITE ACTUATOR

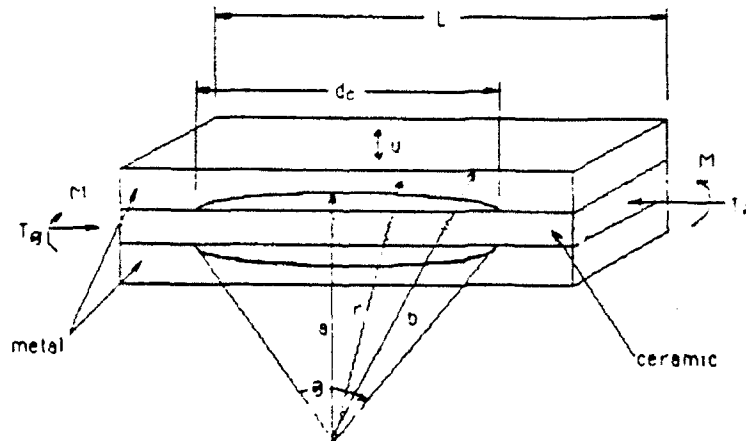


FIGURE 2. Simplified model for displacement magnification.

$$T_{\theta} = \frac{dE_3Y_cA_c}{A_m} \quad (2)$$

where d = piezoelectric strain coefficient of the ceramic,
 E_3 = electric field in the ceramic,
 Y_c = Young's modulus of the ceramic,
 A_c, A_m = cross sectional area of the ceramic and metal, respectively,

and $r \sim a \sim b$.

The normal displacement of the metal produced by the piezoelectric effect of the ceramic is:

$$U_{\theta} = \frac{-M \left(\frac{h_m}{2}\right)^2}{2 Y_m I_m} - \frac{3}{4} \frac{d Y_c d_c}{h_m Y_m \theta} V \quad (3)$$

h_m = thickness of the metal
 Y_m = Young's modulus of the metal
 V = applied voltage
 I_m = moment of inertia of the metal

$$d_{33}|_{\text{eff}} = \frac{U_{\text{pi}}}{V} = \frac{3}{4} \frac{d Y_c d_c}{h_m Y_m \theta} \quad (4)$$

For the electrostrictive effect:

$$T_\theta = \frac{Q \epsilon^2 E^2 Y_c A_c}{A_m} \quad (5)$$

Q = electrostrictive coefficient of the ceramic

ϵ = permittivity

The displacement of the metal by the electrostrictive effect is then:

$$U_{\text{ei}} = \frac{3}{4} \frac{Q \epsilon^2 Y_c d_c}{h_m h_c Y_m \theta} V^2 \quad (6)$$

The transverse displacement at the end of the ceramic bar is:

$$\delta = \frac{dV}{h_c} L$$

and the displacement conversion ratio is:

$$\frac{U}{\delta} = \frac{3}{4} \frac{d_c Y_c h_c}{L \theta Y_m h_m} \quad (7)$$

Equations (3) and (6) explain how the normal displacement U of the metal is related to the transverse piezoelectric or electrostrictive effect of the ceramic. The total displacement is the sum of the displacement described above and the displacement due to longitudinal effects.

The lowest resonant frequency of the actuator is a flextensional mode which is determined mainly by the stiffness of the ceramic in a planar mode and the equivalent mass of the metal plate. The equivalent mass is much larger than the real mass of the metal plate because the vibration velocity of the metal part is much larger than the reference velocity of the PZT. The equivalent mass is

CERAMIC-METAL COMPOSITE ACTUATOR

$$M_e = \frac{\int_0^L \frac{1}{2} \rho_m b h_m \dot{U}^2 \omega^2 dX}{\frac{1}{2} \delta^2 \omega^2} \sim M_m \frac{d_c^2 Y_c^2 h_c^2}{L \theta^2 Y_m h_m^2}$$

$$M_m = \rho_m V_m = \rho_m b h_m L.$$

When the h_c/h_m ratio is high and $k_m \ll k_c$,
the resonant frequency of the lowest flextensional mode is:

$$f_n = \frac{1}{2\pi \sqrt{(M_e + M_m)(k_c + k_m)^{-1}}} \sim \frac{f_c}{\sqrt{1 + (2\pi f_c)^2 M_m k_c^{-1}}}$$

$$= [1 + (2\pi f_c)^2 \frac{M_m k_c^{-1} Y_c^2 h_c^2 d_c^2}{L \theta^2 Y_m h_m^2}]^{-\frac{1}{2}} f_c \quad (8)$$

The M_e is much larger than the real mass of the metal.

Here k_c =stiffness of ceramic

k_m =stiffness of metal plate

f_c =resonant frequency of planar mode of the ceramic itself.

$$f_c = \frac{1}{2\pi \sqrt{M_c k_c^{-1}}}$$

From equation (8) the lowest flextensional frequency f_{fl} is proportional to $\sqrt{h_m}$.

SAMPLE PREPARATION

The composite actuators were made from electroded PZT5A or PMN-PT ceramic disks (11 mm in diameter and 1 mm thick) and brass end caps (from 11 mm to 13 mm in diameter with thicknesses ranging from 0.2 to 3 mm). Shallow cavities from 6 mm to 8.5 mm in diameter and about 150 μ m center depth were

machined into the inner surface of each brass cap. The ceramic disk and the end caps were bonded around the circumference, taking care not to fill the cavity or short circuit the ceramic electrodes. Three kinds of bonding materials have been utilized:

1. Silver foil (25 μm thickness) and silver paste bonding.

This composite was heated to 600°C under stress to solidify the bond. After cooling, the actuator was encapsulated using Spurr's epoxy resin, followed by curing at 70°C for 12 hours. Electrodes were attached to the brass end caps and the PZT ceramic was poled at 2.5 MV/m for 15 minutes in an oil bath held at 120°C.

2. Pb-Sn-Ag Solder Bonding.

The PMN-PT or poled PZT and the brass end caps with the Pb-Sn-Ag solder ring (thickness 50 μm) were heated to 190°C under pressure. After cooling, the composite was encapsulated using epoxy resin.

3. Epoxy Resin Bonding.

The brass end caps and the ceramic were bonded by Emerson & Cuming epoxy resin around the rim at room temperature.

An electrostrictive actuator was made from a multilayer ceramic stack and a brass beam and bonded to the Moonie inner surface with an epoxy (Figure 3). This composite demonstrates that a sizeable displacement can be produced under low driving voltage using a multilayer ceramic stack.

EXPERIMENT RESULTS

The displacement of the composite actuator in the low frequency range was measured with a Linear Voltage Differential Transducer (LVDT) having a resolution of approximately 0.05 μm . The direct piezoelectric coefficient d_{33} was measured at a frequency of 100 Hz using a Berlincourt d_{33} meter. The displacement-frequency dependence was measured with a double beam laser interferometer.

CERAMIC-METAL COMPOSITE ACTUATOR

Resonant frequencies were obtained with a Hewlett-Packard Spectrum Analyzer (HP-3585A) or Network Analyzer (HP-3577A).

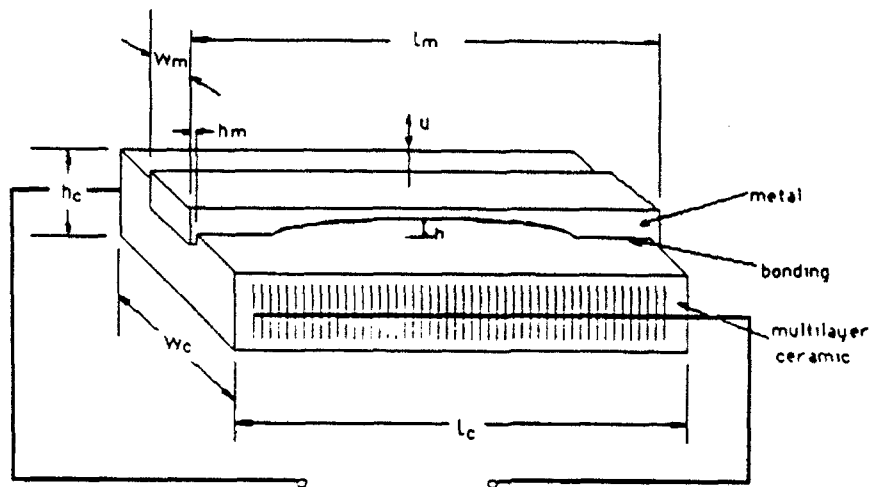


FIGURE 3. Another type of ceramic-metal composite actuator with multilayered ceramic part.

1. Displacement Measurement

Figure 4 shows the displacements versus electric field curves for composite actuators driven by PZT and PMN ceramics. Displacements for the uncapped ceramics are shown for comparison. PMN does not need to be poled because it utilizes the electrostrictive effect rather than piezoelectricity. Dimensions of the PMN composite sample in Figure 6 are as follows: $d=13$ mm, $d_p=11$ mm, $h=150$ μ m, $d_c=6$ mm, $h_p=1$ mm, and $h_m=0.4$ mm. The dimensions of the PZT composite-1 sample are: $d=d_p=11$ mm, $h=50$ μ m, $d_c=7$ mm, $h_p=1$ mm, and $h_m=0.5$ mm. Both of the uncapped PZT and PMN ceramics have the same size, $d_p=11$ mm and $h_p=1$ mm. The experimental results show that the composites produce a strain amplification of about 10 times. A displacement of about 10 μ m can be obtained under a field of 1 kV/mm. By loading these actuators with weights, it is capable of exerting forces in excess of 2 kgf.

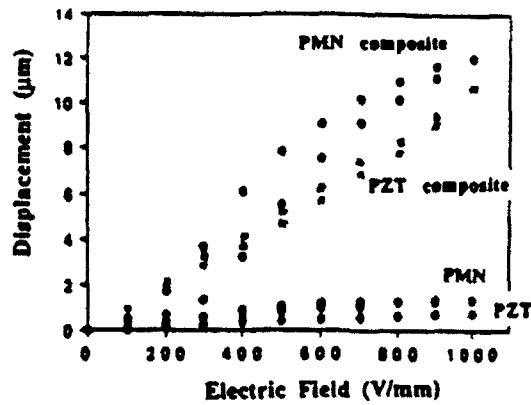


FIGURE 4. Displacements measured for composite actuators driven by PZT and PMN ceramics. Displacement for the uncapped ceramics are shown for comparison.

As shown in Equation 3 and Equation 6, the displacement amplification is dependent on the thickness of metal h_m and cavity diameter d_c . The sample PZT composite-2 with dimensions $d=d_p=11$ mm, $h_p=1$ mm, $h=200$ μ m, $h_m=0.3$ mm, and $d_c=8.5$ mm exhibits sizeable displacements - as large as 20 μ m with a force capability of 0.15 kgf (see Figure 5).

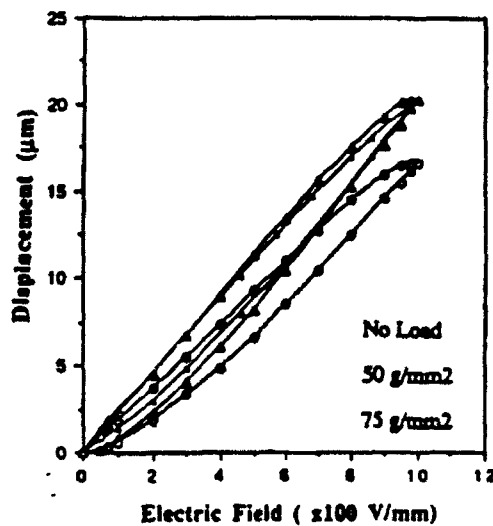


FIGURE 5. Displacement vs. field curves under different exerty forces for the sample PZT composite-2.

CERAMIC-METAL COMPOSITE ACTUATOR

The 124 layer electrostrictive composite actuator shown in Figure 3 gave the displacement exhibited in Figure 6. More than $15\text{ }\mu\text{m}$ displacement can be obtained under an applied voltage of 150V. Notice that this experimental result is obtained with only one metal end-cap on the ceramic stack. If the convex or concave metal end-caps are placed on both sides of the ceramic stack, more than $30\text{ }\mu\text{m}$ displacement will be obtained under the applied voltage of 150V. Displacements for the uncapped multilayer ceramic in the same direction are shown for comparison. The lowest flexensional resonant frequency for the composite is 6.4 kHz.

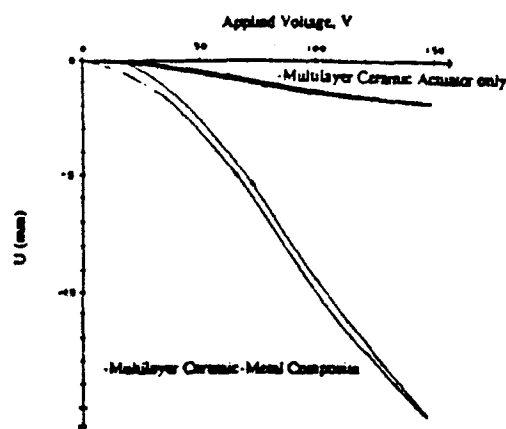


FIGURE 6. Displacement with increase in applied voltage of the multilayer ceramic-metal composite actuator using an electrostrictive ceramic stack and a brass end cap.

2. Thickness Dependence

Figure 7 shows the effective d_{33} coefficient and resonant frequency plotted as a function of the brass thickness. As expected in Eq. (4) and Eq. (8), the effective d_{33} is proportional to $1/h_m$ and the lowest resonant frequency is proportional to $\sqrt{h_m}$. The d_{33} values were measured at the center of the brass end caps using a Berlincourt d_{33} meter. Values as high as 4000 pC/N, approximately 10 times that of PZT5A, were obtained with the Moonie actuator.

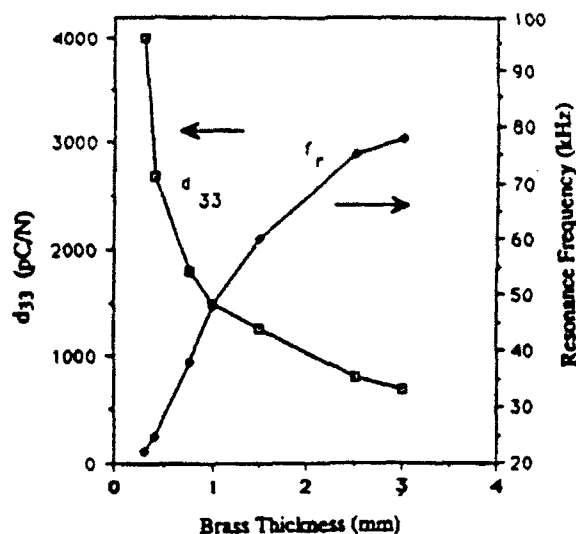


FIGURE 7. Resonance frequency f_r and d_{33} coefficient plotted as a function of the thickness of the brass endcaps.

Piezoelectric effects are largest near the center of the transducer where the flexural motion is largest. The effective values measured as a function of position with a Berlincourt meter are shown in Figure 8. Plots are shown for two brass thicknesses of 0.4 and 3.0 mm. Ample working areas of several mm^2 are obtained with the actuators.

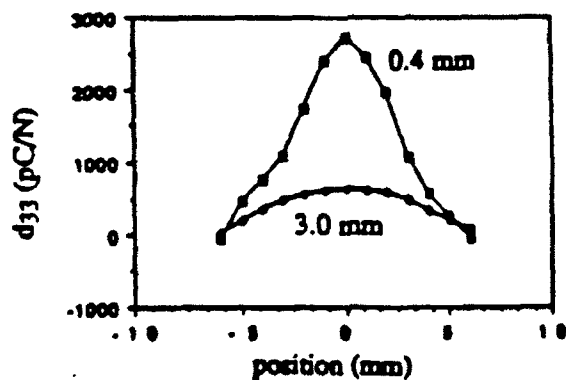


FIGURE 8. Positional dependence of the d_{33} coefficient for two actuators with brass thicknesses of 0.4mm and 3.0mm.

CERAMIC-METAL COMPOSITE ACTUATOR

3. Resonant Frequency-Temperature Dependence

The lowest flextensional frequency of the PZT-brass composite with Pb-Sn-Ag solder bond and without epoxy encapsulation decreases with temperature as shown in Figure 9. This is probably due to the high stress in the PZT ceramic arising from thermal stresses set up by the metal.

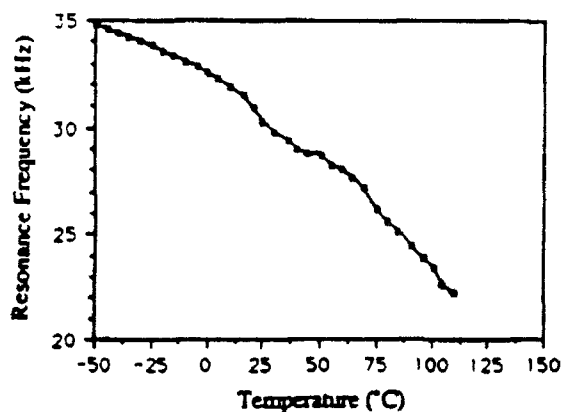


FIGURE 9. Resonance frequency vs. Temperature

4. Electrode Effect

Figure 10 shows the effective piezoelectric d_{33} coefficient of the composite increases with electrode area of PZT. This means that all the PZT is contributing uniformly to the displacement.

5. Creep

Keeping a field of 1 kV/mm on the composite sample with epoxy bonding for two hours, no displacement change was observed by LVDT measurement (see Figure 11) after one hour.

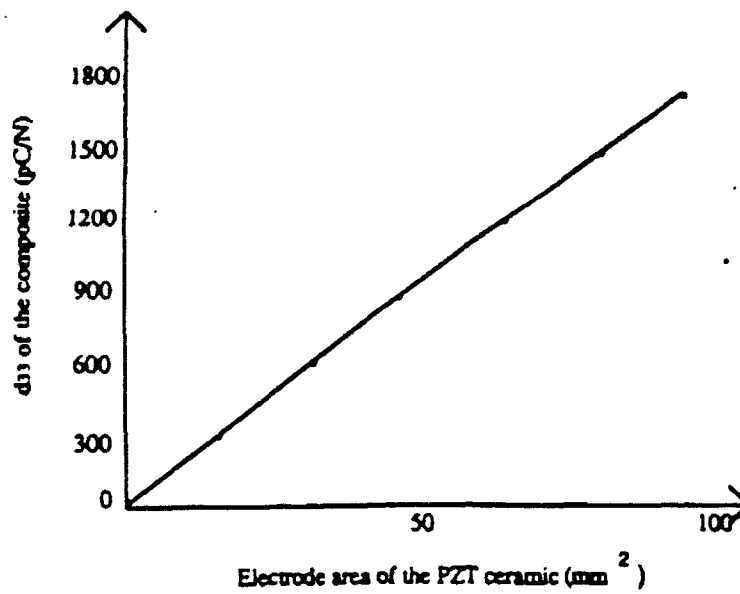


FIGURE 10. Effective d_{33} vs. electrode area of ceramic.

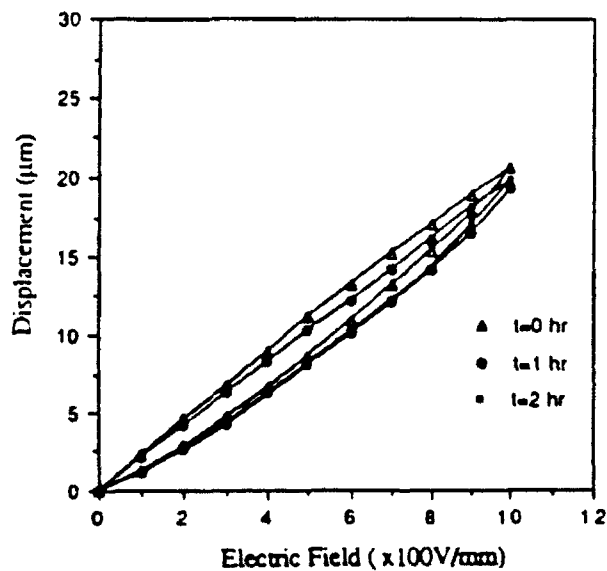


FIGURE 11. Creep under field of 1kV/mm

CERAMIC-METAL COMPOSITE ACTUATOR

CONCLUSIONS

A new type of actuator has been constructed from piezoelectric PZT ceramics bonded to metal end caps. Shallow spaces under the end caps produce substantial increases in strain by combining the d_{33} and d_{31} contributions of the ceramic. Even larger displacements were obtained using PMN electrostrictive ceramics.

The displacement is inversely proportional to the metal thickness.

The displacement is proportional to the area of the driving ceramic.

The creep under 1 kV/mm is very small after one hour.

The lowest resonant frequency is proportional to the square root of the metal thickness.

Further improvements in actuator performance are expected using improved materials and design. Driving voltages can be reduced using multilayer ceramics, and larger displacements can be obtained using multilayer stacks (Figure 12).

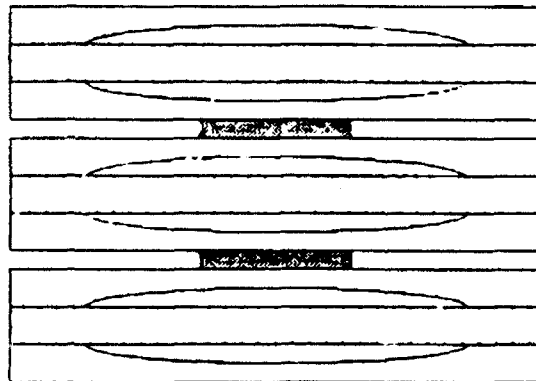


FIGURE 12. Illustration of stacked composite.

ACKNOWLEDGEMENTS

The authors wish to thank Dr. W. Smith, Professor L.E. Cross, Dr. K. Uchino, and Dr. J. Dougherty for their advice, as well as Y. Sugawara, K. Onitsuka, and J. Belsick for work reported in earlier papers [3,6].

REFERENCES

1. K. Uchino, "Piezoelectric/Electrostrictive Actuator," Morikita Publishers, Tokyo, Japan(1986)
2. K. Yoda , H. Morita, T. Mori, T. Shibuya, "Frame Structure for Impact Print Head," Spring Meeting of IECE of Japan, 7-96 (1990) (in Japanese).
3. Q.C. Xu, J. Belsick, S. Yoshikawa, and R. E. Newnham, "Piezoelectric Composites with High Sensitivity and High Capacitance for Use at High Pressure," IEEE Transactions on UFFC (in press).
4. R.E. Newnham, Q.C. Xu, and S. Yoshikawa, (patent) "Transformed Stress Direction-Acoustic Transducer (to the Pennsylvania Research Corporation) U.S. 4,999,819 (March 12, 1991).
5. S. Timoshenko and J. N. Goodier, "Theory of Elasticity," Chapters 4 and 10, 2d ed., New York, McGraw-Hill, 1951.
6. Y. Sugawara, K. Onitsuka, S. Yoshikawa, Q.C. Xu, R.E. Newnham, and K. Uchino, "Piezoelectric and Electrostrictive Composite Actuators," Proceedings of the 1991 International Symposium on Active Materials and Adaptive Structures, Alexandria, VA (in press).